DISSERTATION

FUNCTIONAL CHARACTERIZATION OF NUCLEOSOME ASSEMBLY PROTEINS

Submitted by

Daniel Krzizike

Department of Biochemistry and Molecular Biology

In partial fulfillment of the requirements

For the Degree of Doctor of Philosophy

Colorado State University

Fort Collins, Colorado

Summer 2021

Doctoral Committee:

     Advisor: Karolin Luger

     Alan Kennan
     Jennifer Nyborg
     Laurie Stargell
     Robert Woody

ABSTRACT

FUNCTIONAL CHARACTERIZATION OF NUCLEOSOME ASSEMBLY PROTEINS

The amount of DNA found within the human body will span from the earth to the sun ~50 times. With the DNA providing the genetic blueprint of all living things, it needs to be packaged in a way that allows accessibility. The first step in this packaging involves nucleosomes, large macromolecular complexes made up of histone proteins and DNA. Nucleosomes must remain dynamic as they are constantly assembled and disassembled for processes such as DNA replication, repair, and transcription. Both assembly and disassembly occur in a specific stepwise manner orchestrated by multiple proteins employed by the cell. Specifically, histone chaperones have been implicated in almost every aspect of nucleosome dynamics such as shuttling histones into the nucleus, histone storage, and both nucleosome assembly and disassembly in an ATP-independent manner. While the structures of many histone chaperones have been determined, the mechanism of how they regulate nucleosome dynamics is still largely unknown.

I investigated the mechanism of the nucleosome assembly protein family (Nap family) through several biochemical approaches. The Nap family of proteins are implicated in histone homeostasis through interactions with core histones, histone variants, and linker histones. They are conserved among all eukaryotes from yeast to humans. Members of the Nap family contain a conserved core region flanked by highly disordered N- and C-terminal tails varying in length and charge between species. Using yNap1, we investigated how these tails impact the overall function in regard to histone binding, histone selectivity among core histones and histone variants, and in mediating histone-DNA interactions. We found that the tails are critical for overall function, with the charge of the tails being crucial in regulation.

We also investigated Vps75, another member of the Nap family. Similar to Nap1, Vps75 binds core histones, but also stimulates the acetylation activity of Rtt109, a histone

acetyltransferase. In light of a recent debate regarding the stoichiometry with which these Nap members bind their histone cargo, we characterized the Vps75-histone interaction using core histones H2A-H2B and H3-H4. Comparing Vps75 with yeast Nap1, we found that the mechanism of histone binding is not conserved among these Nap family members. Further expanding on Vps75, we investigated the interaction with Rtt109 in both the presence and absence of H3-H4. We discovered dimeric Vps75 is capable of binding either one histone tetramer or two units of Rtt109 with the ternary complex consisting of only one unit of Rtt109 and one H3-H4 tetramer.

While characterizing Nap family members I became very familiar with Analytical Ultracentrifugation (AUC). AUC is a powerful in-solution technique that provides first-principle hydrodynamic information to determine size, shape, and molecular interactions, making it ideal for the characterization of proteins, DNA, and the interactions among them. As our lab traditionally used AUC to obtain van Holde-Weischet plots, an excellent graphical representation of homogeneity or heterogeneity, we incorporated new analysis techniques for improved accuracy in molecular mass and gross shape determination. Using the added-on fluorescence detection system, we obtained a level of sensitivity and selectivity that was otherwise not possible.

Using the powerful method of analytical ultracentrifugation combined with fluorescent studies, we provide insight into the regulation mechanism of Nap family members along with establishing a framework to study other macromolecular complexes.

They have each provided me with comments, suggestions, and critiques over the years that have improved my research, writing, and presentation skills. With Dr. Woody being across the hall, I bugged him many times while working through both thermodynamic and AUC issues with him never once turning me down. With all the support I have received I don't think I could have asked for a better graduate experience.

TABLE OF CONTENTS

Chapter 1 – Characterization of Nucleosome Assembly Proteins

Introduction: Literature Review

1.1 - Chromatin dynamics and regulation

The human cell contains specific blueprints that are passed down from parents to offspring known as deoxyribonucleic acid (DNA). In humans, these genetic blueprints are encoded within 3 billion base pairs of DNA distributed through 23 pairs of chromosomes. Aligning the DNA in all chromosomes of a single human cell from end to end gives a measurement of ~2 meters. Organizing this DNA to fit inside a 10μm nucleus would be similar to packing ~9.5 miles of string inside a baseball, with the additional challenge that DNA is a negatively charged polymer. This causes the DNA to experience repulsive forces with any DNA in close proximity. Making compaction seem even more implausible is that DNA needs to be organized in a dynamic manner so it is accessible for diverse cellular processes. This is accomplished among all eukaryotic cells with the assembly of chromatin: a dynamic complex of negatively charged DNA molecules interacting with positively charged histone proteins.

Histone proteins are indispensable components of chromatin. Histones make up the foundation of the nucleosome (Figure 1.1), the basic repeating unit of chromatin that is conserved from yeast to metazoans consisting of 146 bp of DNA wrapped around an octameric core [5, 6]. Assembly of the nucleosome begins with the interaction of H3-H4 with DNA forming a tetrasome followed with the addition of two H2A-H2B dimers [7]. Due to the stepwise assembly, nucleosome formation is not a spontaneous process, but rather requires the aid of proteins known as histone chaperones [8]. Although nucleosomes must remain dynamic, through the use of micrococcal nuclease digestion, it has been shown that histones form tight associations with each other and DNA making nucleosomes quite stable [9].
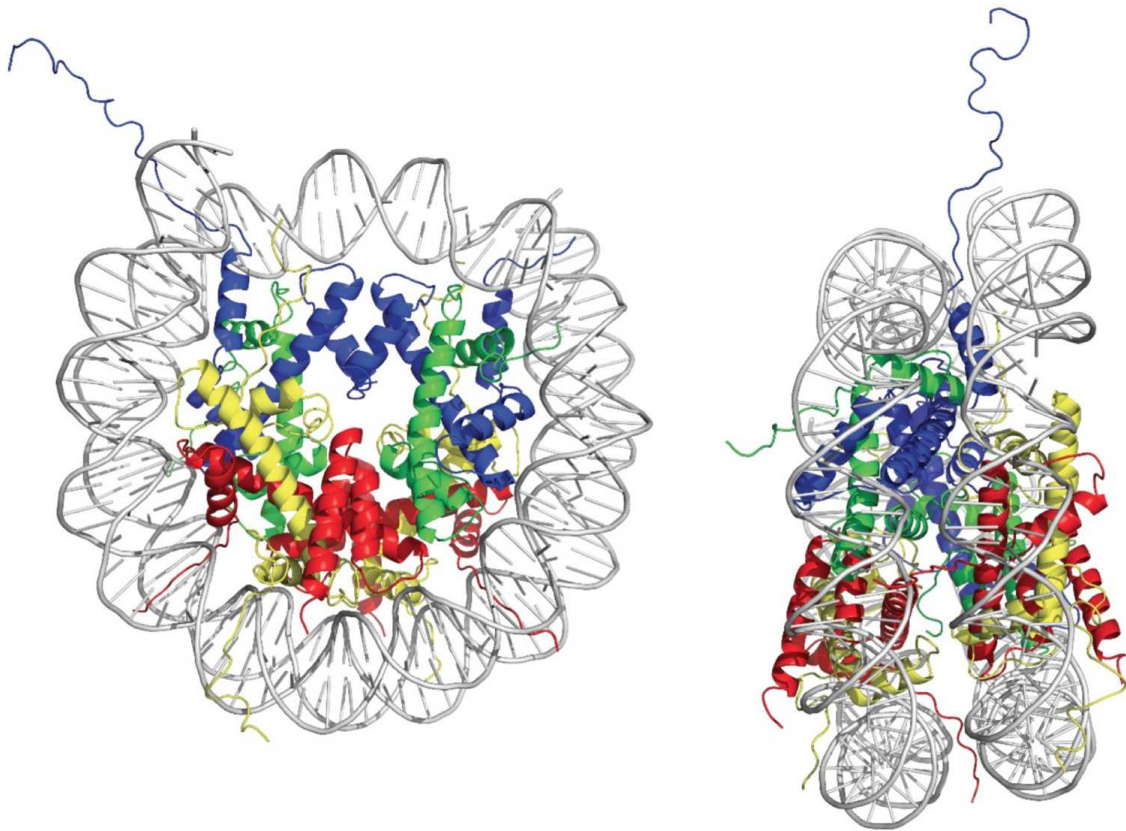
Figure 1.1. Crystal structure of the nucleosome core particle (NCP) (Luger et al, 1997) (PDB ID: 1AOI). 146 bp α-satellite DNA (grey) wraps ~1.65 turns around a histone octamer containing *Xenopus laevis* H2A-H2B (yellow and red) and H3-H4 (blue and green).

Core histones are small (11-15 kDa), basic proteins that are highly conserved among eukaryotes. A variable length N-terminal tail, subject to extensive post-translational modifications, along with a histone fold motif are common among core histones [5, 10]. Within the nucleosome, core histones form an octameric assembly of H3-H4 tetramer flanked by two H2A-H2B dimers. The first step in octamer refolding is heterodimerization of H2A-H2B and H3-H4 that occurs through a "handshake" interaction: an extensive histone-histone interface made up of head-to-tail associations between two histone folds. Histone-fold motifs, composed of three alpha helices separated by two unstructured loops, are highly conserved and have also been found in several protein complexes besides DNA-binding proteins [11]. After heterodimerization, the next step of octamer assembly is association of histones with one another via the 4-helix bundle at the dimer-dimer interface. Specifically, H3-H4 tetramerization occurs through H3-H3 interactions between two H3-H4 dimers. Then, two H2A-H2B dimers associate with each end of the H3-H4 tetramer via the H4:H2B 4-helix bundle completing the histone octamer. The histone octamer contacts the DNA at regular intervals within the nucleosome. Due to the instability of the H4:H2B 4-helix bundle, the octamer is only stable when bound by DNA (completing the nucleosome) or in high salt.

The mononucleosomes described above are interconnected via linker DNA to form long strings of nucleosomes known as nucleosomal arrays (Figure 1.2). These nucleosomal arrays form the 10 nm fiber, or what appears as "beads on a string" when visualized via electron microscopy and atomic force microscopy [12, 13]. Within the nucleus of a human cell, a single chromatin fiber can consist of ~100,000 nucleosomes reaching concentrations greater than 200 mg/ml [14]. To fit the large number of nucleosomes in the cell, further compaction is necessary. This compaction is inhibited by the highly acidic phosphate backbone of DNA. Nucleosome assembly accounts for neutralizing half of the acidic charge leaving the remaining charge to be

neutralized by factors such as chromatin associated proteins, alterations in the ionic conditions, and linker histones. Increasing the ionic strength of the solution induces higher order compaction through intra- and inter-fiber nucleosome interactions that are then stabilized by linker histones.

In the 1970's, it was shown by electron microscopy that purified nucleosome fibers containing linker histones folded into fibers with a 30 nm diameter (Figure 1.2) [15]. Since then, researchers concluded nucleosome assembly is the first order of chromatin compaction followed by nucleosomal arrays making up the 10 nm fiber (Figure 1.2). Intra-fiber interactions mediated by the N-terminal tail of H4 increased folding from the 10 nm fiber to the 30 nm fiber that is then stabilized by linker histones. It has been speculated that the 30 nm fiber takes on either a one-start solenoid, a two-start zig-zag, or a combination of the two structures [16-18]. Additional proteins and/or changes in ionic conditions are then required for higher order structures such as 100 nm and 200 nm complexes that form into large chromatin fibers. For the most part this still holds true, with the exception of the 30 nm fiber [19, 20]. There has been no evidence of such fibers in vivo and recently it has also been shown through SAXS and cryo-EM that both 10 nm fibers and highly condensed chromatin exist in isolated nuclei but lack the 30 nm fiber [21]. Regardless of whether a 30 nm fiber exists, there are several factors involved in nucleosome dynamics contributing to both compaction and relaxation. These factors include histone modifications, histone variants, ATP-dependent chromatin remodelers, DNA methylation, and histone chaperones. Regulation of nucleosome dynamics does not occur due to one specific factor: a combination of all of the listed factors take place simultaneously leading to specific regulation events.

Histone post-translational modifications (PTMs) play a crucial role in the regulation of nucleosome dynamics in a number of ways [22]. PTMs may have an impact on the overall net charge that can alter DNA-histone interactions or inter-nucleosomal interactions resulting in structural changes [23]. PTMs can also recruit effector proteins to facilitate and regulate processes such as transcription, replication, and repair [24]. A vast array of these chemical

modifications exist including acetylation, methylation, phosphorylation, ubiquitylation, and ADP-ribosylation that are enzymatically added and removed in a dynamic fashion [23]. The most extensively studied modifications occur on the tails of histones, primarily in the N-terminal tails [25]. Modifications such as acetylation and phosphorylation are common, altering the charge of histones, thereby disrupting histone-DNA interactions leading to a change in chromatin structure [24].

Variants of the core histones have evolved and are incorporated into nucleosomes for specialized functions regulating chromatin dynamics. Some variants exchange with pre-existing histones resulting in an altered structure of the nucleosome (open/compact chromatin) while others are specific to certain regions of the genome. Unlike canonical histones that are almost exclusively expressed during S-phase and incorporated into chromatin during replication, histone variants are replication-independent and expressed throughout the cell cycle [26]. Similarity among core histones and variants can range from highly conserved to highly divergent. Among core histones, H2A has the largest number of variants and H4 has no known variants. We primarily focused on H2A variants H2A.X and H2A.Z as they are both ubiquitously expressed. H2A.X is involved in double-strand DNA repair and has been found to impair H1 binding [27]. H2A.Z has been found to have several functions including both stabilizing and destabilizing chromatin leading to either inactive or active gene expression. It has also been found to impair H1 binding, allowing for increased accessibility for processes such as transcription [28, 29]. The diverse roles of H2A.Z are determined by specific post-translational modifications, further evidence that nucleosome dynamics is not controlled by one specific event (Reviewed in [30]). Incorporation/removal of these variant histones, from the nucleosome do not occur spontaneously, and needs to be mediated by proteins such as histone chaperones.
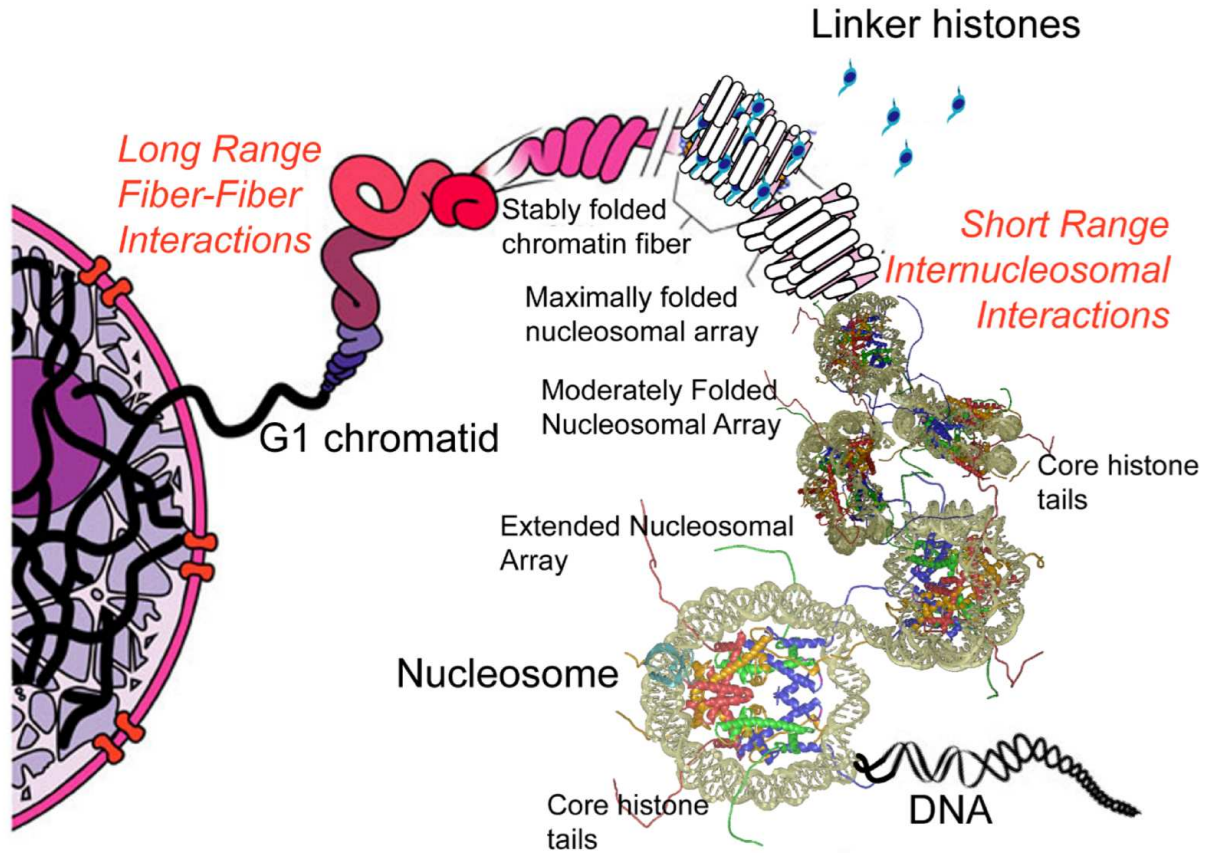
Figure 1.2. Illustration showing what was long believed to be how chromatin is organized within the nucleus of the cell. The first order of compaction begins with the DNA wrapping around the histone octamer forming the nucleosome. Linker DNA connects several nucleosomes forming arrays. These arrays are further compacted into higher order structures with linker histones such as H1 (figure taken from [4]).

1.2 - Functions of histone chaperones

In vitro, the combination of core histones with DNA at physiological salt results in aggregation rather than nucleosome assembly. Nucleosome assembly is a sequential process of two H3-H4 dimers binding to DNA resulting in the formation of tetrasomes. Two copies of H2A-H2B then bind to form the canonical nucleosome. This is accomplished in vitro by systematically lowering the ionic strength as H3-H4 binds DNA at higher ionic strength than H2A-H2B [7]. In vivo, free histones not only bind promiscuously to DNA, but also to other negatively charged cellular components such as RNA [31]. Therefore, in vivo, nucleosome assembly requires a combination of assembly factors. Evidence of this was first discovered in 1978 by Laskey et al. when they found they could not only prevent DNA-histone precipitation, but also form nucleosomes with the addition of small amounts of Xenopus egg homogenate to the DNA-histone mixture at physiological salt [32]. They identified the responsible factor as nucleoplasmin and coined the term "histone chaperone" to describe nucleoplasmin's function [8]. Currently histone chaperones are defined as a diverse family of ATP-independent proteins that facilitate nucleosome (dis)assembly by mediating histone-DNA interactions (Reviewed in [33]).

The acidic nature of histone chaperones likely facilitates their interaction with basic histones, potentially shielding it from electrostatic interactions with DNA and other acidic proteins. Within the cell, histone chaperones are involved in various steps of nucleosome assembly including shuttling histones in and out of the nucleus, histone assembly onto DNA, histone exchange, histone stability in the absence of DNA, and prevention of non-nucleosomal histone-DNA interactions that inhibit nucleosome formation [34-38]. Many histone chaperones are histone-specific, meaning they will bind only to major type histones, linker histones, or histone variants. This is not the case for the histone chaperone Nucleosome assembly protein 1 (Nap1), as it binds both major type and variant histones along with linker histone H1 with low nM affinity [1].

Nucleosomes systematically compact DNA in an ordered fashion allowing for a dynamic transition between compact chromatin (heterochromatin) and accessible chromatin (euchromatin). This dynamic behavior is critical for cellular processes such as transcription, replication, and repair as heterochromatin hinders these processes by acting as a physical barrier [39]. Histone chaperones along with ATP-dependent remodelers aid in maintaining this dynamic nature by destabilizing nucleosomes through processes such as histone variant replacement and nucleosome (dis)assembly. The mechanism of histone chaperones along with cellular regulation of histone chaperones is still poorly understood, partially due to the vast diversity among chaperones. Recent literature has implicated the charged tails of chaperones in regulating histone binding [40-42]. This is further supported by the identification of post-translational modifications that can dramatically alter the charge on the tails [43, 44]. Additionally, it has been shown that altering the chaperones' oligomeric state can correlate with different stages of nucleosome assembly. Specifically, Vps75, a histone chaperone belonging to the Nap1 family, has been shown to have altered binding sites when in different oligomeric states and is able to form multimeric complexes with H3-H4 [45, 46]. Both histone acetyltransferase Rtt109 and histone chaperone Asf1 have been shown to interact with the Vps75:H3H4 complexes, with differences in the multimeric complexes being able to directly impact post-translational modifications [45].

1.3 - The role of Nucleosome assembly protein 1 (Nap1) in histone dynamics

Nap1, originally identified in HeLa cell extracts, is a histone chaperone that is conserved among all eukaryotes from yeast to humans [47, 48]. In higher eukaryotes, there are several homologues of Nap1 (Nap1-like proteins (NAP1L1–NAP1L5) and, SET), while in yeast, Nap1 and Vps75 are the only representatives of the Nap family. Structurally, yeast Nap1 (yNap1) is a homodimer of two 48-kDa polypeptides (Figure 1.3) [48]. Each subunit contains a 47-amino acid long dimerization helix and an α-β domain [48]. A nuclear localization and export sequence occurs within the structure of Nap1 allowing histone shuttling into the nucleus and export out of the

8

nucleus [49-51]. The β-hairpin has also been shown to mediate yNap1 oligomerization, which is dependent on factors such as the ionic strength of the buffer and concentration of Nap1 [52]. Notably, Nap1 family members contain highly disordered N- and C-terminal tails that are thought to be critical for Nap1 function. The tails are unique among species in that they vary in length, sequence, and charge [53]. Post-translational modifications on the C-terminal tail, such as polyglutamylation, further alter the charge along with histone binding [43].

Dimeric yNap1 contains a negative surface on the 'underside' of the α-β domain that is responsible for histone binding; specifically it has been shown to interact with H2B [54]. Our lab has found that yNap1 also stabilizes histones H2A-H2B that otherwise fluctuate between folded and unfolded conformations when free in solution [54]. yNap1 reduced this conformational sampling by stabilizing the hydrogen bonds throughout the histone fold domains in both H2A and H2B [54]. When Nap1 is bound to H2A-H2B it blocks the H2A-H2B interface utilized in the nucleosome, suggesting that H2A-H2B interacts with Nap1 and DNA at similar contact points [54].

Processes like transcription require chromatin accessibility for the cellular machinery. In vitro, Nap1 plays an integral role in transcription by increasing accessibility through histone eviction [55], along with facilitating elongation by RNA polymerase II on chromatin templates [55]. In vivo, Nap1 prevents the formation of atypical chromatin, that is, chromatin containing excess H2A-H2B also impacting transcription. This was accomplished by creating a strain in which *nap1* was deleted resulting in increased H2A and H2B levels bound to DNA [56]. Together we conclude that Nap family members play a significant role in regulating transcription.

Aberrant gene regulation can be linked to many diseases. With histone chaperones being crucial players in proper gene regulation, it is essential to gain a full understanding of their mechanism. Although much effort has gone into characterizing histone chaperones, the mechanism of how they regulate chromatin dynamics is largely unknown. Even though Nap family

members share a conserved core region, they each have different functional roles suggesting that the core region is essential for function, but not selectivity in distinguishing the different roles [38].

There has been debate over the stoichiometry and specificity of Nap family members in complex with histones, further complicating our understanding of these chaperones mechanistically [1, 45, 57-59]. Recent evidence suggests that the interaction between histones and histone chaperones is influenced by ionic strength with different complexes forming based on the salt concentration [45, 46]. By performing in-solution assays, we functionally characterize Nap family members looking at conservation in histone binding, ionic strength-dependence, and histone assembly and disassembly, while also testing how each of these are influenced by the N- and C-terminal tails. We hope our characterization of Nap family members will provide insight into chromatin regulation along with providing a framework for the investigation of other histone chaperones.
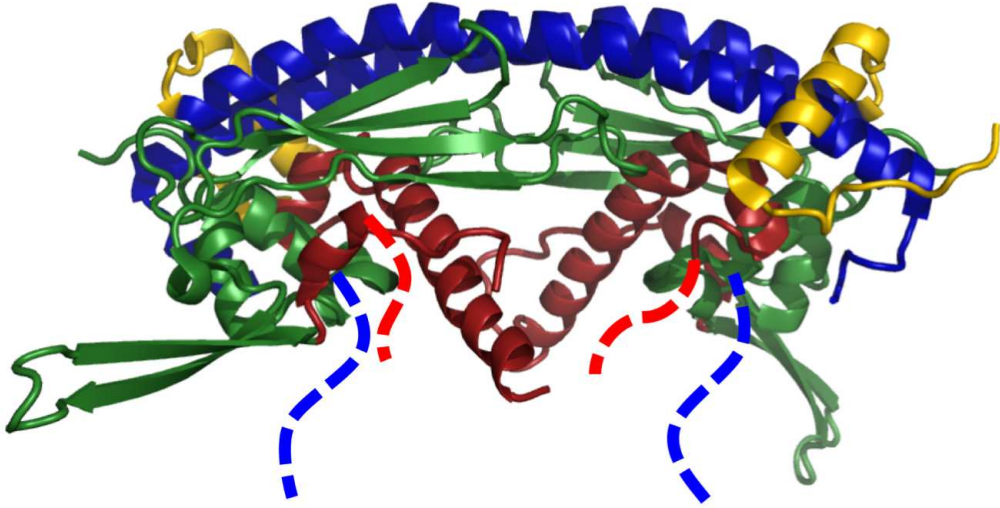
Figure 1.3. Structure of yNap1(PDB ID 2Z2R) solved at 3.2Å. yNap1 exhibits a domed shape architecture composed of long dimerization helices and α/β domains. The N- and C-terminal tails (blue and red dashes) lie on the underside of the α/β domains where histones interact.

Chapter 2 – Mechanistic Insight into the Tails of Nucleosome Assembly Protein 1

2.1 - Summary

Nap1 is a histone chaperone implicated in histone homeostasis, nucleosome formation and gene regulation. Nap1 is a homo-dimer with disordered N- and C-terminal tails that are critical for the prevention of non-canonical histone-DNA interactions in vitro. Although Nap1 has been well characterized, the mechanistic details regarding its chaperoning function are not well defined. Using thermodynamic and biophysical techniques to dissect the mechanism of Nap1, we confirmed that the tails of Nap1 are required to sequester histones from DNA and also play a role in histone selectivity between core histones and histone variants. Specifically, due to the basic nature of histones and the highly acidic C-terminal tail of Nap1, electrostatic interactions play a significant role in histone binding. In line with this, we see diminished binding and loss of selectivity when the C-terminal tail of Nap1 is removed. The C-terminal tail also contributes to the prevention of non-canonical histone-DNA interactions. Lastly, using analytical ultracentrifugation we monitored the ability of Nap1 to prevent histone:DNA aggregation and found that addition of H3-H4 to DNA at low ionic strength resulted in aggregation, which is prevented through the addition of Nap1.

2.2 - Introduction

Eukaryotes have a very complex system for packaging vast amounts of DNA into the nucleus. To accomplish this, the DNA is first wrapped ~1.65 turns around a histone octamer forming the nucleosome core particle [5]. Thousands of nucleosome core particles, connected by 10 – 70 bp of linker DNA, make up a nucleosome array that further compacts to form chromatin fibers, chains of ~100,000 nucleosomes at concentrations exceeding 200 mg/mL within the

12

nucleus of the cell [14]. Nucleosome assembly is a sequential process in which the H3-H4 tetramer must first bind the DNA forming a tetrasome, which is then flanked by two copies of H2A-H2B forming the canonical nucleosome. In vitro, this process is accomplished by mixing DNA and histones at high salt, followed by systematically reducing the ionic strength. H3-H4 binds DNA at higher ionic strengths than H2A-H2B, ensuring the sequential deposition of histones [7]. When histones are added to DNA at low ionic strength, non-specific electrostatic interactions can lead to non-nucleosomal histone-DNA complexes along with aggregation, both of which inhibit nucleosome formation [7]. The cell employs histone chaperones to aid in the assembly of nucleosomes by promoting proper histone assembly and eliminating non-nucleosomal histone-DNA interactions [36, 60]. Critical biological processes, such as DNA replication, repair, and transcription, are all dependent on histone chaperones [34]. The acidic nature of histone chaperones likely assists their interaction with basic histones, potentially shielding electrostatic interactions with DNA and other acidic proteins. While it has been reported that certain histone chaperones are specific to either H2A-H2B, H3-H4 or linker histone H1, the histone chaperone Nucleosome assembly protein 1 (Nap1) binds both core histones and linker histone H1 with low nM affinity [1].

Nap1 is conserved among all eukaryotes, from yeast to humans. In higher eukaryotes, there are several homologues of Nap1, including SET and five Nap1-like proteins. Yeast Nap1 (yNap1) is a homodimer of two 48-kDa polypeptides [48]. The Nap1 monomer contains a 47-amino acid long dimerization helix and an α-β domain [48]. Notably, Nap1 family members contain highly disordered N- and C-terminal tails required for Nap1 function with the mechanism being unknown [36]. Although the core region of Nap members is conserved, the tails deviate in both length and amino acid composition [53]. Dimeric yNap1 contains a negative surface on the 'underside' of the α-β domain that is responsible for histone binding [54, 57]. Within the structure of yNap1 there is also a β-hairpin that contains a nuclear localization sequence [51, 52, 61], allowing Nap1 to shuttle histones from the cytoplasm to the nucleus [49]. The β-hairpin has also

been shown to mediate oligomerization that is also dependent on experimental conditions such as ionic strength and concentration [52, 62].

Although there is a great deal of structural information for Nap1 (and family members), the mechanistic details of how Nap1 binds histones remains unclear. Specifically, conflicting information regarding the stoichiometry the complex formed between Nap1 and histones. It has been suggested that each yNap1 monomer can recognize the histone fold; therefore a yNap1 dimer binds two histone dimers [1, 59]. Similar binding affinities between Nap1 and major type histones or histone variants supported the notion that Nap1 recognizes the conserved histone fold [1]. Using hydrogen/deuterium exchange coupled with mass spectrometry (H/DX-MS) it was observed that H2A-H2B fluctuates between partially folded and unfolded conformations until bound by yNap1 [54]. Two copies of yNap1 in complex with H2A-H2B formed a tetrameric complex causing reduced conformational sampling of H2A-H2B by stabilizing the hydrogen bonds throughout the histone fold domains in both H2A and H2B [1, 54]. This stoichiometry has recently been challenged by a recent low resolution crystal structure indicating that one yNap1 dimer binds one H2A-H2B heterodimer [57]. Thus there is conflicting information about the Nap1:histone interaction that needs to be addressed.

Our lab has shown yNap1 has the ability to bind all core histones and linker histones with low nanomolar affinity, but how it discriminates between the different histones such as H2A-H2B and H3_H4 is still unknown [1, 59]. Andrews et al. found that one of the many roles of yNap1 was to promote nucleosome assembly by eliminating non-nucleosomal (H2A-H2B)-DNA interactions [60]. Further evidence for this role was found using magnetic tweezers. DNA length was monitored during the addition of pre-incubated Nap1-(H2A-H2B) or Nap1-(H3-H4) [63]. The length of DNA remained constant with the addition of Nap1-(H2A-H2B), but decreased with the addition of Nap1-(H3-H4) indicating Nap1 prevents non-nucleosomal (H2A-H2B)-DNA interactions while also depositing H3-H4 [63]. In yeast, deletion of Nap1 leads to aberrant transcription and the formation of non-nucleosomal H2A-H2B•DNA complexes [60].

In humans, Nap1 regulates CENP-B binding by eliminating non-specific CENP-B – nucleosome binding while stimulating CENP-B binding to CENP-A nucleosomes [64]. Another example of a histone chaperone not belonging to the Nap family is Anp32e, a histone chaperone specific for H2AZ. Anp32e also prevents non-nucleosomal interactions by inhibiting the formation of H2AZ-H2B interactions with 601-DNA [65]. In contrast, Anp32a failed to remove the same interactions, indicating that this is not a function of all histone chaperones [65]. Mechanistically there is still much to learn about the various functions of Nap family members such as how do the tails aid in overall Nap function, how does Nap discriminate among histones, and how does the cell regulate histone chaperones?

2.3 - Materials and Methods

2.3.1 - Reagents

Saccharomyces cerevisiae Nap1 and Nap1 tail truncations were expressed and purified as previously described McBryant, Park et al. 2003), with the exception they were from the pHAT4 plasmid. Additionally, all constructs contained mutations D201C, C200A, C249A, C272A, C414A to facilitate labeling. The tail truncations of yNap1 consist of ΔN (encompassing amino acids 74-417), ΔC (1-365), ΔNΔC (74-365), and C-terminal truncations (1-375, 1-385, and 1-395). TEV protease was used to cleave histidine tags from Nap constructs before purification using Mono-Q. Binding assays with H2A-H2B were conducted with and without the histidine tag on yNap1 to determine the impact on binding. *Xenopus laevis* H2A-H2B$_{T112C}$, *Xenopus laevis* H2A-H2B, *Xenopus laevis* H3-H4$_{E63C}$ along with H2A variants were expressed and purified as described previously [66, 67]. All DNA sequences used are based on the "601" nucleosome positioning sequence [68]. 601-207, 601-207x3, and 601-207x12 were prepared as previously described [4, 69] with the exception of 207x12 being purified over the Mono-Q column after digestion in place of size exclusion to purify the 207x12 fragment from digestion enzymes and digested DNA fragments.

2.3.2 - High-Throughput Interactions by Fluorescent Intensity (HI-FI)

FRET assays were conducted in a 396-well plate as described previously [70]. The donor, $H2B_{T112C}$ or $H4_{E63C}$ was labeled with Alexa 488 using a maleimide linkage following the manufacturer's protocol, prior to refolding with H2A or H3. The acceptor, yNap1, was labeled with Atto 647N using a maleimide linkage following the manufacturer's protocol. Excess dye for H2A-H2B, H3-H4, and yNap1 was removed by dialysis followed by buffer exchange over a PD10 column. The final reaction buffer was 20 mM Tris-HCl pH 7.5, 5% (v/v) glycerol, 0.01% (v/v) NP40, 0.01% (v/v) CHAPS, 1 mM DTT, 1 mM EDTA pH 8.0, and 150, 225, 300, 375, or 450 mM NaCl with the final reaction volume being 40 µl. The labeled probe, 488-H2A-H2B or 488-H3-H4 was kept at constant concentration of 1nM while the acceptor, yNap1, was titrated in up to 2 µM. Duplicates were performed for each point in the reaction with control titrations containing only labeled donor or labeled accepter being used to correct for donor bleed-through and direct excitation producing $F_{corrected}$. Samples were pipetted into a microplate and scanned using a Typhoon 8600 variable mode fluorescent imager. Three scans were performed: (Ex./Em.); 488/520 nm – donor only, 633/670 nm – acceptor only, and 488/670 nm - FRET. Fluorescence was quantified using the program ImageQuant TL and the data were analyzed using non-linear regression and fit with GraphPad Prism.

2.3.3 - Electrophoretic mobility shift assays

EMSAs were performed to determine the role of the tails of yNap1 in removing H2A-H2B from DNA. Increasing amounts of yNap1 (0.5X – 10X molar excess to H2A-H2B) was added to equilibrated 601-207 DNA (0.75 µM) with H2A-H2B (1.5 µM). These were mixed in a final buffer containing 20 mM Tris-HCl, pH 7.5, 200 mM NaCl and 1 mM EDTA. Reactions were incubated at 25°C for 15 min and then separated on using 5% native-PAGE running at 150 volts, 4°C, for 60 min. DNA was then visualized with EtBr staining and UV.

16

2.3.4 - Tetrasome and nucleosome assembly

Tetrasomes and trimer tetrasomes were assembled with *Xenopus laevis* H3-H4 onto either 601-207 or 601-207x3 (621bp) by systematically lowering the ionic strength as previously described [4]. Nucleosomes were assembled in the same manner using purified *Xenopus laevis* octamer. The final assembled tetrasomes/nucleosomes were checked for saturation using EcoRI digestion and analytical ultracentrifugation [69]. Trimer tetrasomes assembly was performed by Uma Muthurajan.

2.3.5 - yNap1 histidine tag binding assay

Taking advantage of the histidine tag, 7-fold molar excess yNap1 (WT and tailless) to H2A-H2B was added to equilibrated nucleosomal arrays (0.10 uM) with or without 5X molar excess H2A-H2B. For controls, yNap1, arrays, and arrays containing excess H2A-H2B were also analyzed individually, showing that signal can only come from the presence of DNA. The reactions were performed in buffer containing 150 mM NaCl, 0.1 mg/mL BSA, 10 mM imidazole, and 20 mM Tris-HCL pH 7.5. The samples were loaded onto nickel resin and allowed to incubate for 1 hour. The nickel resin was washed with buffer containing 150 mM NaCl, 0.1 mg/mL BSA, 20 mM imidazole, and 20 mM Tris-HCL pH 7.5. Samples were separated on a 1% agarose gel running at 50V, 25°C, 60 min. The DNA was then stained with SYBR Gold and visualized using UV. The visualization of nucleosomal arrays, arrays with H2A-H2B, and arrays with yNap1 confirmed the arrays did not bind to the nickel column nor yNap1. The samples were then eluted from the nickel beads with buffer containing 150 mM NaCl, 0.1 mg/mL BSA, 500 mM imidazole, and 20 mM Tris-HCL pH 7.5. Samples were separated on a 1% agarose gel running at 50V, 25°C, 60 min. The DNA was stained with SYBR Gold and visualized using UV.

2.3.6 - *Sedimentation velocity analytical ultracentrifugation*

Sedimentation velocity analytical ultracentrifugation (SV-AUC) experiments were performed using a Beckman Coulter Optima XL-I or XL-A analytical ultracentrifuge equipped with an optional Aviv fluorescence detection system (FDS) using either an An50Ti or An60Ti rotor (Beckman Coulter) with standard epon 2-channel centerpiece cells. Samples were diluted to desired concentrations ranging from ~0.2 – ~0.5 OD (absorbance). Alexa 488 labeled samples were set to 1 nM concentration (fluorescence). Sedimentation was then monitored using either the absorbance optics (intensity mode at 260 or 280 nm) or fluorescence optics (emission 488, excitation >505 nm) at 20°C using speeds ranging from 20,000 RPM to 45,000 RPM depending on the sample and rotors used. Partial specific volumes of sample were determined using UltraScan 3 version 2.0. Time invariant and radial invariant noise was subtracted from the sedimentation velocity data by 2-dimensional-spectrum analysis (2DSA) followed by genetic algorithm refinement and Monte Carlo analysis [71-73]. Sedimentation coefficient distributions G(s) were obtained with enhanced van Holde-Weischet analysis [74]. Relative molecular masses (M_r) for self-associating samples were improved upon by also using parametrically constrained spectrum analysis [75]. Calculations were performed on the UltraScan LIMS cluster at the Bioinformatics Core Facility at the University of Texas Health Science Center at San Antonio and the Lonestar cluster at the Texas Advanced Computing Center supported by NSF Teragrid Grant #MCB070038.

2.4 - Results

2.4.1 - *The tails of Nap1 contribute to histone selectivity*

The core region of yNap1, lacking both the N- and C-terminal tails, is sufficient for histone binding [1, 36]. It is unknown however how the length and charge of the tails contribute to both binding and mediating histone-DNA interactions, specifically discriminating between core

18

histones and histone variants. Using an assay developed in our lab, high-throughput interactions by fluorescent intensity (HI-FI) [70], binding affinities between yNap1 and histones were measured. Consistent with our previously published results where (de)quenching was used instead of FRET, we found that yNap1 WT binds H2A-H2B with low nM affinity (Figure 2.1A, Table 2.1) [1]. We then focused on the contribution of yNap1 tails by removing either the N-terminal tail (ΔN), the C-terminal tail (ΔC), or both tails (ΔNΔC). We observed a ~15-fold reduction in the binding affinity for H2A-H2B when both the N- and C-terminal tails of yNap1 were removed (Figure 2.2). Removal of just the N-terminal tail (ΔN) had little impact, as binding was similar to that of WT. Surprisingly, removal of just the C-terminal tail of yNap1 (ΔC) resulted in ~27 fold weaker H2A-H2B binding compared to WT, and ~2 fold weaker than what was observed upon removal of both tails (ΔNΔC). This was unexpected because it was in disagreement with our previous results, likely due to different methods used. The previous method did not allow for equilibration as measurements were taken in short time frames [1, 60]. We also investigated whether the tails had similar effects on the H3-H4 interaction (Figure 2.1B, Table 2.1). Consistent with what was observed for H2A-H2B, we observed similar binding when the N-terminal tail was removed. yNap1 ΔC exhibits weaker binding than when both tails were removed, indicating the N-terminal tail acts as an antagonist for histone binding.

We next investigated the role of Nap1 tails in histone selectivity. Previously published GST pull-down assays with purified proteins reported that yNap1 preferentially binds H3-H4 tetramer over H2A-H2B dimer [59]. This is consistent with yNap1 recognizing the histone fold as they calculated H3-H4 concentration as a tetramer and H2A-H2B as a dimer giving H3-H4 twice the number of histone folds. This was challenged using both in vitro and in vivo techniques where this preferential binding was not observed [36, 60]. The discrepancy is likely due to the high concentrations of protein required to visualize gel shift and pull-down assays making accurate quantification difficult. Therefore, we decided to revisit this along with what, if any, impact the tails of yNap1 have on selectivity using our HIFI assay. The use of fluorescent tags allows for increased

sensitivity making it ideal for determination of low nanomolar dissociation constants [70]. Using

the binding affinities from Table 2.1, we calculated the difference in free energy ($\Delta\Delta G^{o}_{H3-H4/H2A-H2B}$)

between histones H3-H4 and H2A-H2B with yNap1 (Figure 2.2A). We observed preferential

binding with H2A-H2B over H3-H4 by ~1.3 kcal/mol. Removal of the C-terminal tail, consisting of

52 acidic residues, had the biggest impact on selectivity indicating electrostatic interactions could

be one of the mechanisms for selectivity. The exact role of the N-terminal tail containing 9 acidic

and 7 basic residues ($pI_{\Delta N}$ - 4.18 vs WT pI_{WT} – 4.24) still remains inconclusive. We observed

minimal change in selectivity when removing the N-terminal tail, consistent with the notion that

electrostatics play a role in selectivity as the overall charge of yNap1 ΔN is similar to yNap1 WT

(Table 2.3).

Andrews et al. observed nanomolar binding affinities between major type histones and

histone variants suggesting yNap1 recognizes the histone fold within the heterodimers, which was

further supported by hydrogen-deuterium exchange [1, 54]. Using the previously described

approach, we investigated whether the tails functioned in histone selectivity as Andrew's has

shown variability among H2A-H2B variants [1]. We found that WT yNap1 favored H2A-H2B over

variants H2A.Z-H2B and H2A.X-H2B as it bound ~2-3 times tighter (Table 2.1). We next

compared the variants with H3-H4 to determine if yNap1 favored major type histones over

variants. Although we found both WT yNap1 and tailless yNap1 favored the H2A variants over

H3-H4, the difference between the variants and H3-H4 was less substantial when compared to

WT, which supports our hypothesis that the core domain is responsible for binding histones while

the tails function in histone selectivity (Figure 2.2B & C).
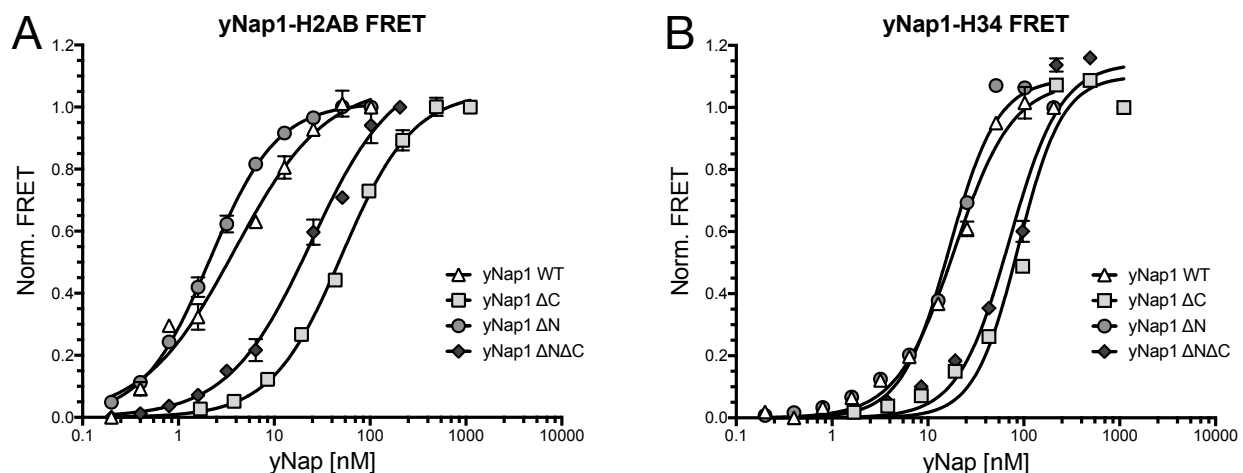
Figure 2.1. The tails of yNap1 impact histone binding. Normalized fluorescence as a function of yNap1 WT (triangles), C-terminal deletion of yNap1 (squares), N-terminal deletion of yNap1 (circles), and N- and C-terminal deletions of yNap1 (diamonds) binding histones H2A-H2B **(A)** or H3-H4 **(B)** at 0.32M ionic strength. Apparent dissociation constants were determined through GraphPad Prism and listed in Table 2.1. Error bars arise from number of replicates listed in Table 2.1.

TABLE 2.1. yNap1-histone binding affinities. Values of the measured disassociation constants calculated for yNap1 binding both core histones and H2A variants at 0.32 M ionic strength. Standard deviations were calculated using the number of replicates (n).

yNap1 construct	H2A-H2B K_D (nM) n = # of replicates	$(H3-H4)_2$ K_D (nM) n = # of replicates	H2A.X-H2B K_D (nM) n = # of replicates	H2A.Z-H2B K_D (nM) n = # of replicates
yNap1 FL	2.01 ± 0.94 n= 3	18.65 ± 0.45 n= 3	5.98 ± 2.62 n= 2	4.04 ± 1.15 n= 4
yNap1 ΔN	1.97 ± 0.38 n= 3	16.66 ± 0.11 n= 2	N/A	N/A
yNap1 ΔC	54.51 ± 3.67 n= 3	95.65 ± 11.11 n= 2	N/A	N/A
yNap1 ΔNΔC	30.64 ± 0.69 n= 3	69.26 ± 2.09 n= 3	42.11 ± 7.30 n= 3	62.83 ± 14.70 n= 3

21

2.4.2 - The tails of Nap1 modulate histone binding through ionic interactions

Expanding on our hypothesis that electrostatic interactions play a critical role in histone selectivity, we measured the ionic contribution in the yNap1-H2A-H2B interaction by determining the apparent K_D as a function of ionic strength. Plotting the log K_D vs log NaCl and determining the slope reveals the ionic contribution between yNap1 and H2A-H2B (Figure 2.3, Table 2.2). Overall, we observed that yNap1 binding is inversely proportional to ionic strength (ranging from 0.81 nM at 150 mM NaCl to 42.11 nM at 450 mM NaCl), along with a correlation between the ionic contribution and the length/charge of yNap1 tails (Table 2.2). Removal of the N-terminal tail of yNap1 had minimal effect on the ionic contribution (compared to wild type) whereas removal of the C-terminal tail resulted in a decrease in the ionic contribution. This indicates the presence of ion pairs within the C-terminal-(H2A-H2B) interaction interface. At high ionic strength the ionic contribution of the C-terminal tail becomes less prevalent as we observe a 48 fold difference in binding between yNap1 WT and ΔC at 225 mM NaCl vs ~10 fold difference in binding at 375 mM NaCl. This is consistent with the notion that ionic interactions contribute significantly to the interaction between H2A-H2B and the C-terminal domain of Nap1.

The C-terminal domain contains 30 negatively charged residues spread throughout the 52 amino acid long tail. Further characterization of this tail was performed to determine how reduction in the charge could impact histone binding, by measuring affinities of yNap1 tail truncations to H2A-H2B. Binding affinities for WT yNap1-(H2A-H2B) and C-terminal truncations of yNap1-(H2A-H2B) were measured at varying ionic strengths enabling us to calculate the difference in free energy ($\Delta\Delta G^{o}_{Mut/WT}$) (Figure 2.4, Table 2.3). $\Delta\Delta G^{o}$ values provide insight into the stability of the yNap1-H2A-H2B interaction using the various tail truncations. Specifically, we can determine the difference in energy required ($\Delta\Delta G^{o}_{Mut/WT}$) between WT yNap1 and the tail truncations of yNap1
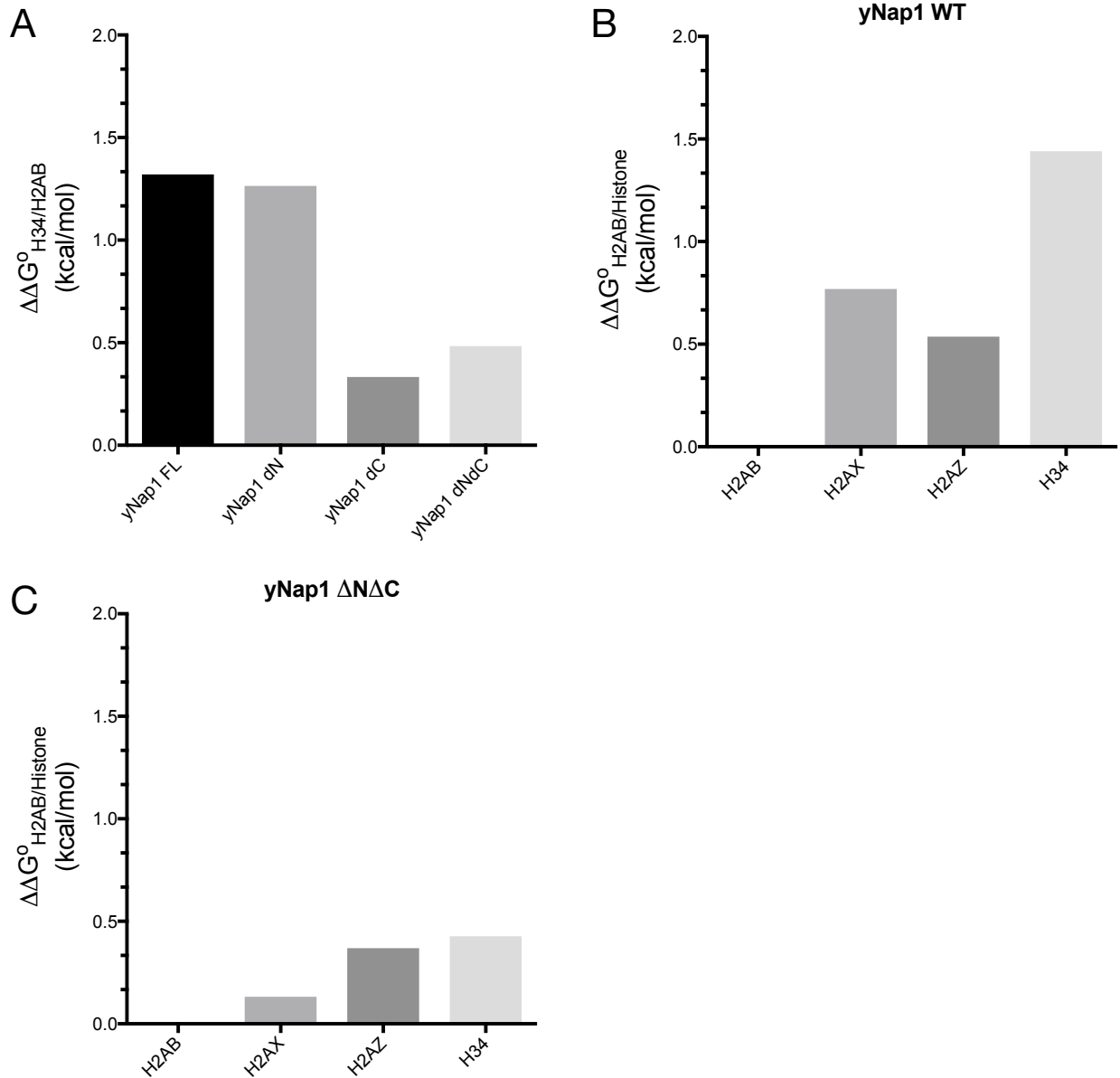
Figure 2.2. Change in free energy (ΔΔG°) indicates the tails of yNap1 impact histone selectivity. ΔΔG° values were calculated for WT yNap1 and yNap1 tail constructs to determine histone selectivity between **A)** H2A-H2B and H3-H4, **B & C)** H2A-H2B and H2A histone variants. **A)** ΔΔG° values indicate H2A-H2B is the preferential binding partner of yNap1 that is independent of the tail contribution. **B)** ΔΔG° values indicate canonical H2A-H2B is preferred over H2A variants and H3-H4. **C)** ΔΔG° values indicate when the tails of yNap1 are removed the energy difference is less substantial suggesting the tails impact histone selectivity.
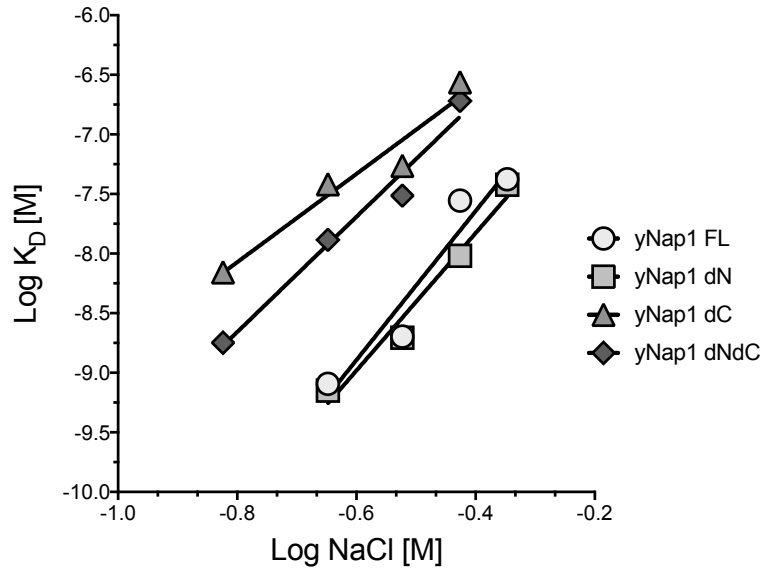
Figure 2.3. Characterization of ionic contribution between yNap1 and H2A-H2B.
Plot showing the Log (K_D) as a function of ionic strength (log NaCl) between yNap1 and H2A-H2B. The slope reveals the ionic contribution between highly acidic yNap1 and basic H2A-H2B. Deletion of the tails resulted in loss of ionic contribution indicating the interaction relies on electrostatic interactions.

TABLE 2.2. yNap1-Histone binding affinities and ionic contribution. Observed apparent dissociation constants for tail deletions of yNap1 and H2A-H2B along with the calculated ionic contribution from Figure 2.3 are shown here.

NaCl (mM)	yNap1 FL K_D (nM) n = # of replicates	yNap1 ΔN K_D (nM) n = # of replicates	yNap1 ΔC K_D (nM) n = # of replicates	yNap1 ΔNΔC K_D (nM) n = # of replicates
150	n/a	n/a	6.95 ± 0.72 n = 4	1.79 ± 0.16 n = 3
225	0.81 ± 0.13 n = 4	0.71 ± 0.25 n = 5	38.13 ± 7.45 n = 3	13.04 ± 1.92 n = 3
300	2.01 ± 0.94 n = 3	1.97 ± 0.38 n = 3	54.51 ± 3.67 n = 3	30.64 ± 0.69 n = 3
375	27.81 ± 6.08 n = 3	9.60 ± 0.78 n = 2	273.80 ± 45.22 n = 5	191.00 ± 8.55 n = 3
450	42.11 ± 8.34 n = 2	37.79 ± 3.71 n = 4	n/a	n/a
Ionic contribution	6.25 ± 1.25	5.77 ± 0.71	3.70 ± 0.63	4.83 ± 0.57

Table 2.3. Comparison of change in free energy ($\Delta\Delta G^{o}$) between WT yNap1 and C-terminal tail truncations when bound to H2A-H2B.

	yNap1 WT	yNap1 ΔNΔC $\Delta\Delta G^{o}$ (kcal/mol)	yNap1 ΔN $\Delta\Delta G^{o}$ (kcal/mol)	yNap1 ΔC $\Delta\Delta G^{o}$ (kcal/mol)	yNap1 1-375 $\Delta\Delta G^{o}$ (kcal/mol)	yNap1 1-385 $\Delta\Delta G^{o}$ (kcal/mol)	yNap1 1-395 $\Delta\Delta G^{o}$ (kcal/mol)
# of acidic C-terminal amino acids	52	0	30	0	8	17	23
# of C-terminal amino acids removed	0	52	0	52	42	32	22
Isoelectric Point (pI)	4.24	4.49	4.18	4.54	4.43	4.32	4.26
225 mM NaCl	N/A	1.65	-0.08	2.28	0.76	0.16	0.12
300 mM NaCl	N/A	1.77	-0.01	1.95	0.80	0.22	-0.02
375 mM NaCl	N/A	1.14	-0.63	1.35	0.41	-0.42	-0.25

when binding histones. A positive $\Delta\Delta G^o_{Mut/WT}$ value indicates that the tail truncations of yNap1 are less favorable to bind histones than WT, whereas a negative $\Delta\Delta G^o_{Mut/WT}$ value indicates that the tail truncations are more favorable to bind histones (Figure 2.4B). The positive change in energy led us to conclude that as the highly acidic C-terminal tail of yNap1 is shortened (thereby reducing charge), binding to histones becomes less favorable. Furthermore, we conclude that the C-terminal domain must contain at least 17 of the 30 negative amino acids before H2A-H2B binding is significantly impacted (Figure 2.4B, Table 2.3). Increasing ionic strength reduces the overall difference in free energy indicating the charged residues impact histone binding more than overall tail length (Table 2.3).

2.4.3 - Oligomeric states of Nap1 are impacted by N- and C-terminal tails

Previous studies have shown that yNap1 self-associates into higher order complexes at low ionic strength due to β-hairpin interactions between yNap1 dimers [52, 57, 62, 76]. Using analytical ultracentrifugation (AUC), we investigated other factors that might impact yNap1 oligomerization such as the charged tails and histone binding. Through fluorescent assays and H-D exchange, our lab has shown a yNap1 dimer will bind two histone dimers. Other labs showed that this is dependent on the ionic strength of the solution [1, 54, 57]. AUC is ideal as it provides first-principles hydrodynamic and thermodynamic information in solution allowing us to mimic physiological ionic strengths. We specifically used sedimentation velocity (SV-AUC) coupled with 2-dimensional spectrum analysis (2DSA) incorporated into UltraScan III (Demeler , Brookes, Cao et al. 2010). Several methods have been developed to analyze sedimentation velocity data, with 2DSA being our preferred choice as it provides a high-resolution description of gross shape (determined by the frictional ratio - *f/f$_o$),* and molecular masses (accuracy dependent on partial
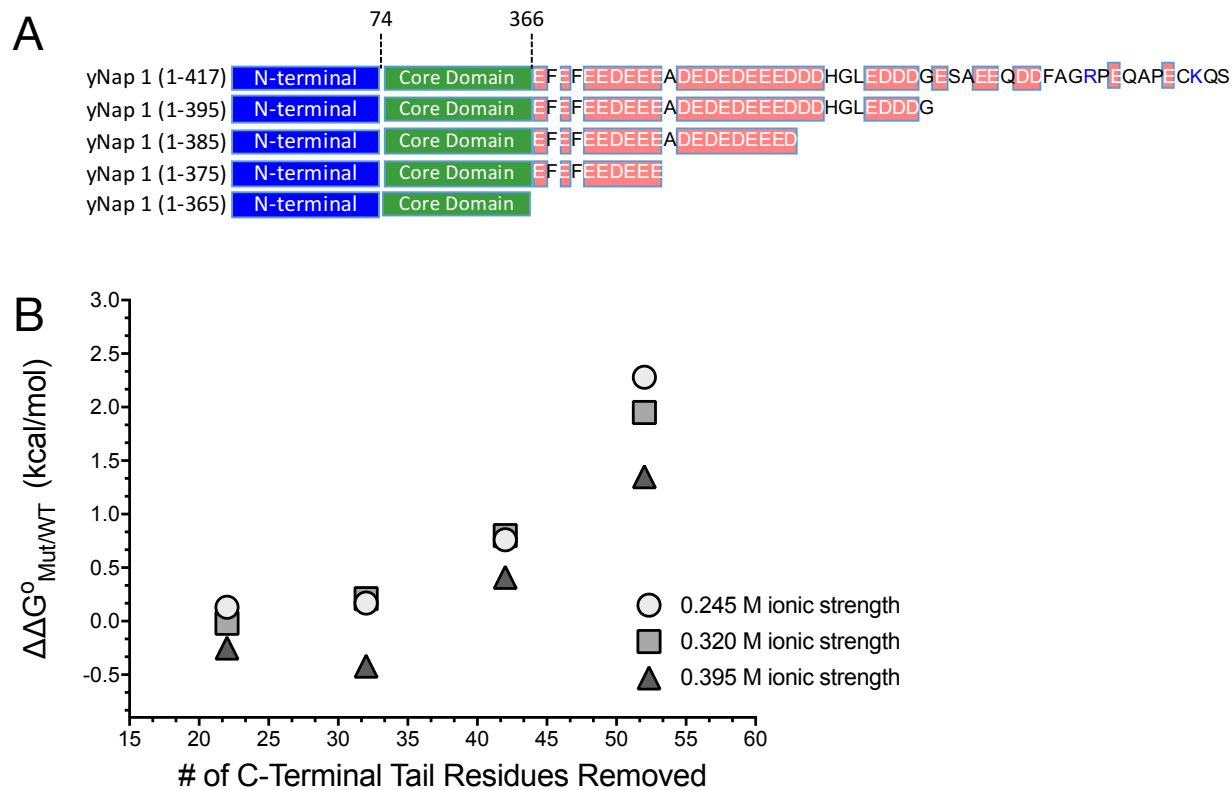
Figure 2.4. (A) Illustration showing different C-terminal tail truncations of yNap1 used, with acidic residues highlighted in **red**. **(B)** The difference in free energy between WT yNap1 and C-terminal tail truncations of yNap1 (shown above) bound to H2A-H2B was calculated at different ionic strengths to determine the impact of tail length/charge.

specific volume) for each species in the solution while also improving the accuracy of sedimentation coefficients [71, 77, 78]. Other programs such as Sedfit can be used for molecular mass determination, but its platform only allows for one frictional ratio per solution, meaning molecular mass determination for heterogeneous mixtures will be less accurate.

To determine how the tails of yNap1 along with histone binding impact oligomerization, we first confirmed the conditions that promote WT yNap1 oligomerization in the absence of histones using SV-AUC. Van Holde-Weischet results, in agreement with previously published results [62], revealed WT yNap1 sediments at ~4.5S at 0.3 M ionic strength and oligomerizes at 0.15 M ionic strength forming species that sediment at ~7.5 S (Figure 2.5A). It has been widely accepted that this 4.5S species is a homodimer, while the exact quaternary structure formed at low ionic strength still remains unclear [62]. With the high resolution analysis of 2DSA, ionic dependent quaternary structures of yNap1 can now be confirmed by molecular mass determination using sedimentation velocity [71]. Using this method, our results confirmed that WT yNap1 fluctuates between a dimeric and tetrameric species. The primary species depends on both ionic strength and concentration (Table 2.4). Although previously published results indicated that the tails of yNap1 did not impact oligomerization, our results (in agreement with the numerical values from their vHW plots) found this not to be true at low ionic strength (Compare Figure 2.5A with 2.5D) [52]. At 150 mM NaCl we observed significant oligomerization when both tails were removed, whereas removal of just the N- or C-terminal tail had minimal affect (Figure 2.5).
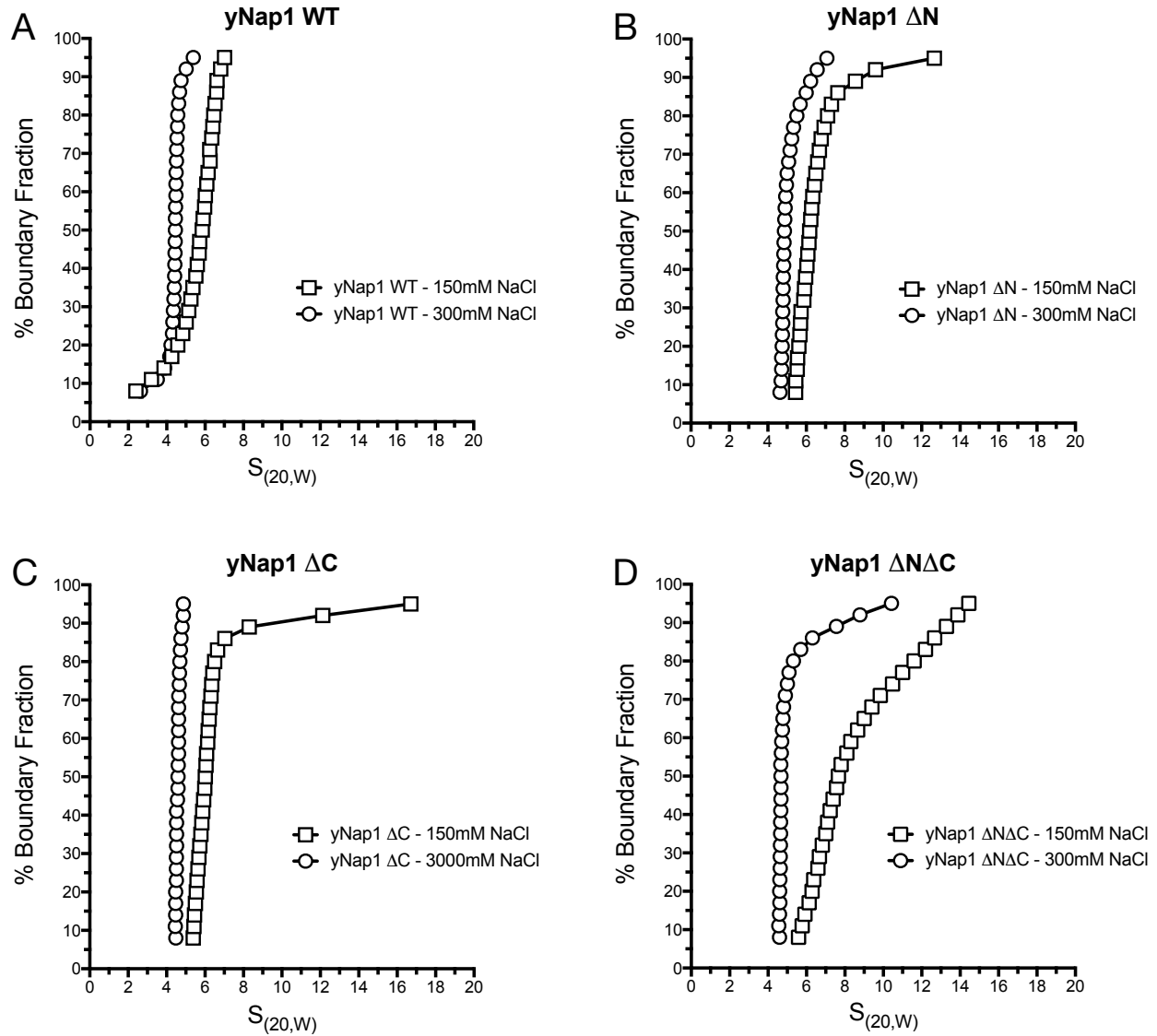
Figure 2.5. The tails of yNap1 impact self-association. Sedimentation velocity was performed at either 150 mM NaCl (squares) or 300 mM NaCl (circles) with **A)** WT yNap1, **B)** yNap1 ΔC (1-365), **C)** yNap1 ΔN (74-417), and **D)** yNap1 ΔNΔC (74-365) to determine the impact of the N- and C-terminal tails at different ionic strengths.

29

As stated previously, the exact nature of Nap1:histone complexes formed at different ionic strengths has remained somewhat a mystery [1, 57, 58]. Data exists showing both Vps75 and Xenopus laevis Nap1 will form large multimer complexes in the presence of histones, but the exact stoichiometry of these complexes is unclear, and it is unknown whether all Nap family members in various species behave in the same manner [45, 58]. Having characterized the ionic dependence of yNap1 alone, we used the same methodology to investigate how the presence of H2A-H2B impacts oligomerization of yNap1 (Figure 2.6). Addition of a 2-fold molar excess of H2A-H2B to WT yNap1 at 300 mM NaCl produced a complex that sediments at ~6.5S, with a molecular mass of ~150 kDa. With yNap1 alone having a sedimentation coefficient of 4.5, 6.5S is consistent with a complex of one yNap1 dimer bound to two H2A-H2B dimers (Figure 2.6A).

To determine if the concentration of yNap1 impacted the complexes formed with H2A-H2B, I used our optional fluorescent detection system for the AUC that allows detection of nanomolar concentrations. Keeping yNap1 constant at 1 nM we titrated H2A-H2B in 0.5, 1, 2, and 10-fold molar excess. Consistent with the absorbance data, we did not observe any component sedimenting faster than ~6.5S (Figure 2.6A).

With the tails of yNap1 impacting oligomerization (Figure 2.5), we investigated whether they also affected histone binding. Unlike WT yNap1, sub-saturating amounts of H2A-H2B (1:0.5 yNap1:H2AB) with tailless yNap1 (ΔNΔC) produced multiple species ranging from 6S to 12S (Figure 2.6B). Due to the heterogeneous nature of this complex, molecular mass determination is prone to larger errors; nevertheless, we observed species with molecular masses ranging from ~70 kDa to 195 kDa (molecular mass data not shown). These molecular masses are consistent with the presence of free yNap1 dimer along with tetrameric yNap1 binding two H2A-H2B dimers. Saturating tailless yNap1 with H2A-H2B (1:1 or 1:2 yNap1:H2AB) disrupts the tetrameric species and a complex with the same 2:2 stoichiometry as WT yNap1 is formed (Figure 2.6B, Table 2.5A).
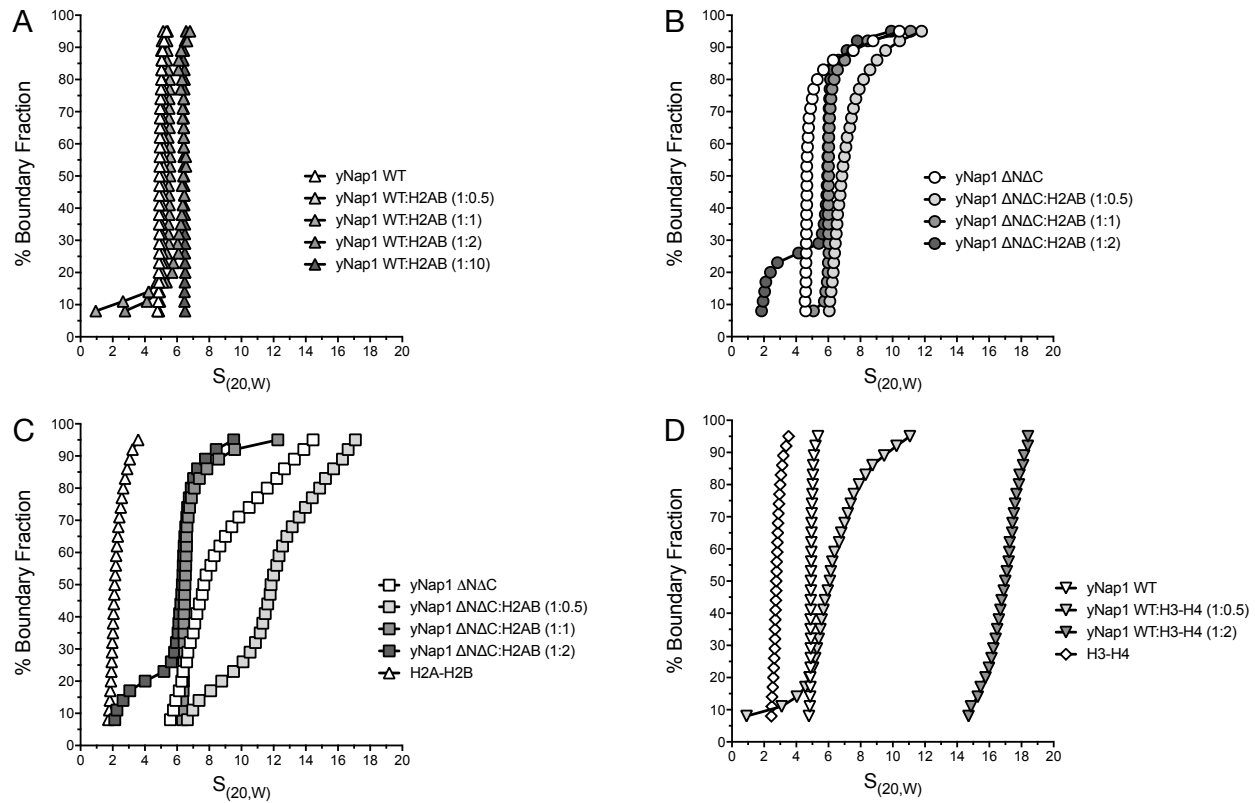
Figure 2.6. yNap1 oligomerization is dependent on histone binding. (A) Sedimentation velocity was performed using WT yNap1 (white triangles) bound to increasing amounts of H2A-H2B from 0.5 fold – 10-fold excess H2A-H2B to yNap1 (grey triangles with shade increasing with concentration) **(B, C)** Sedimentation velocity was performed using yNap1 ΔNΔC with 0-2 molar equivalents of H2A-H2B at either 150mM **(B – squares)** or 300mM NaCl **(C – circles).** yNap1 and H2A-H2B alone are shown in white while 0.5, 1, 2, and 3 molar equivalents of H2A-H2B are shown in light grey, grey, dark grey, and black. **(D)** Sedimentation velocity performed using yNap1 (white triangle) with H3-H4 (white diamond) in either 0.5-fold excess (light grey) or 2-fold excess (dark grey).

Table 2.5A. Measured and theoretical relative molecular masses (M_r) (Da) of yNap1 ΔNΔC-xH2A-H2B complexes at 300mM NaCl.

Abundance (%) and Measured M_r (Da) observed for yNap1:H2A-H2B complexes at 300 mM NaCl				
		Molar equivalents of H2A-H2B added to yNap1		
	Theoretical M_r (Da)	1X H2A-H2B (95% CI)	2X H2A-H2B (95% CI)	3X H2A-H2B (95% CI)
0:1	27928	Not Detected	21.77% - 24105 [17787 – 30422]	33.65% - 24440 [13243-35637]
2:1	95400	Not Detected	Not Detected	Not Detected
2:2	123328	72.23% - 119940 [94580-145290]	58.78% - 132420 [119520-145150]	49.37% - 132960 [111980-153940]

(yNap1:H2AB)

Table 2.5B. Measured and Theoretical relative molecular masses (M_r) (Da) of yNap1 ΔNΔC-xH2A-H2B complexes at 150mM NaCl.

Abundance (%) and Measured M_r (Da) observed for yNap1:H2A-H2B complexes at 150 mM NaCl				
		Molar equivalents of H2A-H2B added to yNap1		
	Theoretical M_r (Da)	1X H2A-H2B (95% CI)	2X H2A-H2B (95% CI)	3X H2A-H2B (95% CI)
0:1	27928	Not Detected	18.68% - 29876 [25685-34067]	30.93% - 25697 [22687-28707]
2:1	95400	Not Detected	Not Detected	Not Detected
2:2	123328	78.19% - 121590 [109030-134140]	63.65% - 129610 [124970-134260]	55.77% - 131830 [121090-142570]

(yNap1:H2AB)

This observation led us to investigate if we could produce more 4:2 yNap1:H2A-H2B species at lower ionic strengths. We found that sub-saturating amounts of H2A-H2B to tailless yNap1 at 150mM NaCl produced even larger complexes than at 300 mM NaCl (Figure 2.6C). These species had S values that ranged from ~6.5 to 21S and molecular masses that ranged from ~111 kDa to 426 kDa (Figure 2.6C). Similar to 300 mM NaCl, saturating tailless yNap1 with H2A-H2B then disrupted formation of larger complexes and bound with a 2:2 yNap1:H2A-H2B stoichiometry (Table 2.5B). Since it has been suggested that yNap1 could possibly form the same ring-like structure as xNap1 in the presence of histones, we can only assume this is also the case [58]. Saturating tailless yNap1 with histones at low ionic strength disrupts these large complexes and binds with the same 2:2 stoichiometry as both WT and tailless yNap1 at 300 mM NaCl (Figure 2.6B & C).

We then wanted to see if these larger complexes could be observed with H3-H4. Addition of saturating amounts of H3-H4 to WT yNap1 produced considerably larger complexes than H2A-H2B (Figure 2.6D). Unlike H2A-H2B, sub-saturating amounts did not produce large complexes (Figure 2.6D). We conclude that both H3-H4- and H2A-H2B-bound yNap1 can form large complexes with sedimentation coefficients similar to those previously published for Xenopus Nap1, where ring-like structures were observed that are dependent on the tails of yNap1, ionic strength, and concentration [58].

2.4.4 - The C-terminal tail of Nap1 is required for eliminating non-nucleosomal H2A-H2B interactions

H2A-H2B binds DNA with low nM affinity resulting in H2A-H2B•DNA complexes [60]. As nucleosome formation requires H3-H4 to bind the DNA first, these H2A-H2B•DNA complexes inhibit nucleosome formation while making the H2A-H2B-enriched chromatin more accessible than canonical chromatin for processes such as replication and transcription [60]. It has been previously shown that yNap1 can remove/exchange H2A-H2B from nucleosomes along with

33

preventing non-nucleosomal interactions by sequestering H2A-H2B from DNA [36, 60]. The C-terminal tail of yNap1 is required for H2A-H2B exchange/removal from nucleosomes but has yet to be investigated with regard to H2A-H2B removal from either naked DNA or linker DNA between nucleosomes [36, 60].

To begin to elucidate the role of the C-terminal tail of yNap1 in this activity we first made sure we could accurately characterize these non-nucleosomal H2A-H2B•DNA complexes by their hydrodynamic properties using sedimentation velocity. Sedimentation velocity allows us to observe how the DNA changes with respect to sedimentation and shape (f/f_o), in addition to allowing us to monitor precipitation/aggregation by measuring changes in OD. If DNA were wrapped around H2A-H2B as it does with H3-H4, we would expect to see a compacted complex compared to DNA alone, resulting in a smaller f/f_o than that observed for DNA. Likewise, if H2A-H2B linearized the DNA into rod-like structures, it could possibly be in a less compacted state than DNA alone, resulting in a larger f/f_o. We observed that the addition of H2A-H2B slightly decreased the frictional ratio and increased the sedimentation coefficient compared to DNA alone, indicating that H2A-H2B binds and compacts the DNA (Figure 2.7A, Table 2.6). We did not observe any aggregation with the addition of H2A-H2B as the OD_{260} values did not decrease. Using more physiologically relevant conditions, we also tested longer fragments of DNA in this assay. Consistent with our results using a single 207-bp repeat, increasing amounts of H2A-H2B to DNA resulted in greater sedimentation coefficients and reduced frictional ratios (Figure 2.7B, Table 2.6). These results suggest that dimer enriched DNA does not increase chromatin accessibility due to preventing compaction, but further testing using nucleosomal arrays could provide further evidence.

After characterizing the H2A-H2B•DNA interaction by sedimentation velocity, we investigated how the addition of yNap1 altered this complex. Consistent with previously published
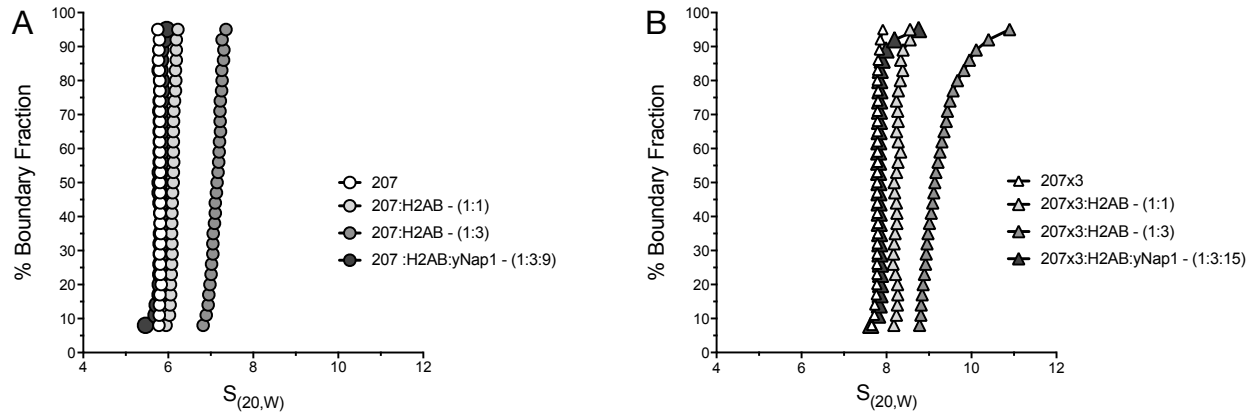
Figure 2.7. yNap1 eliminates non-nucleosomal H2A-H2B-DNA interactions. A) SV was performed to monitor the interaction between H2A-H2B and DNA using 601-207 DNA (white circles), 1 or 3-fold excess of H2A-H2B (grey circles), and 3-fold excess yNap1 (dark grey circles). This demonstrates the ability of yNap1 to remove H2A-H2B from DNA. **B)** 207x3 DNA (white triangles) was also used to determine how DNA length impacted binding with 1 or 3-fold excess H2A-H2B (grey triangles) and 5-fold excess yNap1 (dark grey triangles).

TABLE 2.6. SV was performed to determine sedimentation coefficients ($S_{20, W}$), gross shape (*f/f$_o$*), and amount of aggregation (O.D.) determined with 2DSA. 2 replicates were performed for each sample with the exception of 601-207 + 3X H2AB + yNap1.

Sample	$S_{20,W}$	f/f$_o$	OD$_{sample/DNA}$
601-207	5.73 ± 0.04	3.05 ± 0.04	1.00 ± 0.00
601-207 + 1X H2A-H2B	6.02 ± 0.05	2.82 ± 0.02	0.98 ± 0.03
601-207 + 3X H2A-H2B	6.78 ± 0.38	2.54 ± 0.08	1.00 ± 0.02
601-207 + 3X H2A-H2B + yNap1	6.05	2.80	1.02
601-207x3	8.26 ± 0.28	4.91 ± 0.16	1.00 ± 0.00
601-207x3 + 1X H2A-H2B	8.49 ± 0.05	4.07 ± 0.12	0.95 ± 0.08
601-207x3 + 3X H2A-H2B	9.85 ± 0.37	4.05 ± 0.31	0.88 ± 0.04
601-207x3 + 3X H2A-H2B + 5X yNap1	8.33 ± 0.01	4.35 ± 0.13	1.12 ± 0.20
601-207x12	11.76 ± 0.62	9.13 ± 1.24	1.00 ± 0.00
601-207x12 + 5X H2A-H2B	17.72 ± 0.48	4.21 ± 0.43	0.82 ± 0.04
601-207x12 + 5X H2A-H2B + 5X yNap1	11.57 ± 0.06	8.48 ± 0.06	1.24 ± 0.11

results, H2A-H2B sequestered by yNap1 resulted in both free DNA and yNap1-H2A-H2B complexes (Figure 2.7A & B) [60]. Previous studies have shown that removal of the tails of yNap1 eliminates the ability of yNap1 to remove/exchange H2A-H2B from nucleosomes, but whether this also applies to free DNA has yet to be determined [36]. Using electrophoretic mobility shift assays, we were able to confirm that the tails did in fact impact H2A-H2B sequestering from DNA (Figure 2.14). yNap1 WT sequestered H2A-H2B from DNA at ~1:1 yNap1-(H2A-H2B) ratio (Figure 2.14A), while removal of both the N- and C-terminal tails (yNap1 ΔNΔC), significantly altered this function (Figure 2.14B). Removal of just the N-terminal tail had little to no impact whereas removal of the C-terminal tail (yNap1 ΔC) abolished H2A-H2B removal from DNA completely (Sup. Figure 2.1C). Surprisingly, comparing yNap1 ΔC with completely tailless yNap1 (ΔNΔC) revealed that the N-terminal tail may slightly inhibit the sequestering activity, as tailless yNap1 was able to sequester H2A-H2B at high concentrations whereas yNap1 ΔC was unable to do so using the same high concentrations (Sup. Figure 2.1B & C).

To determine whether H2A-H2B binds to nucleosomal arrays, and what role yNap1 may have in resolving these interactions, we employed SV experiments to monitor both aggregation (OD$_{260}$ values) and sedimentation of 207x12mer arrays. As a control, 207x12mer DNA was also used to compare/contrast any differenced due to the presence of nucleosomes (Figure 2.8A). 207x12mer arrays consist of 12 repeats of 601-207 DNA with each repeat containing one nucleosome. Previous published results found that arrays containing 12 nucleosomes have a sedimentation coefficient of ~28S at 2.5 mM NaCl [79]. Our 207x12mer nucleosomal arrays also had a sedimentation coefficient of ~28S (Figure 2.8B), indicating their proper assembly. Addition of H2A-H2B to these nucleosomal arrays formed large complexes that sediment at ~45S. Addition of yNap1 effectively returns the array to its canonical state of ~28S (Figure 2.8 presumably by sequestering H2A-H2B, suggested by the presence of large 'tail' in the van Holde-Weischet plot in Figure 2.8B). The van Holde-Weischet analysis of

37
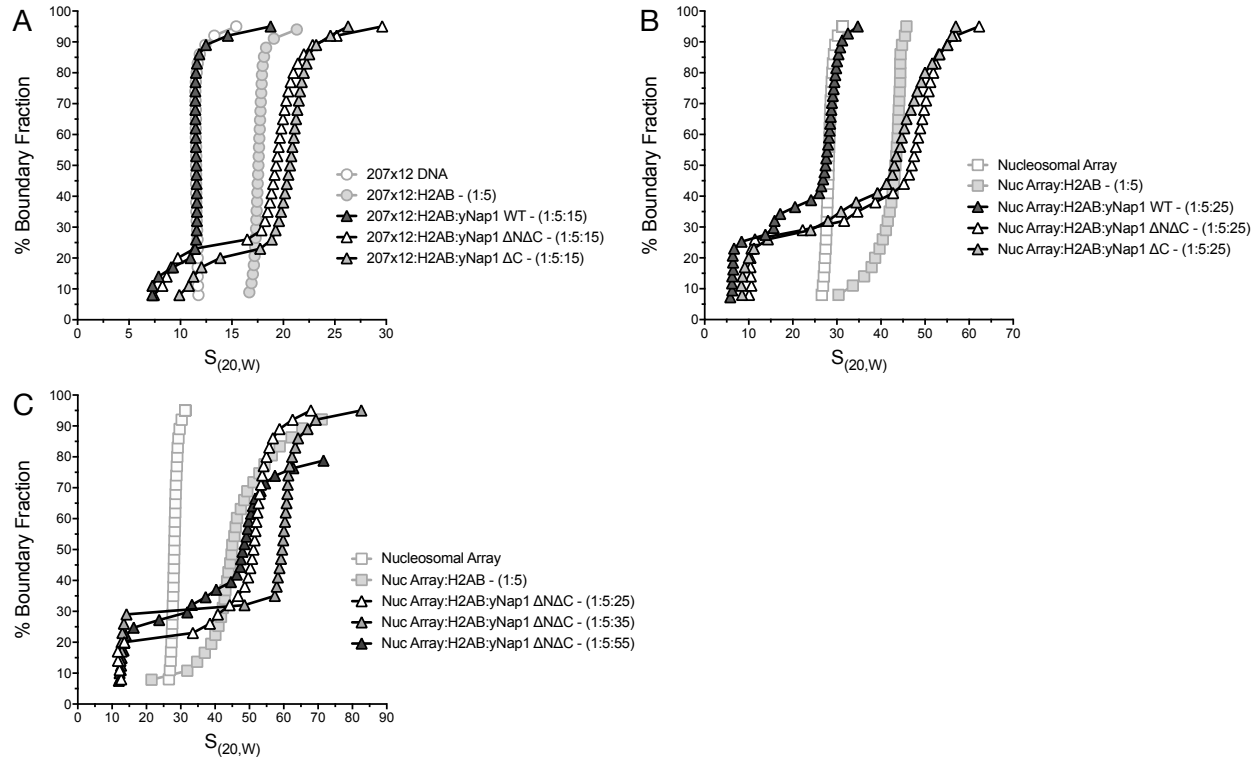
Figure 2.8. Tails of yNap1 impact the removal/prevention of H2A-H2B from both free DNA and nucleosomal arrays. A) SV was performed to monitor how the tails of yNap1 impact the interaction between H2A-H2B and 601-207x12 DNA. Unlike WT yNap1[*], removal of either the C-terminal tail or both tails abolished the ability to remove H2A-H2B from DNA. **B)** SV was performed to monitor how the tails of yNap1 impacted the removal/prevention of H2A-H2B prebound to saturated nucleosomal arrays. Addition of WT yNap1 restored the array to a native state whereas removal of either the C-terminal tail or both tails again abolished this function as was seen in **(A).** * WT yNap1 data is duplicate from figure 6B. **C)** Tailless yNap1 was added to H2A-H2B saturated arrays to determine if excess yNap1:H2A-H2B molar ratios could force H2A-H2B removal. Due to non-ideality the top 15% of 11X yNap1 was not included.

38

these arrays in the presence of H2A-H2B and yNap1 also reveals multiple components that coincide with free yNap1 and yNap1-H2A-H2B complexes (presence of tails in figure 2.8).

We have shown that the tails of yNap1, specifically the C-terminal tail, contribute to both histone binding and sequestering (Figure 2.8A, Sup Figure 2.1B and C), therefore we wanted to confirm that this holds true in the presence of nucleosomes. Using sedimentation velocity, we monitored the changes in sedimentation when tailless yNap1 was added to nucleosomal arrays with excess H2A-H2B (Figure 2.8B). Removal of both yNap1 tails resulted in larger nucleosomal array complexes when compared to WT yNap1 or the H2A-H2B saturated arrays. Since sedimentation is proportional to mass, this could indicate that tailless yNap1 either assembles more H2A-H2B histones onto the array, or that it forms a ternary complex with the H2A-H2B bound arrays. The possibility of a ternary complex was more evident as we observed an increase in sedimentation upon titrating increasing amounts of tailless yNap1 (Figure 2.8B and C).

Taking advantage of the histidine tag attached to the N-terminal tail of yNap1 for purification, we performed pull-down assays to test for the ternary complex. If yNap1 formed a ternary complex with nucleosomal arrays with excess H2A-H2B added, we would expect to see the presence of DNA after washing the samples with low concentrations of imidazole (imidazole wash will remove any non-specific binding) (Figure 2.9). We were unable to detect any significant amount of DNA when 207x12mer arrays were added to yNap1, whereas we did observe the presence of DNA when H2A-H2B was added to the arrays (Figure 2.9). This confirms that yNap1 (WT or tailless) is only able to form a complex with arrays when excess H2A-H2B is added. This is not observed with WT yNap1 in our SV-AUC experiments, suggesting that the complex could be a weak intermediate that is not observed during sedimentation velocity. This also contradicts recent work that suggested both DNA and yNap1 share the same H2A-H2B binding site [57]. If this were the case, yNap1 would bind H2A-H2B after it dissociates from DNA, thereby preventing

39
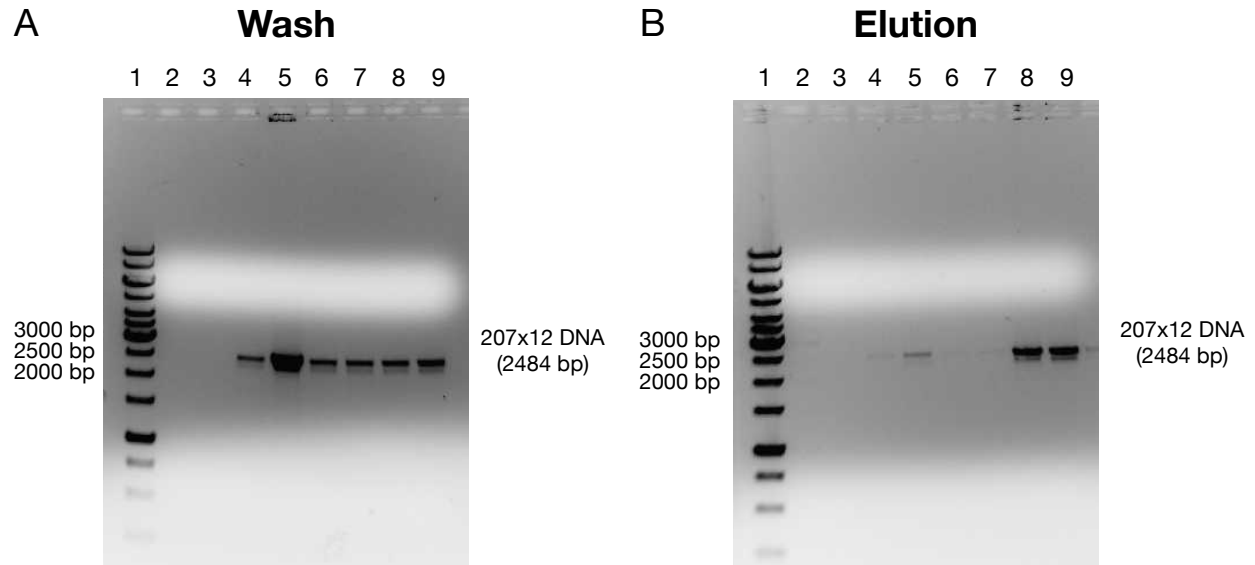
Figure 2.9. Histidine tag pull-down assay indicates that yNap1 forms a ternary complex with H2A-H2B array 1% agarose gel stained with SYBR Gold with the following in lanes 1-9: 1) 1kb ladder, 2) yNap1 WT, 3) yNap1ΔNΔC, 4) 207x12 nucleosomal array, 5) Nucleosomal array + 5X molar excess H2A-H2B, 6) Nucleosomal array + 35X yNap1 WT, 7) Nucleosomal array + 35X yNap1ΔNΔC, 8) Nucleosomal array + 5X H2A-H2B + 35X yNap1 WT (7X excess to H2A-H2B), 9) Nucleosomal array + 5X H2A-H2B + 35X yNap1 ΔNΔC. **A)** Wash step (0.02M Imidazole) for histidine tag binding assay indicates yNap1 alone does not bind 207x12 DNA as it eluted during the prewash. Histones have been shown to bind nickel columns explaining why we see increased amounts of DNA for the array with H2A-H2B vs array alone (excess H2A-H2B bound nickel blocking the array). **B)** Elution of the histidine tagged yNap1 and binding partners was accomplished by washing with 0.5M imidazole. Presence of both yNap1 WT and H2A-H2B indicate yNap1 can form a ternary complex with H2A-H2B saturated arrays.

the formation of a ternary complexes. As we observed previously (Figure 2.6) where the oligomerization state of tailless yNap1 changed when binding histones, it is possible this could hold true with H2A-H2B-saturated arrays, and might also explain the larger complexes.

2.4.5 - Nap1 aids in tetrasome assembly[1]

Nucleosome assembly begins with H3-H4 binding DNA forming a "tetrasome." Tetrasome assembly either requires H3-H4 to be reconstituted on the DNA by systematically lowering the ionic strength, or it requires the aid of histone chaperones, such as Nap1, to prevent insoluble aggregates from forming [8]. Using SV, we investigated tetrasome assembly with and without yNap1.

We first looked at how ionic strength and the number of DNA base pairs influenced tetrasome formation. Tetrasome formation requires DNA to wrap around H3-H4, therefore we hypothesize longer strands of DNA might experience unwanted electrostatic interactions making it difficult for the DNA to wrap around H3-H4. Using 601-207x3 DNA (3 repeats of 601-207), tri-tetrasomes were assembled by setting up several reactions keeping DNA constant and adding different molar ratios of H3-H4 and then systematically lowering ionic strength (Figure 2.10A) [4]. EcoRI digestion was then performed to identify potentially under assembled tri-tetrasomes (presence of free DNA - *data not shown*), followed by sedimentation velocity to determine if the tri-tetrasomes were over-assembled. Tri-tetrasomes have a sedimentation coefficient of ~16S, whereas free 207x3 DNA sediments at ~8S (Figure 2.13A). We then added increasing molar ratios of H3-H4 to DNA at 0.3 M ionic strength to determine if salt reconstitution was in fact necessary for tetrasome formation. From the integral distribution plots (G(s)) obtained from the van Holde-Weischet analysis plots we were unable to determine any substantial differences between free DNA and DNA with the addition of H3-H4 (Figure 2.10A). Since SV revealed minimal

---

[1] Tetrasome assembly via salt reconstitution was performed by Uma Muthurajan.

to no tetrasome assembly with the addition of H3-H4 to DNA at 0.3 M ionic strength (Figure 2.10A), we compared the OD_{260} values to determine if H3-H4 was causing the DNA to aggregate. Using a fixed OD_{260} of 0.4 for DNA, H3-H4 was then added at 0.5, 1, 2, 3, and 4-fold molar excess to DNA. At low molar ratios of H3-H4 to DNA we observed a minimal change in the OD_{260}, however as we titrated in higher molar ratios we began to see a decrease in OD_{260} indicating the excess H3-H4 was likely causing the DNA to aggregate (Figure 2.10B).

There have been reports of unassisted tetrasome formation when H3-H4 is added to single nucleosome repeats of DNA (146 base pairs) at low ionic strength [80]. Although we may have encountered some unassisted tetrasome formation using H3-H4 and 207x3 DNA, the vast majority did not assemble into tetrasomes. We therefore wanted to understand why tetrasome assembly requires the assistance of a histone chaperone or systematically lowering the ionic strength. To determine if assembly was prevented by an energy barrier, we added excess molar ratios of H3-H4 (1, 2, 3, 4, and 6-fold molar excess) to 601-207 DNA at 0.3 M ionic strength and performed sedimentation velocity. As we increased the molar ratio of H3-H4 to 207 DNA we observed an increase in sedimentation. This was unlike what was observed on 207x3 DNA, and indicates that tetrasome formation may have occurred, or at least H3-H4 binds and compacts the DNA similar to what occurs in tetrasomes (Figure 2.11A). In agreement with 207x3, OD_{260} values also decreased with increasing amounts of H3-H4 indicating that the presence of H3-H4 causes the DNA to aggregate (Figure 2.11B). Since H3-H4 increases sedimentation with 207 bp of DNA but not 621 bp (207x3), we conclude that the number of DNA base pairs does in fact play a role in tetrasome formation, as longer strands of DNA are less efficient in spontaneously assembling tetrasomes.

As we have previously shown, addition of H3-H4 to 207x3 DNA at 0.3 M ionic strength yielded minimal (H3-H4)-207x3 products, with the majority of the sample having the same sedimentation coefficient as 207x3 DNA. We therefore wanted to determine how binding of H3-H4 to DNA was affected at different ionic strengths. We monitored the change in sedimentation
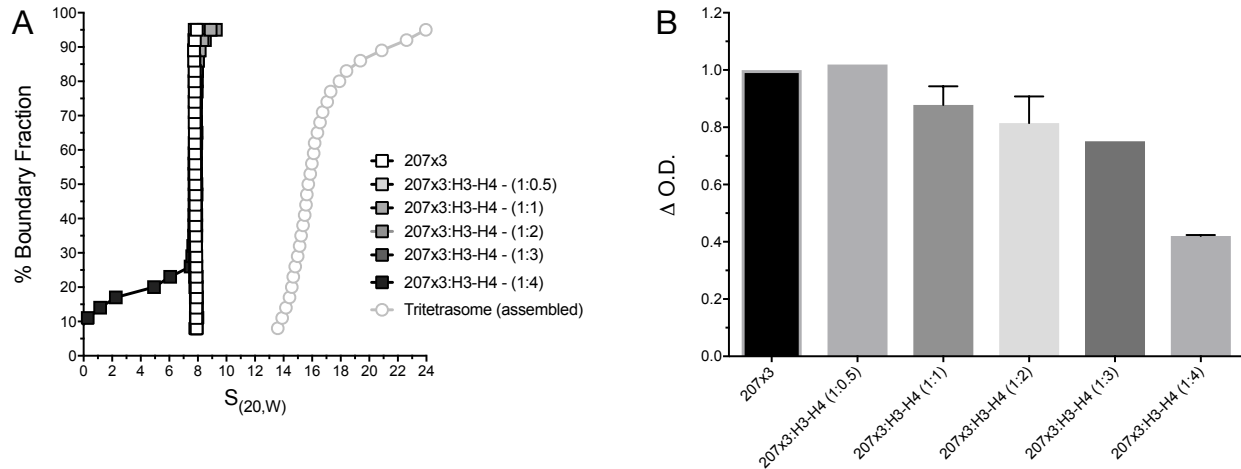
Figure 2.10. Addition of H3-H4 to 207x3 DNA at 300mM NaCl results in little binding and causes aggregation. A) H3-H4 was titrated into DNA at 300mM NaCl from 0.5X to 4X H3-H4:DNA and ran on the AUC. van Holde-Weischet analysis reveals there was minimal binding at all titrations. **B)** Addition of H3-H4 to 207x3 DNA results in decreased OD values indicating aggregation.
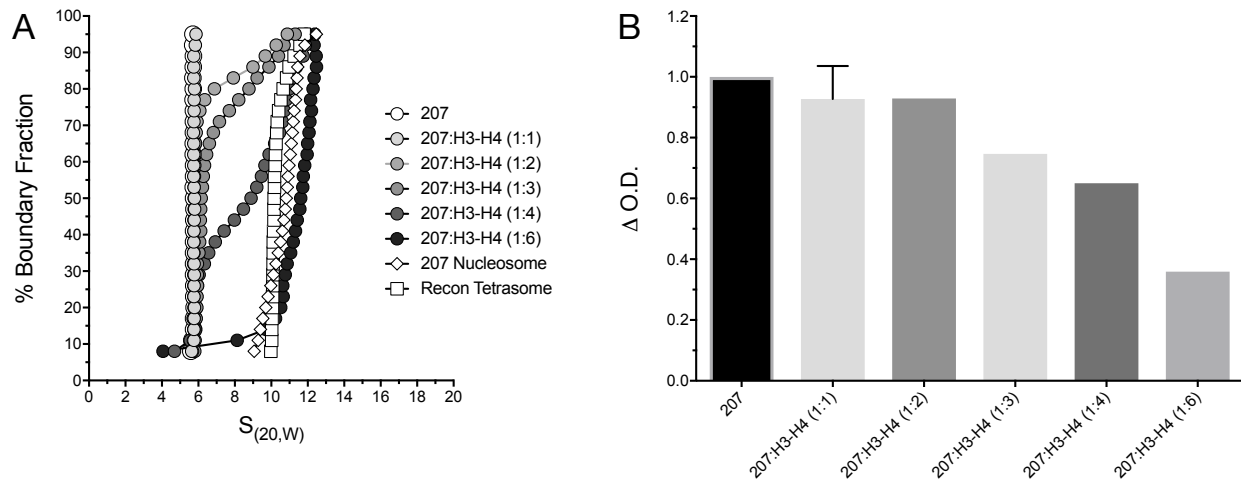
Figure 2.11. Addition of H3-H4 to 207 DNA at 300mM NaCl results in formation of multiple species. A) H3-H4 was titrated from 0.5X to 6X molar ratio into 601-207 DNA at 300mM NaCl with SV performed. We observed multiple species containing DNA and DNA:H3-H4 complexes with increasing amounts of H3-H4. **B)** AUC uses absorbance to measure sedimentation, therefore we can determine amount of aggregation based on the ratio of H3-H4:DNA/DNA control. As H3-H4 is added to the DNA, we observe a decrease in OD values indicating aggregation. *Error bars missing due to lack of replicates

when 3-fold molar excess H3-H4 per DNA repeat of 207x3 DNA was added at different ionic strengths ranging from 0.1 M to 0.6 M in 0.1 M increments. At high ionic strength, we observed increases in sedimentation along with minimal decreases in the OD_{260}. Decreasing the ionic strength resulted in decreased shifts in sedimentation along with decreased absorbance values indicating tetrasome assembly is hindered by unfavorable ionic interactions (Figure 2.12A). Since the ionic strength of the nucleus, where nucleosome formation occurs, is ~0.2 M, the cell employs histone chaperones to assist in formation by preventing these unfavorable ionic interactions. We therefore tested how yNap1 mediates the (H3-H4)-DNA interaction to form tetrasomes, the first step in nucleosome assembly. Using the same setup as above, we investigated how the addition of yNap1 impacts the H3-H4-DNA interaction when 3-fold molar excess H3-H4 was added at different ionic strengths. We found that the addition of yNap1 to H3-H4•DNA complexes resulted in H3-H4 assembly that closely resembled the integral distribution plots (G(s)) of tetrasomes obtained from salt gradient dialysis (Figure 2.13A). Unlike figure 2.12 where we observed a decrease in sedimentation with decreasing ionic strength, in the presence of yNap1 we observed an increase in sedimentation with decreasing ionic strength indicating the complex is becoming more compact.

We conclude by confirming that efficient H3-H4 assembly on DNA requires systematically lowering the ionic strength to prevent improper ionic interactions between H3-H4 and the DNA resulting (i.e. aggregation). Aggregation can also be prevented with histone chaperones such as Nap1, as it likely functions in a similar manner as salt dialysis preventing improper ionic interactions.

2.5 - Discussion

In 1978 Laskey et al. discovered that the addition of histones to DNA at low ionic strength resulted in aggregation instead of nucleosome formation due to nonspecific ionic interactions

between the highly basic histones and acidic DNA [8]. They also observed that aggregation could be reversed with the addition of an acidic protein isolated from Xenopus egg extracts. This acidic protein, Nucleoplasmin, was termed a "molecular chaperone" as it promoted nucleosome assembly by neutralizing the basic histones and preventing incorrect ionic interactions. In keeping with our previous published results, along with the original definition coined by Laskey, we have investigated how Nap1 aids in preventing ionic interactions between histones and DNA [8].

Through the use of thermodynamic assays and sedimentation velocity, we have been able to shed light on potential ways in which yNap1 aids in nucleosome assembly. yNap1 binds core histones and linker histones with low nanomolar affinity, leading to the question, can yNap1 differentiate between canonical histones and histone variants for the different cellular processes? Since Nap1 family members all consist of a conserved core region flanked by non-conserved N- and C-terminal tails with the latter being highly charged, we investigated the effect of these tails on histone binding and selectivity. We found that the highly acidic C-terminal tail contributes to histone binding through ionic interactions, whereas the N-terminal tail has minimal ionic contributions when binding histones. Although the N-terminal tail didn't appear to impact binding, when coupled with the removal of the C-terminal tail, we observed diminished histone selectivity between major type histones and variants. With the addition of post translational modifications, such as polyglutamylation, which further alters the charge of the tails, it is plausible the tails could be one of several ways the cell regulates Nap1, and potentially other histone chaperones [43].

A recent publication suggests that yNap1 binds H2A-H2B with a 2:1 stoichiometry [57], which is in disagreement with our results and previously published results [1, 54, 57]. To obtain a crystal structure, Aguilar-Gurrieri et al. (2016) removed the tails from yNap1 [57]. By employing sedimentation velocity experiments we were able to confirm that the tails contribute to the oligomerization state of yNap1 and yNap1•H2A-H2B. Specifically, we found that WT yNap1 bound H2A-H2B with a 2:2 stoichiometry, while tailless yNap1 was able to form larger complexes with H2A-H2B when H2A-H2B was added at sub-saturating amounts. Due to the large impact of both

yNap1 tails when binding H2A-H2B, the discrepancy between our stoichiometry and the recent crystal structure of tailless yNap1 bound to H2A-H2B with a 2:1 stoichiometry, could be due to the lack of tails.

Sedimentation velocity experiments also confirmed that aggregates form when H3-H4 is added to DNA at low ionic strength. This aggregation is likely caused by improper ionic interactions between the basic H3-H4 and acidic backbone of DNA that can be eliminated with the addition of yNap1. We propose that yNap1 has several functions during nucleosome assembly with the propensity to mediate DNA:histone interactions being dependent on the tails. Specifically, yNap1 prevented H2A-H2B from binding DNA promiscuously, an interaction that inhibits tetrasome formation. Due to highly basic charge of H3-H4 and acidic charge of DNA, tetrasome formation does not occur without the aid of histone chaperones or salt dialysis. The role of histone chaperones, or in our case, yNap1, could be to prevent incorrect ionic interactions that would prevent DNA from being able to wrap around H3-H4 to complete the tetrasome. Once tetrasome formation has occurred, yNap1 may also deliver H2A-H2B to complete the nucleosome.

Assembled nucleosomes act as potential roadblocks for cellular processes such as transcription and replication, therefore they must remain dynamic. Histone variants have been shown to play significant roles in nucleosome dynamics, with Nap1 aiding by exchanging H2A-H2B with histone variants [36]. The mechanism by which Nap1 differentiates between major type histones and histone variants is poorly understood. By using binding affinities to determine histone selectivity, we found that the tails contribute to differentiation indicating regulation may be due to charge alteration of the C-terminal tail through modifications such as polyglutamylation [43]. Together, we conclude that Nap1 plays a critical role in chromatin dynamics with the tails providing a possible link into how Nap1 is regulated.
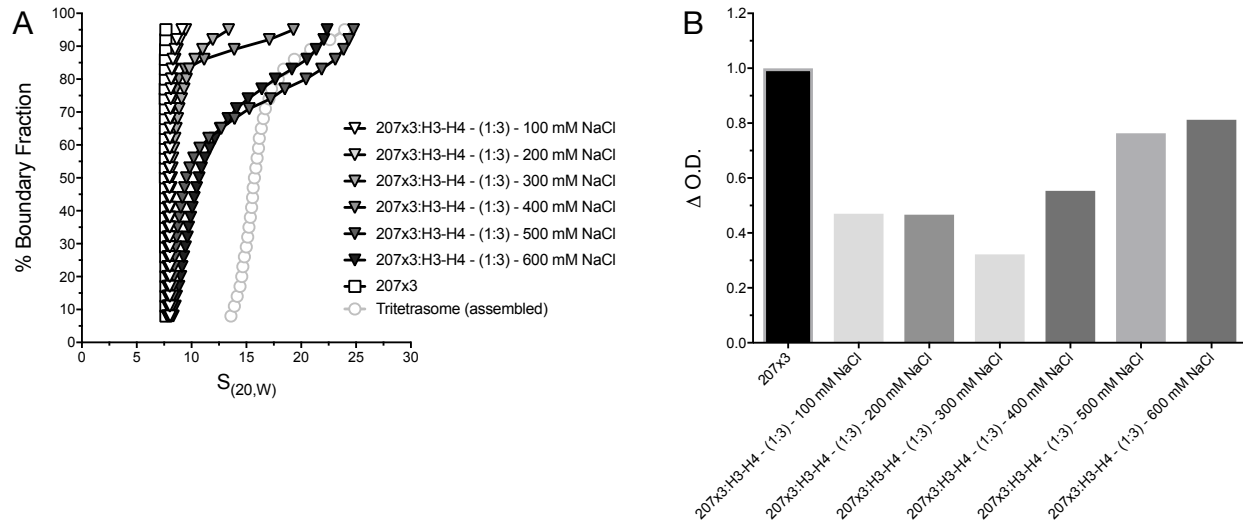
Figure 2.12. Ionic strength affects H3-H4 binding and aggregation. **A)** 3X H34(dimer) was added to 207x3 DNA at different ionic strengths (100- 600 mM NaCl) and allowed to equilibrate for 30 min. vHW analysis reveals that H3-H4 binding is dependent on ionic strength of buffer as higher ionic strengths results in increased binding. Salt recon assembled tri-tetrasome taken from figure 2.13 is shown in circles as a control. **B)** OD values calculated from ratio of DNA:H3-H4/DNA alone. With the exception of 300mM NaCl, we see a trend where low ionic strength leads to increased aggregation, which is evident with the decrease in OD values.
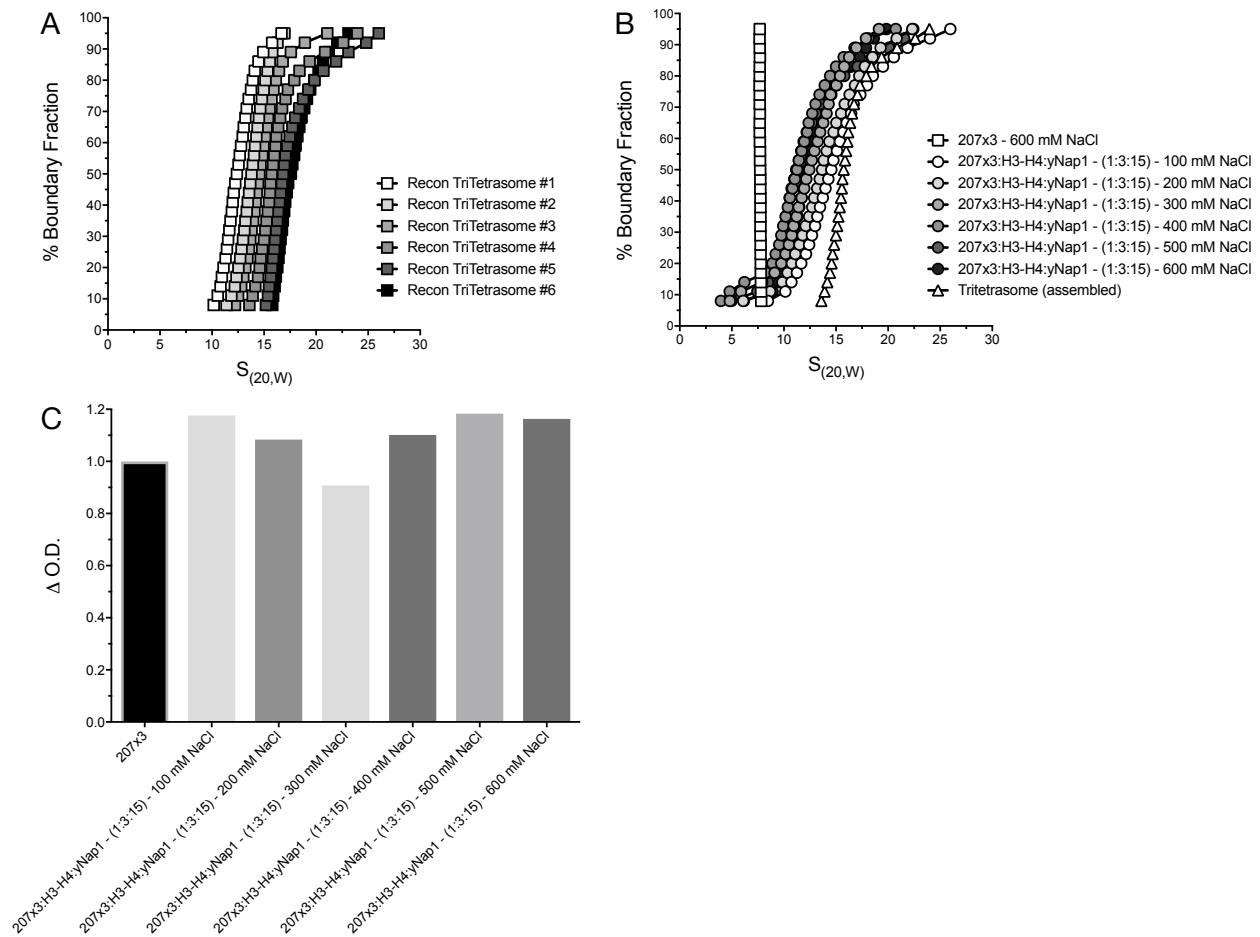
Figure 2.13. Nap1 aids in H3-H4 assembly onto DNA. **A)** Trimer tetrasomes (tri-tetrasomes) were reconstituted by adding 0.7 – 1.2-fold molar excess H3-H4 to 601-207x3 DNA and systematically lowering the ionic strength from 2 M NaCl to 250 mM NaCl, followed by dialysis into a buffer containing no salt. Sedimentation velocity was performed to monitor the saturation level of each tri-tetrasome. **B)** 3X H3-H4 dimer and 5X yNap1 were added to 207x3 DNA at different ionic strengths (100 mM – 600 mM NaCl) and allowed to equilibrate for 30 min. vHW analysis reveals that yNap1 aids in H3-H4 binding as we observe similar binding at all ionic strengths that closely resembles **(A).** Tri-tetrasome shown in **(B)** is taken from Recon Tri-tetrasome #4 from **(A). C)** OD values calculated from ratio of DNA:H3-H4:Nap/DNA. There were minimal changes in OD between the different ionic conditions indicating yNap1 functions as a H3-H4 chaperone by preventing aggregation and aiding in H3-H4 assembly on DNA.
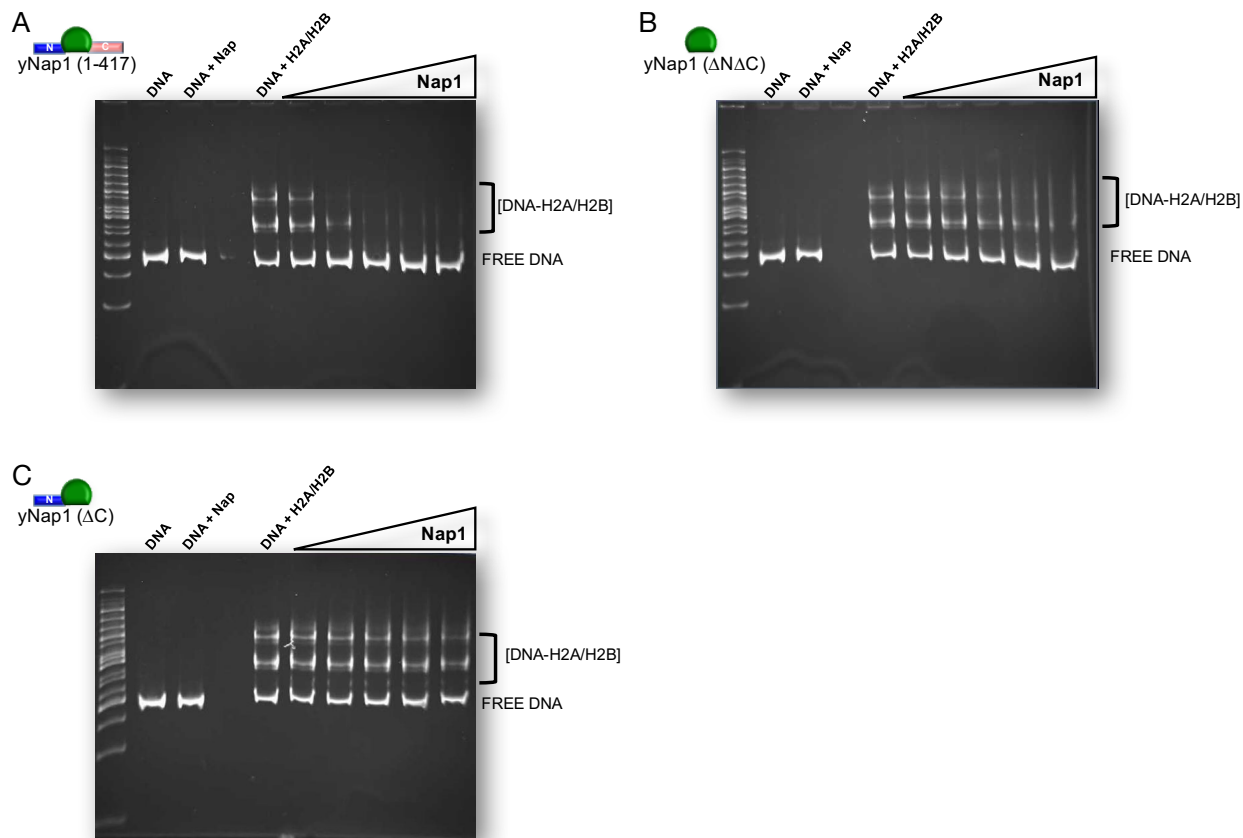
Figure 2.14. yNap1 removes H2A-H2B from DNA. yNap1 was added to preassembled 601-207 DNA and H2A/H2B (H2A-H2B was added in 7-fold molar excess) and then samples run on a 5% native gel and stained with EtBr. **A)** yNap1 WT completely removes H2A/H2B from DNA at a 1:1 yNap1 to H2A-H2B molar ratio whereas **(B)** tailless yNap1 required ~5:1 yNap1 to H2A-H2B molar ratio. **C)** Unlike WT yNap1, removal of the C-terminal tail results in loss of H2A-H2B removal activity. no shadows on figure. Labels are too small.

49

Chapter 3 – Analytical Ultracentrifugation Reveals Asymmetry in Vps75, RTT109 and Histone H3-H4 Complexes[2]

3.1 - Summary:

Vps75, a histone chaperone belonging to the Nap family, has been characterized as a homodimer that self-associates into tetrameric species at physiological ionic strengths. Using sedimentation velocity analytical ultracentrifugation (SV-AUC), we show that Vps75 forms a tetramer at low ionic strength and binds histones while in this tetrameric structure. Saturating Vps75 with histones splits the tetrameric species into a dimeric species bound to the histone cargo. Likewise, Rtt109, a histone acetyltransferase that is activated by Vps75, also splits the Vps75 tetramer, primarily forming asymmetric complexes that consist of both 2:1 and 2:2 Vps75:Rtt109 complexes. In the presence of H3-H4, the second Rtt109 in the Vps75:Rtt109 complex is displaced, resulting in a Vps75:Rtt109:H3-H4 ternary complex.

3.2 - Introduction:

Eukaryotic cells package vast amounts of chromatin, DNA in complex with histones, within the nucleus. The basic repeating unit of chromatin is known as the nucleosome: 147 bp of DNA wrapped around a H3-H4 tetramer flanked by two H2A-H2B dimers [5]. Compacting DNA is absolutely essential for DNA to be packaged within the nucleus in a dynamic manner that allows access for processes such as transcription, replication, and repair. There are several mechanisms that aid in nucleosome assembly and disassembly, including histone post-translational modifications, histone variant incorporation, ATP-dependent chromatin remodelers, and histone chaperones.

---

[2] This work was performed in collaboration with Sheena D'Arcy. Daniel Krzizike performed and analyzed all sedimentation velocity AUC experiments. Both Sheena D'Arcy and Daniel Krzizike contributed to writing this chapter, which will be submitted as a manuscript. Different fonts here.

Originally identified as proteins that prevent histone-DNA aggregation while aiding in nucleosome assembly, histone chaperones have now been implicated in almost all aspects of chromatin dynamics (Reviewed in [8, 37, 38, 81])[82, 83]. There are several classes of histone chaperones with the nucleosome assembly protein (Nap) family being one of the most characterized (Reviewed in [36, 37]) [84]. Nap family chaperones are structurally conserved, primarily adopting a dimeric species that is involved in cellular processes such as nucleosome assembly and disassembly, histone exchange and eviction, histone transport and storage, and histone post-translational modifications(Reviewed in [38, 85]). Yeast Vps75, a structural homolog of Nap1 and the only other member of the Nap family in yeast, was originally identified in a genomic screen for vacuolar protein sorting in budding yeast [86, 87]. Similar to Nap1, Vps75 binds both core histone complexes, H2A-H2B and H3-H4, with high affinity [1, 88].

Likewise, both Vps75 and Nap1 can bind Rtt109 (Regulator of Ty1 Transportation 109), a histone acetyltransferase that, together with histone chaperone Asf1, acetylates H3K56 [88, 89]. Although Nap1, Vps75, and Asf1 are all capable of binding Rtt109 in vitro, only chaperones Vps75 and Asf1 are capable of stimulating Rtt109 acetylation [88-90]. Rtt109 is specific to acetylating lysine residues in histones H3 and H4, but is unique in the fact that its selectivity is altered by Vps75 and Asf1 [91]. Specifically, evidence indicates that Vps75 will promote Rtt109 acetylation of H3K9 and H3K23, whereas Asf1 will promote Rtt109 acetylation of H3K56 [92-94]. Recent evidence suggests Asf1-H3-H4 may act as a substrate for the Vps75-Rtt109 complex, enhancing total H3-H4 acetylation when compared to the complex without Asf1 [91].

The difference in Rtt109 selectivity could be due to different conformations of H3-H4 when in the presence of Vps75 and/or Asf1, respectively [89, 91, 95]. Previous publications show that one Vps75 dimer binds one H3-H4 tetramer, whereas Asf1 'splits' the tetramer, and binds only one H3-H4 dimer [96, 97]. Although there have been extensive efforts to characterize these interactions, conflicting results make understanding the interactions quite challenging. Specifically, conflicting crystal structures of the Vps75:Rtt109 complex indicate the stoichiometry

to be either 2:2 or 2:1 [85, 98]. The stoichiometry of both Vps75 and Nap1 in complex their histone cargo has come into question as other groups have found that both Vps75 and Nap1 dimers bind only one histone dimer [57, 59, 76]. It has also been suggested that when Vps75 and Nap1 self-associate into tetrameric species, they remain tetramers even when bound to their histone cargo [45, 57, 59]. In this work, using both SEC-MALS (size exclusion chromatography coupled to multi-angle light scattering) and SV-AUC (sedimentation velocity analytical ultracentrifugation), we look to resolve the stoichiometry of Vps75 to both H3-H4 and Rtt109 along with the ternary complex of Vps75:Rtt109:H3-H4. We specifically investigated the ionic dependence of each of these proteins along with the impact ionic charge had on stoichiometry. By characterizing these proteins in complex with one another we hope to gain a better biochemical understanding of how histone chaperones might impact the selectivity of histone acetyltransferases such at Rtt109.

3.3 - Materials and Methods:

3.3.1 - Protein expression and purification

Saccharomyces cerevisiae Nap1 and Nap1Δβ (missing residues 288-305) were expressed using the pBAT4 plasmid and purified as described previously [99]. They contained mutations C200A, C249A, C272A to facilitate labeling. An alternative Nap1 labeling mutant (D201C, C200A, C249A, C272A, C414A; used in Fig. 4b), Nap1ΔD (missing residues 1-180) and ΔD+Δβ (missing residues 1-180 and 288-305) were expressed using the pHAT4 plasmid and purified using standard Ni-NTA and Mono-Q chromatography. *S. cerevisiae* Vps75, *S. cerevisiae* H2A-H2B-T118C and *Xenopus laevis* H2A-H2B were expressed and purified as described previously [66, 67].

3.3.2 - Analytical ultracentrifugation

Sedimentation velocity experiments were performed using a Beckman Coulter Optima XL-A or XL-I analytical ultracentrifuge. Samples were diluted to an OD of 0.3 to 0.5 and placed in standard Epon 2-channel centerpiece cells. Sedimentation was then monitored using the absorbance optics at 229 or 280 nm at 20°C. Data were collected using speeds of 30, 35, 45, or 50 krpm with either an An60Ti or An50Ti rotor. Partial specific volumes were determined using UltraScan3. Time invariant and radial invariant noise were subtracted from the sedimentation velocity data by two-dimensional spectrum analysis (2DSA) [100], followed by genetic algorithm refinement and Monte Carlo analysis [72, 73, 100]. Sedimentation coefficient distributions G(s) were obtained with enhanced van Holde-Weischet analysis [101]. Calculations were performed on the UltraScan LIMS cluster at the Bioinformatics Core Facility, University of Texas Health Science Center, San Antonio; and the Lonestar cluster at the Texas Advanced Computing Center, supported by NSF Teragrid Grant #MCB070038.

Resulting values were further refined by fitting the partial specific volume, assuming the molecular mass (M) was a multiple of a Nap1/Vps75 homodimer. Sedimentation plots and relative molecular masses were determined using the model-independent enhanced van Holde-Weischet method, and two-dimensional and/or parametrically constrained spectrum analysis [100-102].

3.3.3 - Size exclusion chromatography coupled to multi-angle light scattering

100 µl of 2 mg/ml Nap1ΔD or Nap1 ΔD+β were injected onto a Superdex 200 10/300 GL column using an ÄKTA purifier HPLC system (GE Healthcare). This system was directly connected to a Dawn Heleos II multi-angle light scattering instrument and a REx refractive index detector (Wyatt Technologies). The column buffer was 20 mM Tris pH 7.5, 1 mM TCEP, 150 mM NaCl and the flow rate was 0.3 ml/min. Data were analyzed with ASTRA 5 (Wyatt Technologies), using the refractive index to determine protein concentration.

3.4 – Results:

3.4.1 - Sedimentation of the Vps75-histone complex depends on ionic strength

To determine the molecular mass and stoichiometry of the complex between Vps75, RTT109 and H3-H4, we first characterized the ionic dependence of each component using SV-AUC. Dimerization of Vps75 is well-established and salt-dependent tetramerization has been previously observed using other techniques [46, 66, 103]. SV-AUC is ideal for solution state characterization because it provides first principles hydrodynamic information about size and shape of the sample while in solution without having to modify or label the sample. Using SV-AUC, we first examined the sedimentation behavior of Vps75 alone at 150 mM and 300 mM NaCl (Fig. 3.1A). At 300 mM NaCl, Vps75 has a sedimentation coefficient (S) of 4.0, while at 150 mM NaCl, Vps75 sediments at 5.8 S. Molecular masses *(M)* obtained with two-dimensional spectrum analysis (2DSA) indicate the increased sedimentation coefficient value occurs because Vps75 dimers self-associate into tetramers (Table S3.1A).

We next added 0.5 to 3 molar equivalents of H3-H4 to Vps75 (Fig. 3.1C & E). We calculated one mole of Vps75 to be a Vps75 monomer, and one mole of H3-H4 to be an H3-H4 heterodimer, not an $(H3-H4)_2$ heterotetramer. At both 150 and 300 mM NaCl, addition of H3-H4 causes an increased sedimentation curve (curve shifts to higher S-value), with high molar equivalents also resulting in a tail at 2 to 3S. Based on the sedimentation of H3-H4 alone (Fig. S3.1A), this tail likely corresponds to unbound H3-H4. The key observation is that the complexes formed between Vps75 and H3-H4 at the two salt concentrations have different sedimentation coefficients. At 300 mM NaCl, the complex sediments at ~ 7S, while at 150 mM NaCl the complex sediments at ~ 9S. Molecular masses determined from 2DSA (>250 kDa, data not shown) suggest complexes larger than 2:2 at both salt concentrations.

To aid in determining the exact stoichiometry for Vps75 and H3-H4 complexes, we investigated the Vps75:H3-H4 interaction using the Vps75 tetramer mutant (TM) that is unable to form tetramers (Vps75-TM; R164D, K169E, K170E) [104]. At both 150 mM and 300 mM NaCl,

Vps75-TM sediments at 4.0 S (Fig. 3.1B), confirming that this construct is exclusively dimeric in our experiment. Titration of 0.5 to 3 molar equivalents of H3-H4 to Vps75-TM has a similar effect to that of WT-Vps75 with H3-H4 at both ionic strengths (Fig. 3.1C & E vs D & F). In fact, the data obtained for Vps75-TM and WT-Vps75 at 300 mM NaCl are virtually identical (compare Fig. 3.1C to 3.1D). As observed for WT-Vps75, there is a difference in the sedimentation of the complexes formed between Vps75-TM and H3-H4 at the two salt concentrations. At 300 mM NaCl the complex sediments at ~7 S, while at 150 mM NaCl the complex sediments up to 9 S. The difference in sedimentation coefficients between 150 mM and 300 mM NaCl indicates Vps75 binds H3-H4 asymmetrically. The use of Vps75-TM however allows us to exclude tetramer formation by Vps75 as the reason for the increased S-value at 150 mM NaCl when compared to 300 mM NaCl.

3.4.2 - The Vps75 tetramer splits into two histone-bound Vps75 dimers

We next tested whether the salt-dependent difference in sedimentation coefficients between Vps75:H3-H4 complexes was due to H3-H4 oligomerization. H3-H4 is known to form an $(H3-H4)_2$ hetero-tetramer in solution, but can also exist as a dimer based on ionic conditions which can make stoichiometry determination more challenging [105]. To eliminate the potential complications caused by the different oligomerization states of H3-H4, we analyzed complexes with H2A-H2B, as it is a structural homolog of H3-H4 that binds Vps75 with high affinity [66], but is predominantly dimeric in solution [106]. We titrated 0.5 to 3 molar equivalents of H2A-H2B against Vps75 at 150 mM and 300 mM NaCl (Fig. 3.2A & C). At 300 mM NaCl, addition of H2A-H2B causes a slight increase in sedimentation (Fig. 3.2A), while at 150 mM NaCl, addition of H2A-H2B causes a noticeable increase at 0.5 molar equivalents followed by a decrease at 1 and 2 molar equivalents (Fig. 3.2C). This sequential increase and decrease as H2A-H2B is titrated at 150 mM NaCl suggests that saturation of the Vps75 histone-binding sites splits the Vps75 tetramer into two histone-bound dimers. Similar experiments with Vps75-TM confirmed this
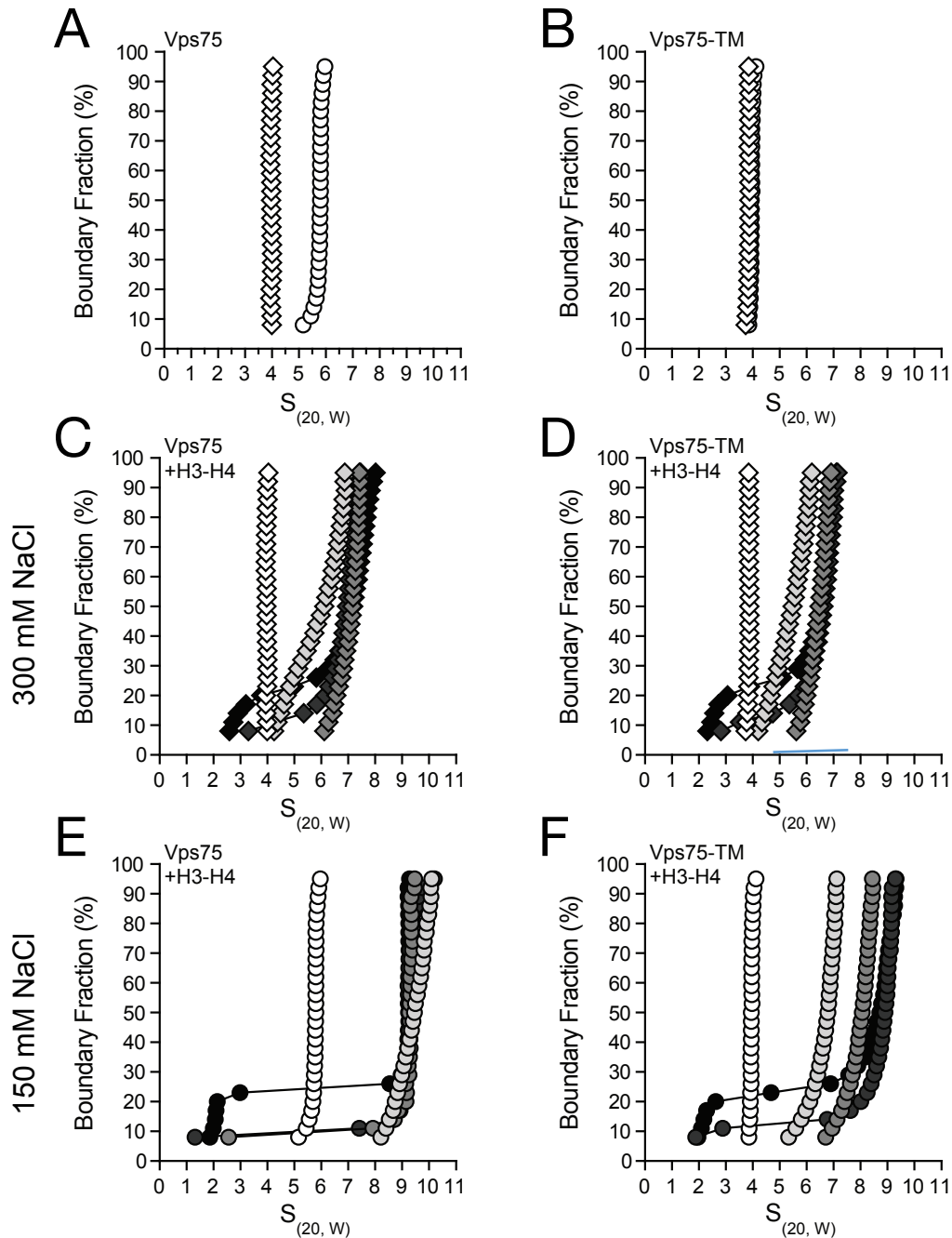
Figure 3.1. Ionic Strength Influences the Sedimentation of Complexes between Vps75 and H3-H4

Sedimentation velocity of **(A)** Vps75 or **(B)** Vps75-Tetramer Mutant (TM) with 0 to 3 molar equivalents of H3-H4 **(C-D).** Experiments were done in the presence of 150 mM (circles in **A, B, E, & F)** or 300 mM NaCl (diamonds in **A, B, C, & D)**. Vps75 or Vps75-TM alone is shown in white, while Vps75 **(C & E)** or Vps75-TM **(D & F)** with 0.5, 1, 2 or 3 molar equivalents of H3-H4 is shown in light grey, grey, dark grey or black respectively.

suggestion, as removing Vps75 tetramer formation eliminates the sequential increase and decrease (Fig. 3.2B & D). Molecular masses obtained using two-dimensional spectrum analysis further support this, as they are indicative of complexes containing Vps75 and H2A-H2B at 4:1, 4:2 and 2:2, but not 4:3 or 4:4 molar ratios (Table S3.1B). Notably, the sequential increase and decrease in sedimentation also occurs, albeit more subtly, when H3-H4 is titrated at 150 mM NaCl (Fig. 3.1C), and is eliminated when using Vps75-TM (Fig. 3.1D). Hence, histone saturation splits the Vps75 tetramer into two histone-bound Vps75 dimers.

We further investigated the splitting of the Vps75 tetramer by H2A-H2B using disulphide crosslinking between two Vps75-N70C chains. These crosslinks occur in a salt-dependent manner (Fig. S3.2A) and produce a cross-linked species that is tetrameric at both 150 mM and 300 mM NaCl (Fig. S3.2B). We monitored cross-linking of Vps75-N70C with and without H2A-H2B, and observe a reduction in cross-linking in the presence of H2A-H2B (Fig. S3.2C). A previous study reported a similar cross-linking result with Vps75-K78C and H3-H4 [104]. Combined with the aforementioned sedimentation data, our cross-linking data confirms that histones split the Vps75 tetramer into two histone-bound Vps75 dimers.

3.4.3 - The Vps75 dimer binds histones asymmetrically

The salt-dependent difference in sedimentation coefficients observed with Vps75 and H3-H4 also holds true for Vps75 with H2A-H2B. As discussed above, at 300 mM NaCl the Vps75-H2A/H2B complex sediments at ~ 4.5 S, while at 150 mM NaCl the complex sediments at ~ 6 S (Fig. 3.2C). We also note a difference in the appearance of a tail, indicative of unbound H2A-H2B [see [106] for H2A-H2B sedimentation]. At 300 mM NaCl, the tail first occurs at 1 molar equivalent, while at 150 mM NaCl it first occurs at 2 molar equivalents. Taken together, these two observations suggest that the number of H2A-H2B dimers bound per Vps75 dimer differs at the two salt concentrations. Molecular masses from two-dimensional spectrum analysis further suggest that the stoichiometry of the complex between Vps75 and H2A-H2B is 2:1 at 300 mM

NaCl, and 2:2 at 150 mM NaCl (Table S3.1B-C). This is likely due to salt effects independent of Vps75 oligomerization, as similar results are obtained for Vps75-TM (Fig. 3.2B).

To further confirm that the observed difference in sedimentation is due to a difference in mass rather than shape, we measured complex stoichiometry using a Job plot. Vps75 labeled with Alexa-488 was mixed with H2A-H2B labeled with Atto-647N at varying molar ratios (Fig. 3.2E). This produces a parabolic curve with a maximum at 0.50 at 150 mM salt, indicating a stoichiometry of one Vps75 dimer with one H2A-H2B dimer, or in this specific case, one Vps75 dimer with two H2A-H2B dimers. Increasing the salt concentration to 300 mM causes the maximum to shift to 0.58, towards a stoichiometry of 2:1. It is likely that the maximum doesn't shift completely to 0.67 as an excess of H2A-H2B may artificially force weak binding of a second H2A-H2B. This shift in stoichiometry also implied using SV-AUC by the elevated molecular mass of the complex formed by Vps75 with 2 molar equivalents of H2A-H2B (Table S3.1C). Altogether, the data reveal an asymmetry that essentially limits the function of one of the two H2A-H2B-binding sites.

In terms of RTT109, however, the histone ligand is H3-H4, not H2A-H2B. To test if asymmetric binding applies to H3-H4, we used an H3 mutant unable to form tetramers (TM-H3-H4; H3 L126A, I130A, C110E) [107]. TM-H3-H4 elutes later than H3-H4 in size-exclusion chromatography (SEC) (Fig. S3.1B) indicating a dimeric species and, unlike H3-H4, has no salt-dependent shifts in sedimentation (Fig. S3.1A). We analyzed the sedimentation of Vps75 with 0.5 or 1 molar equivalents of TM-H3-H4 at 150 mM and 300 mM NaCl (Fig. 3.2F). At 150 mM NaCl, we observe an increase in sedimentation at 0.5 molar equivalents consistent with Vps75 remaining a tetramer while binding one H3-H4 dimer, followed by a decrease at 1 molar equivalent consistent with one Vps75 dimer binding two H3-H4 dimers. As described above, this demonstrates that binding of TM-H3-H4 also splits the Vps75 tetramer. The use of TM-H3-H4 also prevents the larger species observed with wild-type H3-H4 (compare Fig. 3.1C,E and 3.2F). This suggests that complexes with wild-type H3-H4 contain additional H3-H4 that aren't directly
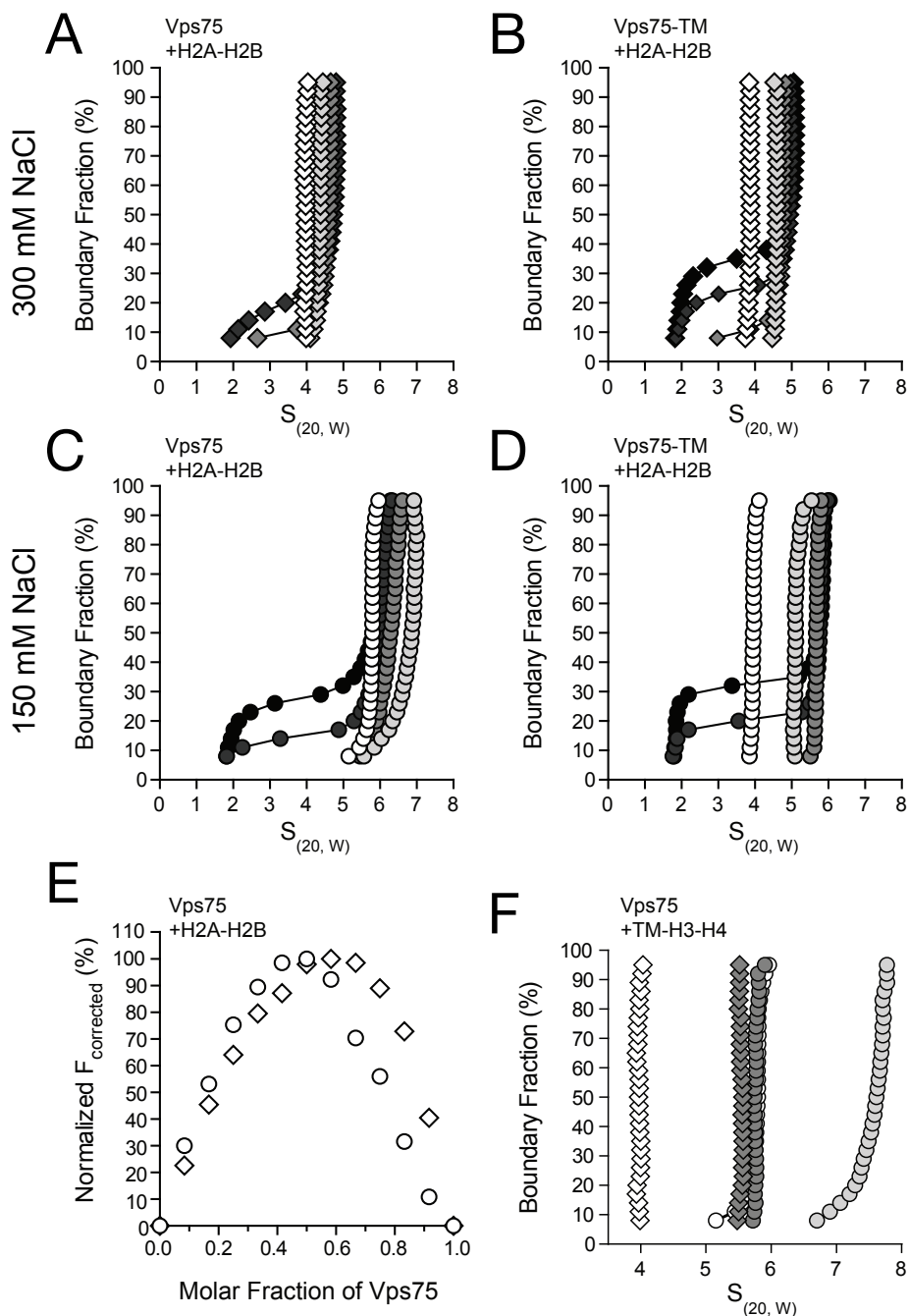
Figure 3.2. The Vps75 Dimer Binds Histones Asymmetrically

Sedimentation velocity of **(A)** Vps75 or **(B)** Vps75-TM with 0 to 3 molar equivalents of H2A-H2B. Experiments were done at (**A & B**) 300 mM (diamonds) or **(C & D)** 150 mM (circles) NaCl. Vps75 or Vps75-TM alone is shown in white, while Vps75 or Vps-75-TM with 0.5, 1, 2 or 3 molar equivalents of histones is shown in light grey, grey, dark grey or black respectively. **(E)** Job plot with Alexa-488 Vps75 and Atto-647N H2A-H2B at 150 mM (circles) or 300 mM (diamonds) NaCl. The curves are representative of three independent experiments and each data point is the mean of duplicate measurements within a replicate. Error bars are plus/minus one standard error of the mean and are too small to be visible. **(F)** Sedimentation velocity of Vps75 with 0 to 1 molar equivalent of TM-H3-H4, colored as in A.

contacting the primary Vps75 dimer. Despite this, the complexes formed between Vps75 and TM-H3-H4 at 150 mM NaCl are still sediment at a slightly larger value than those at 300 mM NaCl (Fig. 3.2E). Molecular masses from two-dimensional spectrum analysis suggest that this slight shift reflects an additional H3-H4 binding a to Vps75 dimer at 150 mM NaCl forming a 2:2 complex compared to 300 mM NaCl forming a 2:1 complex (Table S3.1D). Therefore, the salt dependence change in stoichiometry indicates the Vps75 dimer binds both H2A-H2B and H3-H4 asymmetrically.

3.4.4 - Asymmetric histone-binding is not conserved in Nap1

We next asked if Nap1 displays asymmetry in histone binding similar to Vps75. Nap1 is a structural homolog of Vps75 capable of binding H2A-H2B, H3-H4 and RTT109 [66, 108]. Like Vps75, Nap1 forms a homo-tetramer at 150 mM NaCl [104], but unlike Vps75, Nap1 cannot activate RTT109 histone acetyltransferase [66]. We examined complexes between Nap1 and H2A-H2B at 150 mM and 300 mM NaCl (Fig. 3.3A & B). These complexes have similar sedimentation profiles and notably lack an unbound H2A-H2B tail. Molecular masses from two-dimensional spectrum analysis suggest that a 2:2 species is formed at both salt concentrations (Table S3.1E). These data show that H2A-H2B splits the Nap1 tetramer. They also show that asymmetry in histone binding is not conserved in Nap1, and thus may be a unique feature of Vps75.

3.4.5 - The Vps75 dimer binds RTT109 asymmetrically

In addition to binding H3-H4, Vps75 also directly interacts with RTT109 [89]. Using sedimentation velocity, we characterized RTT109 alone, as well as in complex with Vps75. RTT109 does not exhibit salt-dependent oligomerization and sediments at 3.4 S at both 150 mM and 300 mM NaCl (Fig. S3.3A). We titrated 0.5 to 1 molar equivalents of RTT109 against Vps75 (Fig. 3.4A & B). At 300 mM NaCl, the addition of 0.5 molar equivalents of RTT109 causes a large
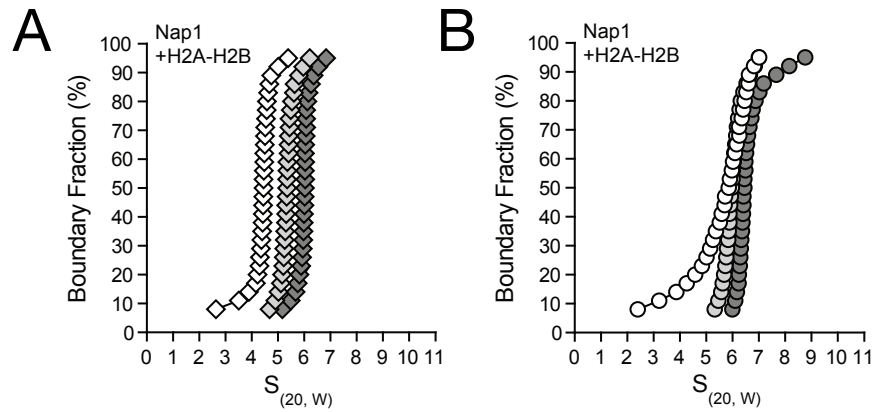
Figure 3.3. Nap1 binds histone H2A-H2B symmetrically
(A & B) Sedimentation velocity of Nap1 with 0 to 1 molar equivalents of H2A-H2B. Experiments were done in the presence of **(A)** 300 mM (diamonds) or **(B)** 150 mM NaCl (circles). Nap1 alone is shown in white, while Nap1 with 0.5 or 1 molar equivalent of H2A-H2B is shown in light grey or grey respectively.

increase in sedimentation (Fig. 3.4A). Addition of 1 molar equivalent does not further increase this sedimentation curve, but results in the appearance of a tail on the van Holde-Weischet plot that is tending toward the sedimentation coefficient of unbound RTT109. In contrast, at 150 mM NaCl, 0.5 molar equivalents of RTT109 do not cause an increase in sedimentation, while 1 molar equivalent does (Fig, 3.4B). An initial increase is not observed as RTT109 splits the Vps75 tetramer, as shown previously by others [104]. Addition of 1 molar equivalent produces a tail that is notably smaller than the analogous tail at 300 mM NaCl. The final complex formed when Vps75 is mixed with 1 molar equivalent of RTT109 also sediments faster at 150 mM NaCl (6.7S) than at 300 mM NaCl (5.9 S). Combined with molecular masses obtained from 2DSA (Table S3.1F-G), these observations suggest that the Vps75 dimer binds both one and two copies of RTT109 at 150 mM NaCl while only binding one copy at 300 mM NaCl. This asymmetry is similar to that observed for Vps75 complexes with either H2A-H2B or H3-H4.

We also analyzed Vps75, RTT109 and their complexes at 150 mM NaCl using size exclusion chromatography coupled to multi-angle light scattering (SEC-MALS). SEC-MALS measures the weight-average molecular mass of all complexes present in a sample. We analyzed Vps75 and RTT109, as well as Vps75 with 0.5, 1 and 2 molar equivalents of RTT109 (Fig, 3.4C). Unbound Vps75 elutes at 11.9 ml, while unbound RTT109 elutes at 15.3 ml (Fig, 3.4C, dotted). Vps75 with 0.5 molar equivalents of RTT109 elutes as a single peak between unbound Vps75 and unbound Rtt109 at 12.6 ml (Fig. 3.4C, solid grey). The measured molecular mass suggests a 2:1 complex. Further increasing the amount of RTT109 causes the major peak to elute earlier and have greater amplitude. The measured molecular masses fall between 2:1 and 2:2 complexes, suggesting a mixture of both. An unbound RTT109 peak also emerges, and at 2 molar equivalents (20 nM RTT109 with 10 nM Vps75) has an amplitude greater than RTT109 alone (10 nM RTT109) (Fig. 3.4C, compare solid and dotted black). Taken together, these data suggest that while a 2:2 complex can form, the binding of the second RTT109 is transient as we see both complexes with SV-AUC and SEC-MALS. Inequality between the two RTT109-binding sites in a

Vps75 dimer has been reported previously based on sedimentation equilibrium experiments [103]. Hence, asymmetric binding between Vps75 and Rtt109 is impacted by ionic strength.

3.4.6 - RTT109 does not stably interact with H3-H4 or TM-H3-H4

The final binary interaction for us to characterize within the Vps75, RTT109, H3-H4 complex, is that between RTT109 and H3-H4. To ascertain if such an interaction occurs in our experimental system, we performed sedimentation analysis on RTT109 with 0.5 to 2 molar equivalents of either H3-H4 or TM-H3-H4 (Fig. S3.3B-C). There is no shift in the sedimentation of RTT109 as H3-H4 or TM-H3-H4 is titrated. Rather, a tail appears between 2 and 3 S, suggestive of unbound H3-H4 or TM-H3-H4. RTT109 thus does not stably interact directly with H3-H4 or TM-H3-H4 in the absence of Vps75 in our experimental system.

3.4.7 - H3-H4 displaces some RTT109 from a 2:2 Vps75:RTT109 complex

Having characterized all possible binary interactions, we next used sedimentation velocity to characterize the ternary complex between Vps75, RTT109 and H3-H4. We started by titrating H3-H4 against an equimolar mixture of Vps75 and RTT109 (Fig. 3.5A). Addition of 0.5 molar equivalents of H3-H4 causes a large increase in sedimentation and the appearance of a tail. The sedimentation plot is right-shifted compared to the binary complexes of Vps75 with either H3-H4 or RTT109. Increasing H3-H4 to 1.0 molar equivalent causes a subtle decrease in sedimentation and an increase in the magnitude of the tail. Comparison with sedimentation curves for unbound H3-H4 and unbound RTT109 (Fig. 3.5A, faded) reveals that the tail likely represents unbound RTT109. This means that titration of H3-H4 against an equimolar complex of Vps75 and RTT109, causes some RTT109 to be displaced. The data show that the Vps75 dimer cannot simultaneously bind H3-H4 and two copies of RTT109, however, it can bind one each of H3-H4 and RTT109 simultaneously.
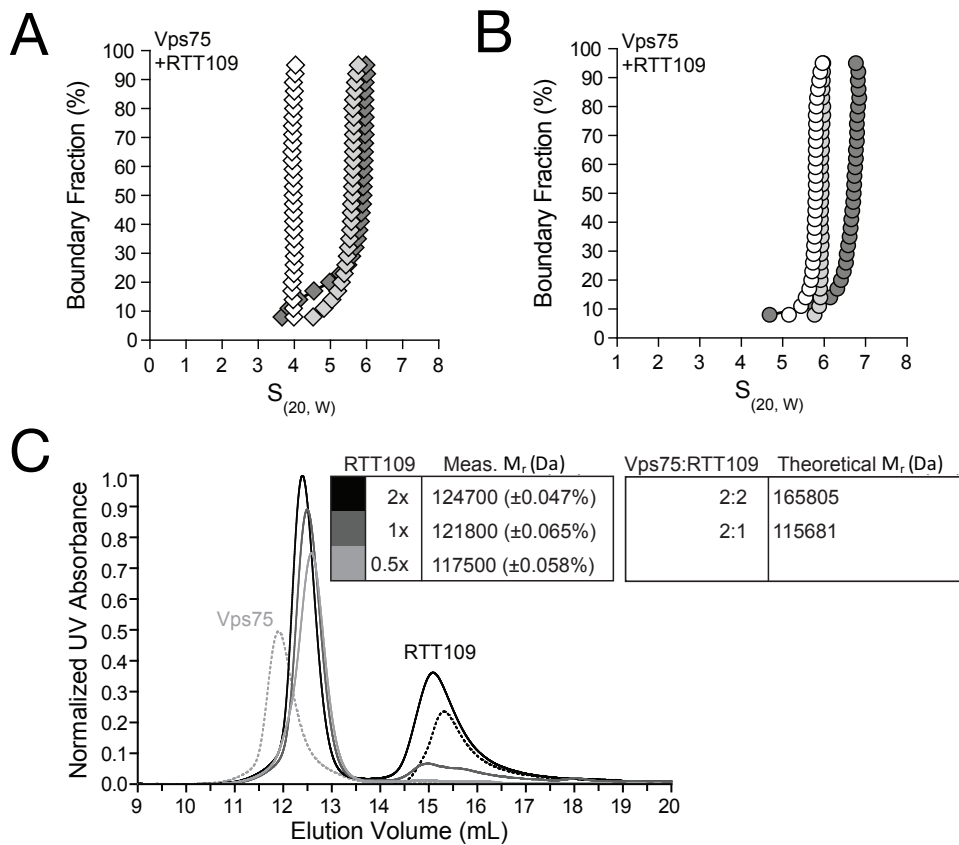
Figure 3.4. The Vps75 Dimer Binds RTT109 Asymmetrically
(A & B) Sedimentation velocity of Vps75 with 0 to 1 molar equivalents of RTT109 **(A)** 300 mM (diamonds) or **(B)** 150 mM NaCl (circles), Vps75 alone is shown in white, while Vps75 with 0.5 or 1 molar equivalent of Rtt109 shown in light grey or grey respectively. **(C)** SEC-MALS of 10 nM Vps75 (dotted grey), 10 nM RTT109 (dotted black) and 10 nM Vps75 with 5, 10 or 20 nM RTT109 (light grey, dark grey or black respectively). Experiments were done at 150 mM NaCl. Tables show the relative molecular masses (M_r) measured using MALS compared to theoretical molecular masses.

We next wondered if RTT109 was being displaced because of the 'extra' copies of H3-H4. As described above, the 'extra' copies of H3-H4 do not directly contact Vps75 and are not seen when using TM-H3-H4. We analyzed a 1:1:0.5 mix of Vps75, RTT109 and TM-H3-H4 (Fig. 3.5B). The resulting sedimentation plot displayed an increase in sedimentation when compared to Vps75 in complex with H3-H4, or Vps75 in complex with RTT109. The plot also has a tail comparable to that seen with wild-type H3-H4, indicative of unbound RTT109. Thus like H3-H4, addition of TM-H3-H4 to an equimolar complex of Vps75 and RTT109, causes some RTT109 to be displaced. The RTT109 displacement observed with wild-type H3-H4 is not due to the 'extra' H3-H4 copies, but rather due to H3-H4 outcompeting Rtt109 for Vps75 binding.

3.4.8 - The Vps75 dimer simultaneously binds one RTT109 and one H3-H4

Our result that an equimolar mixture of Vps75, RTT109, and H3-H4 forms a ternary complex along with containing unbound RTT109, suggests that the Vps75 dimer binds a single RTT109, and either one or two copies of H3-H4. To investigate this further, we titrated H3-H4 against a 1:0.5 mix of Vps75 with RTT109 (Fig. 3.5C). Addition of 0.5 molar equivalents of H3-H4 causes a large increase in sedimentation similar to that observed with the 1:1 mixture of Vps75 and RTT109 (compare Fig. 3.5A and C). A key difference, however, is that the large tail indicative of unbound RTT109 is not observed. Increasing H3-H4 to 1 molar equivalent does not further increase the sedimentation, but does create a small tail. H3-H4 has a low extinction coefficient and this small tail likely corresponds to unbound H3-H4. These data show that H3-H4 does not displace RTT109 when Vps75 and RTT109 are mixed at 1:0.5. The lack of a shift and the appearance of a tail as H3-H4 is increased from 0.5 to 1.0 molar equivalent further suggest that the ternary complex contains only a single copy of H3-H4 tetramer. To avoid the 'extra' copies of H3-H4 and the similar sedimentation of binary and ternary complexes (as seen in Fig. 3.5C), we again made use of TM-H3-H4. TM-H3-H4 was titrated against a 1:0.5 preformed mixture of Vps75 with RTT109 (Fig. 3.5D). Addition of 0.5 molar equivalents of TM-H3-H4 causes a clear increase
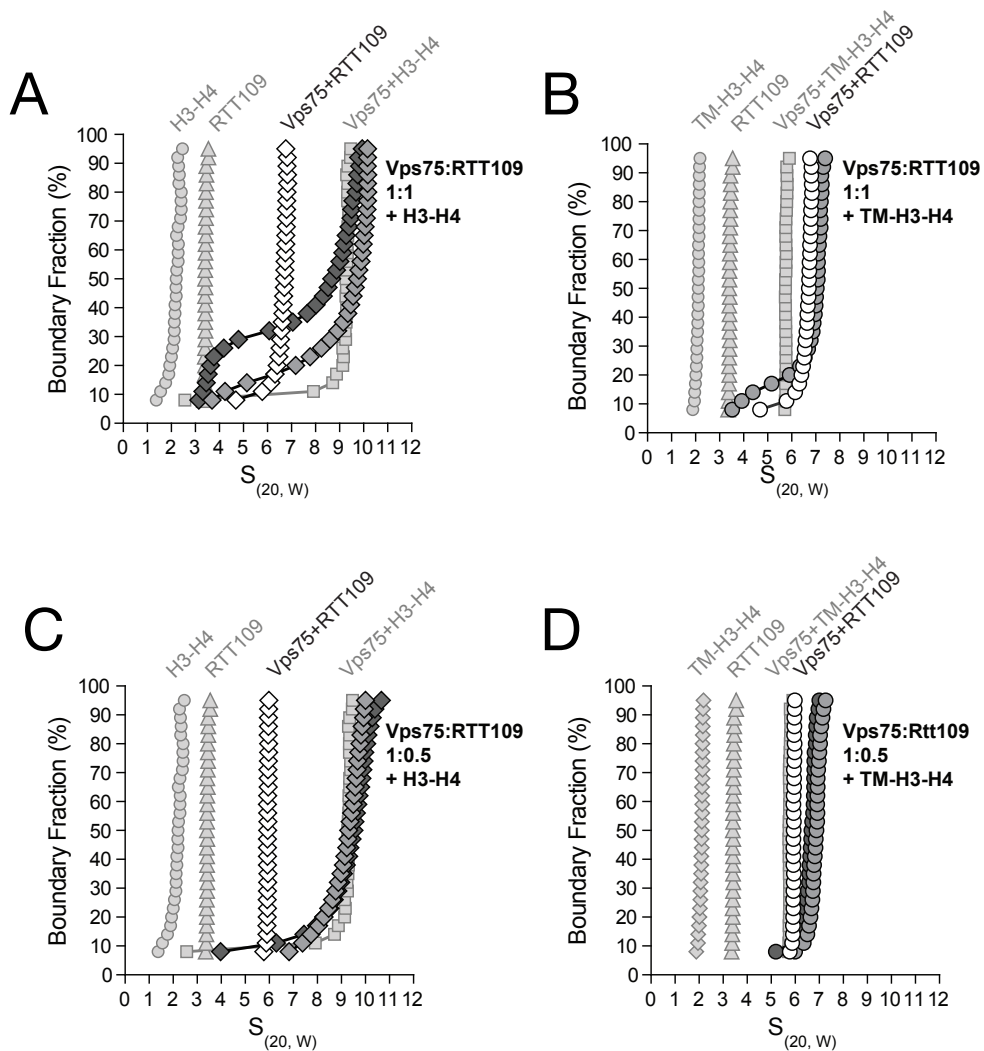
Figure 3.5. The Vps75 Dimer Simultaneously Binds One RTT109 and One H3-H4
Sedimentation velocity of complexes with Vps75, RTT109 and H3-H4 (A, C) or TM-H3-H4 (B, D). Vps75 and RTT109 were mixed 1:1 (A-B) or 1:0.5 (C-D) at 150 mM NaCl. Vps75 with RTT109 is shown in white, while Vps75 with RTT109 and 0.5 or 1 molar equivalent of histones is shown in light grey or grey respectively. For reference, plots are also shown for H3-H4 (faded circles), TM-H3-H4 (faded diamonds), RTT109 (faded triangles) and a 1:1 mix of Vps75 or Vps75-TM with H3-H4 (faded squares).

66

in sedimentation compared to Vps75 in complex with H3-H4, or Vps75 in complex with RTT109. Unlike other mixed samples, the sedimentation plot is also vertical, suggesting a homogeneous mixture with little to no unbound components or exchanging species. Similar to H3-H4, increasing TM-H3-H4 to 1.0 molar equivalent does not further increase the sedimentation, but does create a small tail likely due to unbound H3-H4. Altogether, these results strongly suggest that the stoichiometry of the complex between Vps75, RTT109 and H3-H4 is 1:0.5:0.5. In other words, the Vps75 dimer simultaneously binds one copy of RTT109 and one copy of H3-H4. It seems that the complex is most stable in this asymmetric configuration.

3.5 - Discussion:

Characterizing the interactions between histones, histone chaperones, and histone acetyltransferases is likely to provide key insights into chromatin regulation as each one can be linked to several diseases. Recent work studying the stoichiometry between histone chaperones and their histone cargo has created confusion due to conflicting results [45, 57, 97]. Like Nap1, past evidence suggests that one Vps75 dimer interacts with two core histone dimers [97]. But this has recently been challenged suggesting that both Nap1 and Vps75 can self-associate into higher order structures while still binding their histone cargo [109]. Determining the correct stoichiometry for Vps75 and its histone cargo is essential when trying to understand processes such as Rtt109 acetylation, as the selectivity of acetylation could be based on whether Rtt109 interacts with histone dimers or histone tetramers [45, 46, 57, 58]. In this study, we used sedimentation velocity analytical ultracentrifugation (SV-AUC) and SEC-MALS to quantitatively shed light on the complex interactions of Vps75, core histones H2A-H2B and H3-H4, and Rtt109.

Solution states of Nap1 have previously been reported using SV-AUC, but this has yet to be done with Vps75 [52, 62]. We therefore used SV-AUC to confirm previous reports that both Nap1 and Vps75 self-associate at low ionic strengths [46, 62]. In agreement with the published literature, we observe sedimentation profiles that are consistent with a dimeric species at 300 mM

NaCl and a tetrameric species at 150 mM NaCl (Fig. 3.1A, 2A) [46, 62]. Using two dimensional spectrum analysis (2DSA) to obtain accurate molecular masses, we were able to further confirm that Vps75 primarily adopts a dimeric structure at 300 mM NaCl and a tetrameric structure at 150 mM NaCl (Table S3.1) [71, 78].

It has been suggested that a Vps75 tetramer is capable of binding histones at low ionic strength [45]. Using SV-AUC we characterized the interactions between Vps75 and histones H2A-H2B or H3-H4 at different ionic strengths. Unlike Nap1, we found Vps75 binds histones H2A-H2B asymmetrically meaning it primarily forms complexes with either a 2:1 or 2:2 stoichiometry based on ionic strength whereas Nap1 forms complexes with a 2:2 stoichiometry at all ionic strengths tested. Interestingly, we found Vps75 tetramer will not split into dimers when sub-saturating amounts of H2A-H2B is added at low ionic strength. Under these conditions, we found the Vps75 tetramer will bind two H2A-H2B dimers, but then as H2A-H2B is increased, the Vps75 tetramer will split forming 2:2 Vps75:H2A-H2B complexes.

Characterizing Vps75 with H3-H4 was less clear than H2A-H2B. Similar to previously published results [45], we observed addition of H3-H4 to Vps75 formed complexes with a stoichiometry greater than 2:2 Vps75:H3-H4. It has been speculated these complexes could be two Vps75 dimers bridged together by a H3-H4 tetramer [45]. We were able to test this by using a mutant of Vps75 that is unable to form tetramers. If two Vps75 dimers are bridged together by a H3-H4 tetramer, we wouldn't expect to see a change in sedimentation when using the tetramer mutant of Vps75. We also would expect to see a difference in sedimentation between the Vps75:H2A-H2B complexes and the Vps75:H3-H4 complexes. This is exactly what we observed, the complexes formed between Vps75-TM and H2A-H2B sediment at ~5.5 S whereas both the Vps75-TM:H3-H4 and WT-Vps75:H3-H4 complexes sediment at ~7 S (Compare Fig 3.1 and 3.2). The fact that H2-H2B is unable to bridge two Vps75 dimers, whereas the H3-H4 tetramer can, indicates the Vps75 dimer interacts with only one of the two H3-H4 dimers.

The asymmetric binding observed using different ionic strengths between Vps75 and histones still left us asking what are the large complexes (S-value of ~9.5) that form at 150 mM NaCl? Knowing that a Vps75 tetramer in complex with one histone dimer sediments at ~5.5 S while two histone dimers (or one tetramer) sediments at ~7 S, along with these large complexes only form with H3-H4 and not H2A-H2B, we speculated that these complexes consist of two H3-H4 tetramers and one Vps75 tetramer. To test if we were correct, we used a mutant of H3-H4 unable to form tetramers. Similar to H2A-H2B, addition of sub-saturating amounts of H3-H4-TM to Vps75 at low ionic strength formed complexes consistent with Vps75 remaining a tetramer, whereas saturating amounts of H3-H4-TM split the Vps75 tetramer and formed complexes with a sedimentation coefficient of ~5.5 S (Fig 3.2F). Together we conclude that a Vps75 dimer binds histone asymmetrically based on ionic strength with two distinct binding sites that are capable of binding either two histone dimers or two histone tetramers. When Vps75 dimer binds two histone H3-H4 tetramers, the second copy of H3-H4 in each tetramer is then capable of interacting with a second Vps75 dimer.

One of the many roles of Vps75 is also stimulating H3-H4 acetylation in the presence of histone acetyltransferase Rtt109 (Reviewed in [109]). The binding interactions between Rtt109 and Vps75 have been investigated, but the stoichiometry for this interaction is unclear. Crystal structures have been solved of the complex indicating that Vps75 and Rtt109 bind in either a 2:2 or 2:1 stoichiometry [85, 98]. Using a combination of SEC-MALS and SV-AUC we were able gain insight into these interactions in solution, by determining the stoichiometry at different ionic strengths. Similar to histone binding, we found Vps75 also binds Rtt109 asymmetrically as it formed both 2:1 and 2:2 Vps75:Rtt109 complexes based on ionic strength confirming that the stoichiometry determined from both crystal structures are correct (Fig 3.4, Table S3.1F-G) [85, 98]. The difference in the van Holde-Weischet plots between the different ionic strengths also indicates that Rtt109, like histones, splits the Vps75 tetramer and binds one Vps75 dimer. Unlike histones, sub-saturating amounts of Rtt109 do not form large complexes when bound to the

69

Vps75 tetramer. We also observed that Rtt109 does not form stable complexes with H3-H4 dimer or tetramer in the absence of a histone chaperone such as Vps75 (Fig S3.3).

Since we found Rtt109 does not stably interact with H3-H4 (Fig. S3B-C), we looked at how H3-H4 impacted the Vps75:Rtt109 complex. We found when H3-H4 was added to preformed Vps75:Rtt109 complexes with a stoichiometry of 2:2, the sedimentation coefficient increased along with the appearance of unbound Rtt109. The amount of unbound Rtt109 was drastically reduced when using preformed Vps75:Rtt109 complexes with a 2:1 stoichiometry suggesting H3-H4 outcompetes the second Rtt109 and forms a ternary complex of one Vps75 dimer, one Rtt109, and one H3-H4.

One variable that was still a bit of a mystery was the state of H3-H4. Was it binding the complex as a dimer or tetramer? From our previous experiments we concluded the H3-H4 tetramer does in fact bind Vps75 as larger sedimentation coefficients were observed when compared to TM-H3-H4 (Fig. 3.1E, Fig. 3.2F). Using TM-H3-H4 in place of wild type, we repeated these experiments adding TM-H3-H4 to the Vps75:Rtt109 complex and observed similar results where one Rtt109 was displaced from the 2:2 Vps75:Rtt109 complex in the presence of H3-H4. We also observed a decrease in the sedimentation coefficient when using TM-H3-H4 compared to WT H3-H4, suggesting that only one copy of TM-H3-H4 bound to the Vps75:Rtt109 complex. Taken together, our data indicate that both Rtt109 and H3-H4 have the ability to split the Vps75 tetramer into a dimeric species with the stoichiometry varying between a 2:2 and 2:1 complex. The addition of H3-H4 to the Vps75-Rtt109 complex displaces one Rtt109, forming a ternary complex that contains one Vps75 dimer, one Rtt109, and one H3-H4 tetramer.

It has been shown that residue specific acetylation of H3 by Rtt109 is altered by which histone chaperone is bound. Vps75 and will cause Rtt109 to acetylate different H3 residues than Asf1 individually, but when all three are in complex with H3-H4 the activity of Rtt109 is enhanced with the mechanism of why still unclear [91]. Our work provides a biochemical understanding of how these complexes come together showing that Vps75 is capable of binding one Rtt109 and

one H3-H4 (tetramer or dimer), with Vps75 only directly interacting with one H3-H4 dimer leaving the second H3-H4 dimer open to interact with other proteins such as a second Vps75 dimer or Asf1. With Asf1 splitting H3-H4 tetramer into dimers, the enhanced activity of Rtt109 could be due to a more efficient delivery system as Asf1 makes H3-H4 more accessible. Similarly, the difference in activity between Asf1 and Vps75 could be due to the different conformations resulting in altered accessibility of H3-H4 to Rtt109, based on whether H3-H4 exists as a tetramer or dimer. Clearly, much remains to be learned on how these chaperones, acetyltransferases, and histones come together and their role in regulating chromatin dynamics.

Chapter 4 – Expanding the capabilities of AUC through improved analysis and fluorescence detection

4.1 - Introduction to analytical ultracentrifugation

4.1.1 - Brief History of AUC

Analytical ultracentrifugation (AUC) is an integral instrument in many fields including biochemistry, biophysics, and pharmaceuticals as one of the most versatile techniques for characterizing the solution-state behavior of macromolecules. Relying only on the principle of mass and fundamental laws of gravity, AUC provides precision and accuracy when characterizing size, shape, and homogeneity of macromolecules and macromolecular interactions. With the ability to characterize macromolecules from a few hundred to several hundred-million Daltons in mass, AUC is the ideal technique for many applications.

The concept of centrifugation has been around for centuries dating back to the 1700's when an English military engineer invented a whirling arm apparatus to determine drag. It wasn't until the late 1800's where it was used as a separation technique to separate cream from milk. In the 1920's a Swedish scientist named Theodore Svedberg came up with the conception of AUC while visiting the University of Wisconsin. He devised a method to measure the size distribution of colloids by applying an intense centrifugal field while monitoring the motion of the concentration boundary using optical absorbance. After several failed attempts, Svedberg built the first successful model in 1924 [110, 111]. Using the drive unit from a cream separator, Svedberg was able to generate a centrifugal field intense enough to sediment the colloids. Svedberg's contribution to building the first AUC along with laying down the theoretical foundation for sedimentation earned him the Nobel prize in 1926 [112].

The first vacuum ultracentrifuge was invented by Edward Pickel who later cofounded Spinco in 1946 (Spinco was later sold to Beckman Coulter). Spinco produced the first commercially available Model L ultracentrifuges and Model E analytical ultracentrifuge. With the

development of the Spinco Model E in 1950, AUC climaxed with thousands of institutions using the Model E resulting in a vast amount of information accumulated in the 60's and 70's regarding protein size, shape, and interactions. Although many associate analytical ultracentrifugation with advances in understanding protein structure, it also led to advancements in nucleic acids. Specifically, Vinograd and colleagues developed density gradient equilibrium to examine DNA using the analytical ultracentrifuge [113]. Using this technique, they looked at pH-induced conformational changes of polyoma DNA that led to the discovery of supercoiled DNA [114].

The Model E analytical ultracentrifuge was a very large analog device that was difficult to use and maintain. Even with the difficulties, it was the instrument of choice for most institutions when characterizing proteins until the development of simpler and cheaper techniques such as size-exclusion chromatography and gel electrophoresis. These simpler techniques, although not as accurate as AUC, combined with the lack of technological advances and difficulties associated with the Model E, caused a rapid decline in the use of AUC. In 1992 Beckman Coulter introduced the Proteomelab XL-A and in 1997 the Proteomelab XL-I, causing a resurgence in the technique. The new models used a much smaller footprint than the Model E, were much easier to use and maintain, and included improved optics. With the new hardware, the software also evolved leading to improved user interface and analysis methods. Like the Model E before it, the Proteomelab XL series has now become outdated, leading to the development of new optics that allow multi-wavelength detection. Although several groups have built their own multi-wavelength detection systems, these won't be commercially available until the release of Beckman Coulter's new Optima AUC and the CFA developed by Spin Analytical.

4.1.2 - Basic sedimentation theory

AUC experiments can be performed using two fundamentally different methods, sedimentation equilibrium (SE) and sedimentation velocity (SV). Historically, these two complementary methods provide distinctly different information, as SV provides first-principles

hydrodynamic information about size and shape, and SE provides first-principles thermodynamic information on buoyant molecular mass, stoichiometry, and association constants [115, 116]. In both experiments, macromolecules are exposed to a centrifugal field causing redistribution of molecules and forming a concentration boundary. Sedimentation velocity monitors the rate at which this concentration boundary moves whereas sedimentation equilibrium monitors the distribution of the concentration boundary when an equilibrium is reached between two opposing transport processes, sedimentation and diffusion. With advancements in optical detection and data analysis, it is now possible to obtain SE information using SV with the added benefits of also obtaining sedimentation coefficients and hydrodynamic information. As our lab primarily uses SV, my main focus in this chapter will be SV.

4.1.3 - Sedimentation velocity

Sedimentation occurs during a sedimentation velocity experiment due to a gravitational field applied to the macromolecule [117, 118]. There are three forces that act on the molecule (Fig. 4.1). The first, centrifugal force (F_c), is the force on the molecule due to the gravitation field and is proportional to the mass of a single particle (m) and acceleration (Eqn. 1). As we primarily use relative molar mass (M) instead of the mass of a single particle (m), we can convert m to molar mass using Avogadro's number (N). The acceleration is determined by the rotor speed (ω^2) the distance the molecule is from the axis of rotation (r).

$$F_c = m\omega^2 r = \frac{M}{N}\omega^2 r \tag{1}$$

The second force that acts on the molecule is the buoyant force (F_b), which is the counterforce exerted on the molecule by the mass of the solvent (m_s) that is displaced as the particle sediments, as can be seen in equation 2.

$$F_b = -m_s\omega^2 r \tag{2}$$

The mass (m) can be obtained from eqn 3 if both the solvent density (ρ) and partial specific

$$F_b = \omega^2 r m_s - (buoyancy)$$
$$F_d = -fv - (viscous\ drag)$$

$$constant\ velocity = v$$
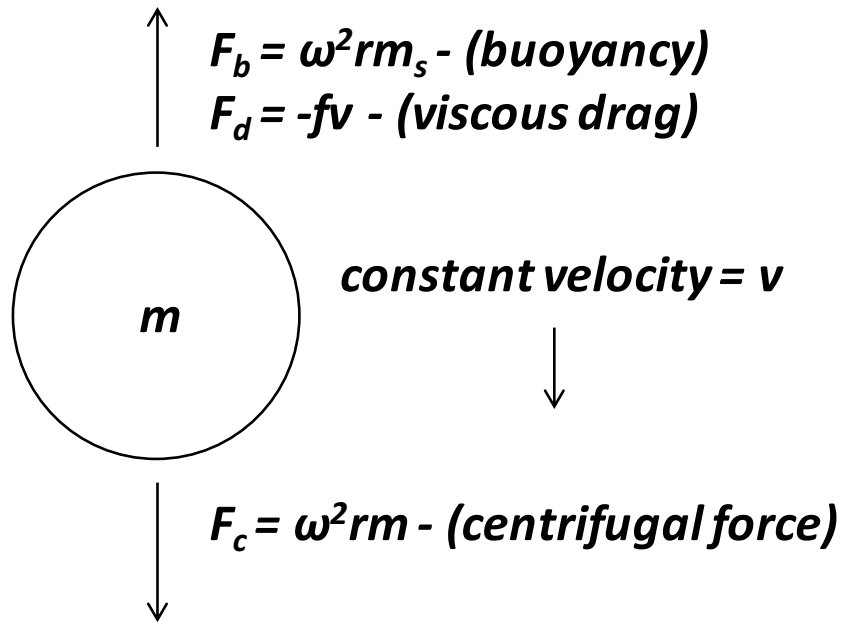
$$F_c = \omega^2 r m - (centrifugal\ force)$$

Figure 4.1. Forces acting on a molecule during sedimentation
Three forces act upon a molecule during sedimentation, centrifugal force (F_c), buoyant force (F_b), and viscous drag (F_d). At constant velocity, the net force is equal to 0, therefore the forces balance out.

volume ($\bar{v}$) are known. The partial specific volume is the volume in mL that each gram of solute occupies in solution. Theoretical values for the partial specific volume can be calculated based on the amino acid sequence for each species, which may not always be accurate as it is dependent on factors such as buffer conditions, overall charge of the species, and interactions. Accurate partial specific volumes are critical as a 1% error will lead to a 3% error in the obtained molecular mass [119].

$$m_s = m\bar{v}\rho = \frac{M}{N}\bar{v}\rho \tag{3}$$

The third force exerted on the molecule is the frictional force (F_d) due to the frictional drag the molecule experiences as it sediments through the viscous fluid:

$$F_d = -fv \tag{4}$$

where f is the frictional coefficient that is based on the molecule's shape and v is the velocity at which the molecule moves through the cell. Once the sample reaches terminal velocity the velocity becomes constant, there can be no net force, resulting in the sum of the three forces to equal 0:

$$F_C + F_b + F_d = 0 \tag{5}$$

By substituting the mass of the solvent (m_s) with the molecules mass (m_p) and applying it for each of the forces we can get:

$$\frac{M}{N}\omega^2 r - \frac{M}{N}\bar{v}\rho\omega^2 r - fv = 0 \tag{6}$$

Further rearrangement placing all the terms that relate to the molecule on the left side and the experimental condition terms on the right side results in the equation for sedimentation:

$$\frac{M(1-\bar{v}\rho)}{Nf} = \frac{v}{\omega^2 r} \equiv s \tag{7}$$

with the term ($\frac{v}{\omega^2 r}$) equaling the velocity of the particle per unit gravitational acceleration; otherwise known as the sedimentation coefficient (s). From the equation 7 it becomes evident that sedimentation is directly proportional to the molar mass (M) and inversely proportional to the

76

frictional coefficient (*f*). Even though equation 7 displays molar mass, it is not possible to accurately determine the molar mass without knowledge of the frictional coefficient.

During a sedimentation velocity experiment the solute experiences two different transport processes that are independent of one another. The first, sedimentation due to the centrifugal force, causes the molecules to sediment towards the bottom of the cell (Fig.4. 2). As the molecules sediment, a boundary is formed between the depleted region and the sedimenting molecules (Fig. 4.2). This boundary can spread due to the second transport process - diffusion (Fig. 4.3A). Since the net force applied to the molecules is zero, the boundary spreading is independent of sedimentation (Fig. 4.3B). By monitoring both the shape and motion of the boundary as it moves down the cell both the sedimentation coefficient and the diffusion coefficient (*D*) can be determined. The Stokes-Einstein relationship states that diffusion, like sedimentation, is also inversely proportional to the molecule's frictional properties as can be seen here [120]:

$$D = \frac{RT}{Nf}$$
(8)

The ratio of these two transport processes, termed the Svedberg equation (equation 9) [120], removes the unknown frictional component, leaving molar mass (*M*) as the only variable that needs to be determined, as *s/D* are transport processes monitored by the AUC while partial specific volume and density can be determined theoretically or through measurement:

$$\frac{s}{D} = \frac{M(1 - \overline{v}\rho)}{RT}$$
(9)

Rearrangement of equation 9 allows us to solve for mass:

$$M = \frac{sRT}{D(1 - \overline{v}\rho)}$$
(10)

Descriptions of both transport processes, sedimentation and diffusion, in a sector-shaped cell can be explained using the Lamm equation [121]:

$$\frac{\delta C}{\delta t} = \frac{1}{r}\frac{\delta}{\delta r}\left(s\omega^2 rC - Dr\frac{\delta C}{\delta r}\right)$$
(11)
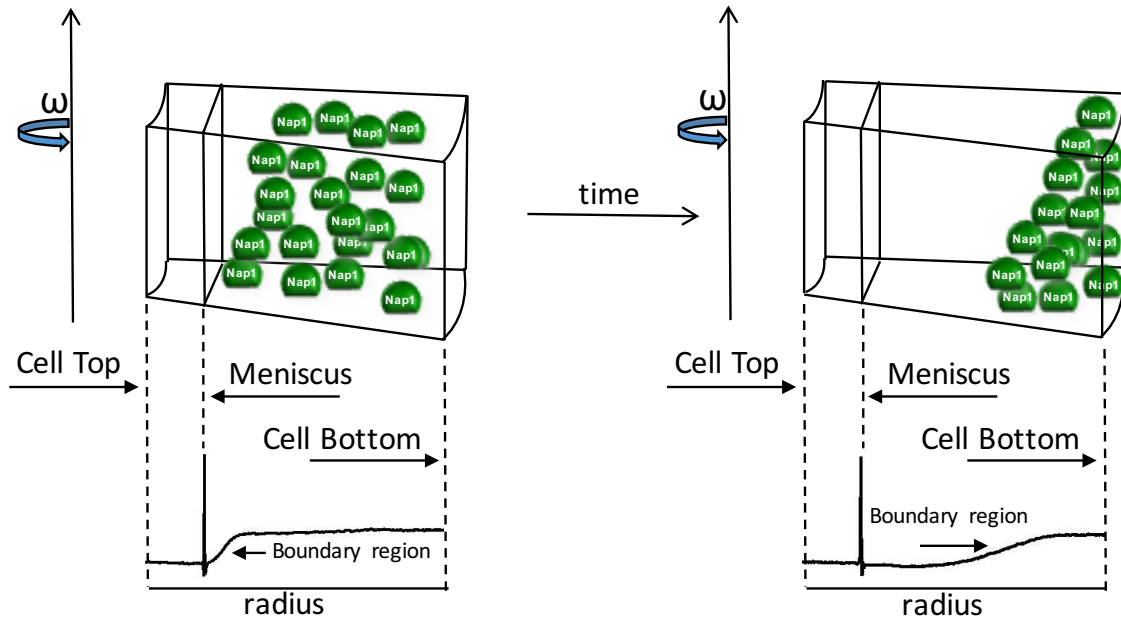
Figure 4.2. Boundary formation due to sedimentation
During sedimentation the sample sediments from the meniscus to the bottom of the cell over time. During sedimentation a boundary is created between the depleted region and the highly concentrated region (illustrations showing boundary region are scans taken from a yNap1 sedimentation velocity experiment). This boundary can be measured using either absorbance, interference, or fluorescence.

where C is the concentration as a function of radius (r) and time (t), s and D are the sedimentation and diffusion coefficients, and ω is the angular velocity of the rotor. By modeling the entire concentration boundary, the Lamm equation describes both sedimentation as it concentrates the solute near the outer radius of the cell and diffusion as it tries to equalize the solute concentration throughout the cell [117]. The Lamm equation was initially used to describe individual non-interacting solutes, but due to the evolution of software analysis, it can now be used to describe heterogeneous mixtures along with associating systems [71, 77, 122-124].

4.1.4 - Sedimentation equilibrium

Sedimentation equilibrium has always been the gold standard in molecular mass/stoichiometry determination [116, 125]. Unlike other methods such as size-exclusion chromatography, which are relative methods, both sedimentation equilibrium and sedimentation velocity are absolute methods as they do not require calibration standards. Similar to sedimentation velocity, sedimentation equilibrium monitors the concentration profile. Unlike sedimentation velocity experiments where the concentration boundary is measured as a function of time, sedimentation equilibrium experiments measure the concentration boundary as a function of radius, and is therefore invariant of time. When an equilibrium is reached between the two transport properties, sedimentation and diffusion, the position of the boundary is recorded. Using a variation of the Lamm equation (equation 11), this concentration boundary can be modeled:

$$s\omega^2 rC - D\frac{\delta C}{\delta r} = 0 \tag{12}$$

As the above equation shows, the net transport is zero resulting in the sedimentation transport process equaling the diffusion transport process. Experimentally this is achieved by producing a centrifugal force great enough to cause sedimentation, but not high enough to cause the sample to pellet. Once equilibrium has been reached, the solute's concentration increases exponentially towards the bottom of the cell. Since diffusion is proportional to concentration, the exponential

can be shifted using different concentrations. Alternatively, since sedimentation is proportional to the centrifugal force, the exponential can also be shifted by using different speeds. This exponential can then be fitted using the following equation:

$$M = \frac{2RT}{(1-\bar{v}\rho)\omega^2} * \frac{\delta(lnc)}{\delta r^2}$$

(13)

where *M* is the molar mass of the molecule. Although this produces a molar mass, it is dependent on both angular velocity (ω) and concentration. Therefore, performing several runs varying concentration and speed, and plotting the log (*concentration*) vs (*radius*)^2 will yield a slope representing a molar mass with increased accuracy [126].

4.2 - Analytical ultracentrifugation instrumentation and optical systems

The current Beckman Proteomelab XL-A/I series analytical ultracentrifuges are based on the Optima XL ultracentrifuge with the addition of an optical system that monitors either absorbance or interference. Similar to the ultracentrifuges these AUCs are based off, they require accurately controlled speed and temperature. With the added optical system, it is possible to accurately record the concentration distribution of the sample while spinning at speeds of up to 60,000 rpm with a temperature range of $0 - 40^o$ C. At such, high angular velocities frictional heating and turbulence can occur, therefore the rotor is spun in a vacuum chamber to minimize these effects.

Analytical ultracentrifuges are capable of spinning up to 60,000 rpm, which translates into a centrifugal force of 250,000 x g. This means that a mass of 1 gram would experience an apparent weight of 250 kg. Besides the need to withstand this amount of force, the rotor must also allow the passage of light. The two available rotors (4 and 8 hole), are made of titanium house the cells containing samples. These cells are made up of a sector-shaped centerpieces sandwiched between two windows (quartz or sapphire). Depending on the experiment being performed,
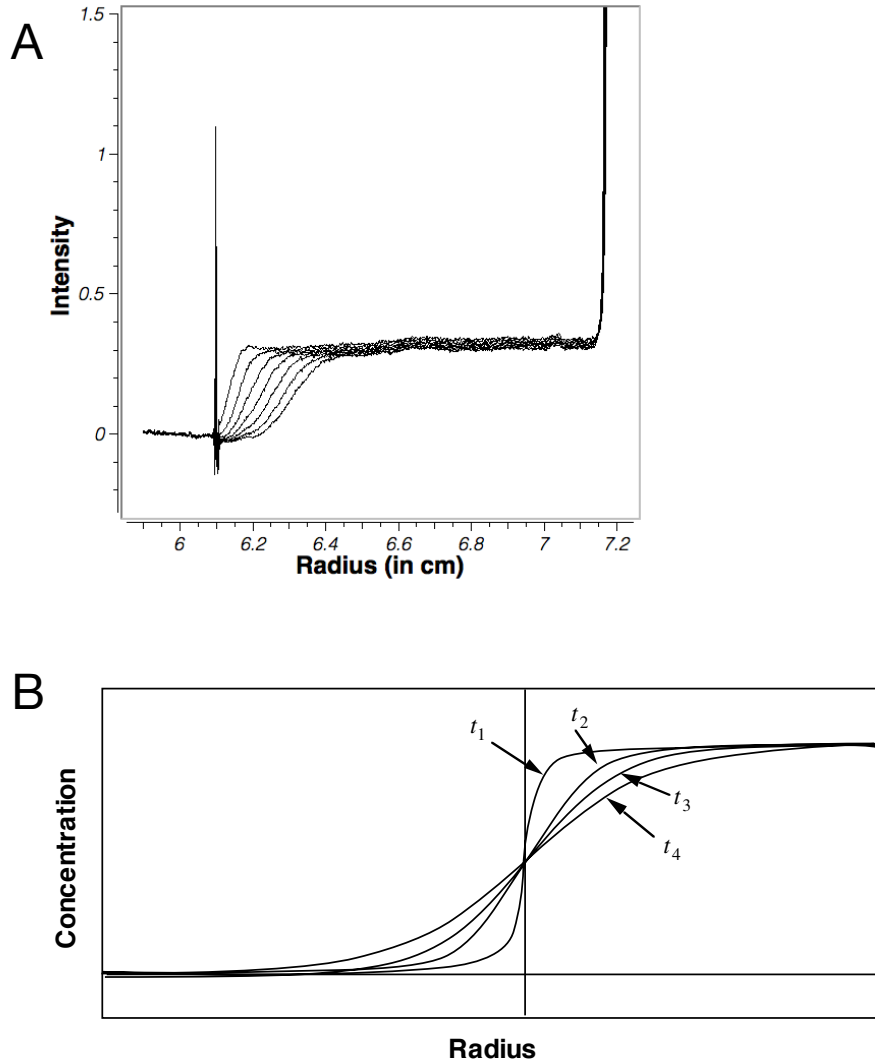
Figure 4.3. Boundary formed during sedimentation is impacted by diffusion

A) As the sample sediments over time the shape of the boundary will spread due to diffusion. **B)** Sedimentation and diffusion are separate transport processes, therefore the shape of the boundary may change due to diffusion (compare t_1 to t_4), but the midpoint as a function of radius will remain the same (Figure B was taken from [2, 3] with permission from Beckman).

several different centerpieces are available. Our lab primarily uses 2-channel sector shaped centerpieces either made from titanium or reinforced epoxy. These 2-channel centerpieces are ideal for sedimentation velocity as they provide a long path length resulting in higher resolution separation. Since sedimentation equilibrium occurs when an equilibrium is reached between the sedimentation and diffusion transport processes that occur towards the bottom of the cell, a shorter path length is ideal to decrease the time it takes for this equilibrium to be reached. This is achieved by using 6-channel centerpieces, that also have the additional benefit of holding more samples. No matter which centerpiece is used, it is essential for the centerpieces to be sector shaped as the sedimenting sample moves along radial lines. If the centerpiece contained compartments with parallel sides the sedimenting molecules would collide with the walls creating turbulence.

4.2.1 - Methods of Detection

As mentioned previously, the analytical ultracentrifuge uses an optical system to monitor a concentration distribution at different radial positions. There are currently two different optical systems available for the Beckman Coulter Proteomelab XL series analytical ultracentrifuges. The XL-A is equipped with UV/Vis absorbance optics (Fig 4.4) while the XL-I comes equipped with both UV/Vis absorbance optics and Rayleigh interference optics. Rayleigh interference optics are ideal for non-absorbing samples as they measure the refractive index. An additional fluorescent detection system (FDS) made by Aviv is also available for either instrument. All three optical systems are complementary and have strengths and weaknesses. Since our lab primarily uses a XL-A with the additional Aviv FDS, these two detection systems will be discussed here.

4.2.1.1 - Absorbance

Absorbance optics are the most widely used system due to the broad wavelength range, ease of use, and broad detection range from ~0.1 OD to 1.0 OD (Fig. 4.4). The XL-A/I instruments
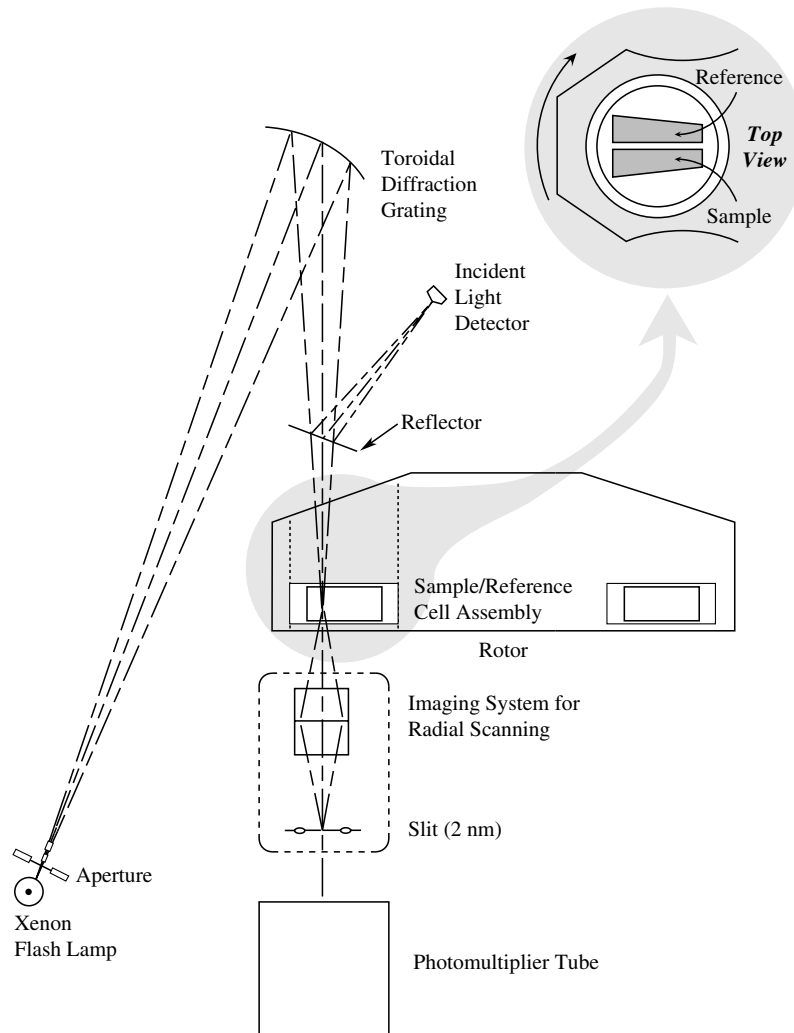
Figure 4.4. Schematic of the Beckman Coulter XL series absorbance optical system
The light path in an absorbance optical system of the current Beckman Coulter XL-A/I. A xenon lamp allows the use of wavelengths between 190-800 nm, with the monochromator yielding specific wavelengths. The light then passes through the sectors of the cell (inset above) into a slit below that moves allowing for measurement at different radial positions (Figure taken from [2]).

are equipped with a double-beam spectrophotometer that monitors both sample and reference channels of the cell simultaneously. The Beer-Lambert law is used to determine concentration as the absorbance signal is directly proportional to the solute concentration:

$$A = \varepsilon c l \tag{13}$$

with (*A*) being the absorbance signal, epsilon being the solute's extinction coefficient, (*c*) being the concentration, and (*l*) being the sample path length (typical centerpiece has a path length of 1.2 cm). Similar to stand-alone double beam spectrophotometers, the optical system simultaneously measures the difference between the reference channel and the sample channel. Although this corrects for absorbing buffers, it also causes an increase in the noise associated with the optical system due to measuring both channels. Because of this, we collect our data using intensity mode. The intensity (*I*) can then be converted to pseudo-absorbance ($A = \frac{I_o}{I}$) with the UltraScan software [78]. While some have reported the ability to place sample in the reference sector, essentially doubling the amount of samples being run, we have found that this causes the PMT to adjust throughout the run, creating large variations in the intensity.

4.2.1.2 - Fluorescence Detection

Currently the Aviv FDS is the only commercially available fluorescence detection system for the XL series analytical ultracentrifuges. It was originally developed by Tom Laue and then sold to Aviv Biomedical [127]. The FDS is equipped with a laser that excites at 488 nm with the emitted light then passing through a band-pass filter only allowing light in the 505 – 565 nm range. This, in theory, places a limitation on the fluorescent probes that can be used, as the excitation and emission wavelengths of FDS cannot be changed. In practice, selection of a good fluorophore, such as Alexa 488, that can conjugate to several different reactive groups, is resistant to photobleaching, and is insensitive to changes in pH will be the most ideal.

The FDS has several benefits over other modes of detections, such as high sensitivity (detection in the low nM to high pM range is possible), has high selectivity (only measures

fluorescently labeled molecules), high throughput (sample can also be placed in the reference channel doubling the number of samples per experiment), and rapid detection (simultaneously scans all cells) [115, 127-130].. The high sensitivity of the FDS, compared to absorption optics, opens the door to new applications such as detection and characterization of molecular interactions that either cannot be observed with the traditional optics or bind too tightly to obtain accurate binding affinities.

4.3 - Improved data analysis allows for both relative molecular mass and shape determination using sedimentation velocity

4.3.1 - Analysis using two-dimensional spectrum analysis (2DSA)

AUC analysis methods have rapidly evolved since the introduction of the Beckman Coulter XL series analytical ultracentrifuge. Although there are several different methods and programs available, the software packages most commonly cited in the literature are UltraScan and SEDFIT/SEDPHAT [78, 131, 132]. Until recently, our lab primarily used the van Holde–Weischet analysis method available in UltraScan [78, 131, 132]. This method provides a graphical representation of the data by plotting an integral sedimentation coefficient distribution, G(s) (Fig. 5). The main advantage of this method is its ability to separate the two transport processes; sedimentation and diffusion [133]. Sedimentation is proportional to the first power of time whereas diffusion is proportional to the square root of time. The van Holde-Weischet method extrapolates the sedimentation coefficient to infinite time, therefore minimizing the diffusion contribution as it is outweighed by the sedimentation transport process [74, 133]. Although this provides an excellent graphical representation of the homo/heterogeneity of the sample, it also has limitations due to minimizing the diffusion contribution that includes molecular mass and gross shape determination.

Since becoming involved in performing AUC experiments, I began to transition the lab from solely using the van Holde-Weischet analysis to a method that provides quantitative information

on additional parameters such as molecular mass, gross shape, and relative abundance of multi-component systems, while also providing sedimentation coefficients with improved accuracy. This is accomplished by using two-dimensional spectrum analysis (2DSA) coupled with Monte-Carlo analysis, which is now incorporated into the UltraScan analysis software [71, 72, 78, 134]. 2DSA provides a high-resolution analysis through the use of a dynamic grid method that fits the sedimentation and frictional ratio parameters. From equation 8, this is only possible by also modeling diffusion. Specifically, 2DSA builds a 2-D grid of frictional ratios and sedimentation coefficients in which a simulation is performed for each sedimentation and diffusion coefficient pair using the Lamm equation [71]. With non-negatively constrained least-squares (NNLS), each combination of the simulated solutions is fitted linearly to the experimental data [71, 135]. In our opinion, 2DSA is a superior method for both homogenous and heterogeneous samples because it models the entire boundary, does not assume a constant shape (f/f_o) for all species in the sample, and only requires input using the model-independent van Holde-Weischet analysis [71].

4.3.2 - Two dimensional spectrum analysis yields accurate relative molecular masses

Traditionally, when performing sedimentation velocity, high rotor speeds are suggested to increase the sedimentation resolution. While this is ideal when using van Holde-Weischet analysis, this is not the case for 2DSA as high rotor speeds decreases the diffusion resolution. In the case of heterogeneous samples, the experiment should ideally be performed at multiple speeds to collect the entire range of information, thereby yielding accurate molecular mass and shape information along with sedimentation coefficients for all species.

Brookes et al state 2DSA analysis not only provides accurate means for molecular mass determination, but also provides a higher level of accuracy for sedimentation coefficient determination when compared to using the van Holde-Weischet analysis [71]. Therefore, we wanted compare the accuracy of 2DSA and van Holde-Weischet analysis while also determining how factors such as heterogeneity, partial specific volume, and rotor speed impacted the accuracy

86

of molecular mass determination with either DNA or DNA-protein complexes. Using 601-207 DNA, we directly compared the sedimentation coefficients produced from these two analysis methods, and also determined the molecular mass accuracy obtained from 2DSA. Four replicates were performed varying either the DNA concentration or speed to determine the reproducibility of molecular mass using different conditions. Van Holde-Weischet analysis reveals that each of the replicates is homogenous, with sedimentation coefficients of ~5.8S (Fig. 4.5A). Increasing concentrations also allowed us to test for non-ideality (repulsive forces causing backward bending of vHW curve) which was not observed (Fig. 4.5B). With 2DSA analysis, we were able to determine molecular mass, gross shape, and sedimentation coefficients from the same data (Table 4.1). Our 601-207 DNA sample has a calculated molecular mass of ~128kDa. With 2DSA analysis, we determined molecular masses of our four replicates ranging from 123 kDa – 128.99 kDa, with a 4.5% variation. We also looked at the variation in sedimentation coefficients between van Holde-Weischet analysis and 2DSA. With the van Holde-Weischet analysis we determined a 3.59% variation between the four replicates compared to 0.70% variation using 2DSA (Table 4.1). Therefore, although van Holde-Weischet provides an excellent graphical representation of the data, 2DSA does in fact provide a higher level of accuracy while also aiding in van Holde-Weischet analysis by removing time and radial invariant noise.

We next investigated how heterogeneous mixtures would impact molecular mass accuracy by using the same 207-bp DNA with the addition of H2A-H2B histones. H2A-H2B was added to the DNA to create a 1:1 molar ratio and two replicates of SV-AUC were performed. Heterogeneity was determined from both van Holde-Weischet analysis and 2DSA-GA-MC (Fig 4.6A-C). Using 2DSA we obtained an average molecular mass of 150.99 kDa, in excellent agreement with the theoretical molecular mass for a 1:1 DNA-(H2A-H2B) of 155.58 kDa (Table 4.2). Similar to 207 DNA, we found a slight difference in sedimentation coefficients when using van Holde-Weischet analysis compared to 2DSA, with the values obtained from 2DSA having a lower standard
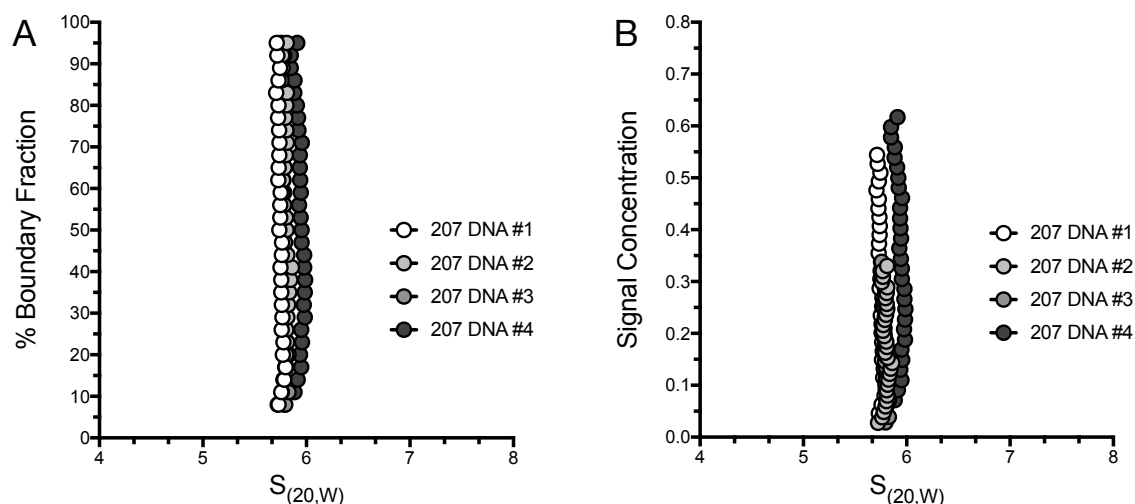
Figure 4.5. van Holde-Weischet analysis provides excellent graphical representation
van Holde-Weischet analysis of 601-207 DNA illustrates sample homogeneity and allows to represent the data either as **A)** fraction bound as a function of sedimentation or **B)** signal concentration as a function of sedimentation.

Table 4.1. Summary of van Holde-Weischet analysis and two-dimensional spectrum analysis of 601-207 DNA.

Sample	vHW $S_{20,W}$	2DSA $S_{20,W}$	f/f_o	Measured MW (Da) (Theoretical – 128,101)	Speed (rpm)	Signal Concentration (OD)
601-207 #1	5.79	5.73	3.32	126,120	35,000	0.3477
601-207 #2	5.74	5.77	3.30	126,600	30,000	0.3548
601-207 #3	5.95	5.75	3.26	123,280	30,000	0.6468
601-207 #4	5.81	5.74	3.36	128,990	35,000	0.5734
Average	5.82	5.75	3.31	126,248	N/A	N/A
Std Dev	0.09	0.02	0.04	2,342.92	N/A	N/A

deviation (compare Table 4.1 & 4.2). Addition of H2A-H2B caused slightly less accurate molecular masses when compared to DNA alone, which is likely caused by uncertainties in the partial specific volume (1% error in partial specific volume causes 3% error in MW) [2]. Measuring the partial specific volume with a densitometer would likely result in greater accuracy [136].

Lastly, we performed an experiment in which we added 3-fold molar excess of H2A-H2B over 601-207 DNA (Fig 4.7). Again, with two replicates, we observed what appeared to be homogenous curves using van Holde-Weischet analysis, with a slight difference in the sedimentation coefficients (Fig 4.7A). Pseudo-3D plots generated from 2DSA analysis revealed the presence of two species that weren't apparent from the van Holde-Weischet plot (Fig. 4.7). Although the van Holde-Weischet analysis generally provides a graphical representation of the data, it can be very challenging to distinguish two species with similar S values. Molecular masses were then obtained for each species using 2DSA with the first species having a molecular mass of 174.42 kDa and the second having a molecular mass of 181.52 kDa (Table 4.3). From these values, we conclude that the complex is likely a mixture of 1:1 (155.58 kDa) and 1:2 (183.28 kDa) DNA-H2AB complexes (Table 4.3). The decrease in molecular mass accuracy can again likely be attributed to the partial specific volume due to inability to assign an individual partial specific volume for each species.

4.3.3 – Analysis summary

Sedimentation velocity is an excellent method for characterizing macromolecules in solution. Traditionally sedimentation velocity was primarily used to determine hydrodynamic information such as size and shape, with sedimentation equilibrium providing information on molecular mass, stoichiometry, and association constants. With advancements in both AUC hardware and software analysis, it has become possible to obtain sedimentation equilibrium information using sedimentation velocity [71]. Using this methodology, we found that we could accurately determine the molecular mass of 601-207 DNA along with obtaining accurate

Figure 4.6. Graphical representations illustrating homogeneity
A) van Holde-Weischet analysis of 601-207 DNA + 1X H2A-H2B shows homogenous species. **B & C)** Pseudo-3D plots illustrating solute distributions for the 2DSA GA-Monte Carlo results of 601-207 DNA + 1X H2A-H2B confirm homogeneity for both replicates (#1 and #2).
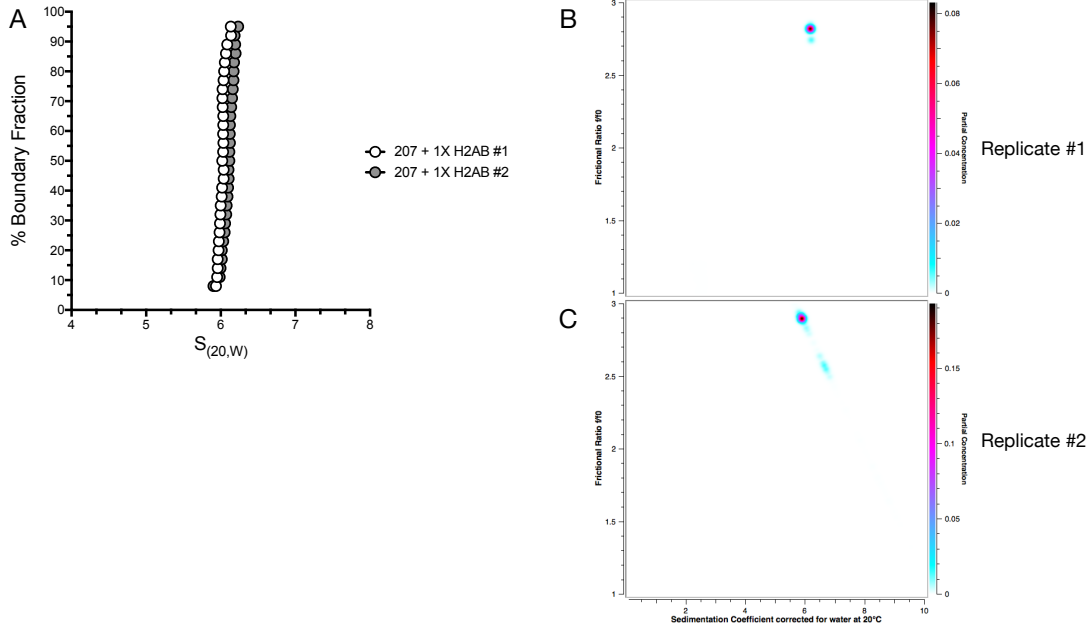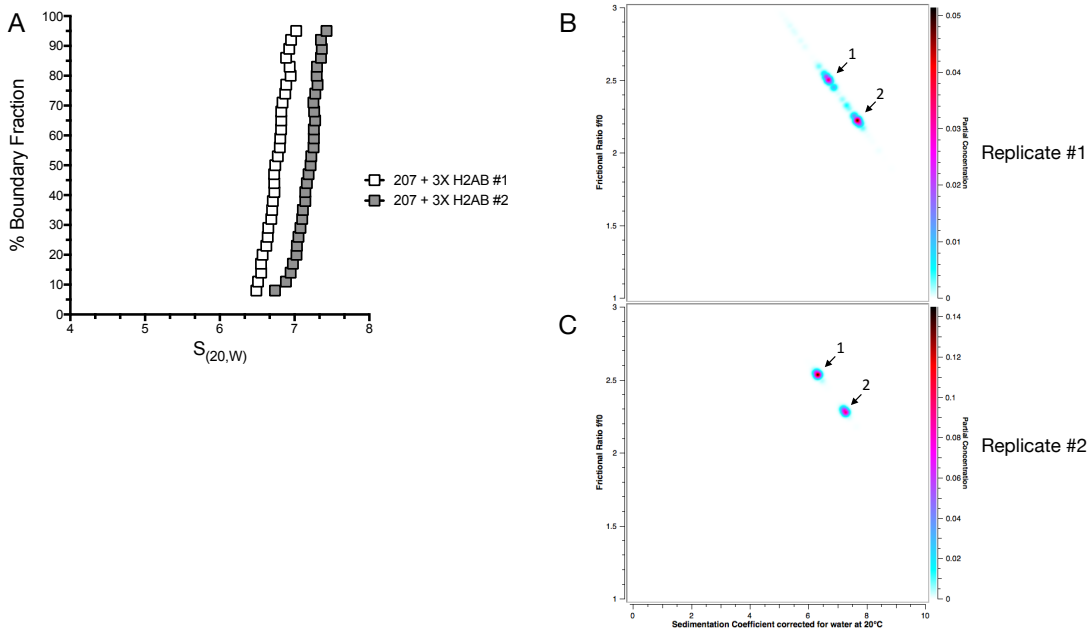

Figure 4.7. Graphical representations illustrating homogeneity
A) van Holde-Weischet analysis of 601-207 DNA + 3X H2A-H2B shows heterogeneous species. **B & C)** Pseudo-3D plots illustrating solute distributions for the 2DSA GA-Monte Carlo results of 601-207 DNA + 3X H2A-H2B confirm heterogeneity as two species are present for both replicates (#1 and #2).

Table 4.2. Summary of van Holde-Weischet analysis and two-dimensional spectrum analysis yielding results for $S_{20,W}$, *f/f$_o$*, and molecular mass of 601-207 DNA + 1X H2A-H2B.

	207 + 1X H2AB #1	207 + 1X H2AB #2	AVG/STDEV
vHW $S_{20,W}$	6.02	6.11	6.07 ± 0.06
2DSA $S_{20,W}$	5.91	5.89	5.90 ± 0.01
f/f$_o$	2.83	2.90	2.87 ± 0.05
Molecular Weight (Da)*	148830	153140	150985 ± 3047

*Theoretical mw for (1:1) DNA:H2A-H2B = 155809

hydrodynamic information. By varying both rotor speed and concentration, we were also able to confirm that neither impacted the overall sedimentation coefficients obtained (Table 4.1). Comparing sedimentation coefficients determined by either van Holde-Weischet analysis or 2DSA gave similar results with 2DSA being slightly more accurate (Table 4.1). We also found that heterogeneous mixtures impacted the accuracy of molecular mass determination for H2A-H2B:DNA complexes. The decrease in accuracy was proportional to the amount of H2A-H2B added, resulting in increased heterogeneity. This likely isn't due to the actual analysis, but due the inability to accurately assign partial specific volumes for each species. Overall, we determined that 2DSA analysis not only produced sedimentation coefficients with a higher level of accuracy than van Holde-Weischet analysis, but could also differentiate between species with similar sedimentation coefficients and mass. Therefore, a combination of both 2DSA and van Holde-Weischet analysis is ideal as 2DSA provides superior quantitative results whereas the van Holde-Weischet analysis provides an excellent graphical representation.

4.4 - Fluorescence Detection System (FDS) – a sensitive and selective method of molecular detection

4.4.1 - Introduction to fluorescence detection – Fluorescence vs absorbance

AUC provides first-principles hydrodynamic and thermodynamic information by monitoring a concentration boundary as a function of radius. The Beckman Coulter XL-A/I monitors this boundary using either absorbance optics or interference optics. Although these optics are widely used for characterization of macromolecules in solution, there are restrictions on the concentrations and complexity of the solutions being analyzed. The Aviv Fluorescence Detection System (FDS) increases the detection limit of the AUC by several orders of magnitude. This increased sensitivity over the traditional optics allows for the characterization of small quantities of materials along with the detection of high-affinity binding interactions, and in principle allows for the analysis of complex mixtures.

Both the absorbance and interference optics that come with the XL series AUCs monitors either the total absorbance or total change in refractive index of the solution. Although this technique is acceptable for many applications, it does pose challenges when dealing with complex mixtures of species having similar absorbance spectra or having similar hydrodynamic properties, making them virtually indistinguishable. By fluorescently labeling the species of interest, the FDS provides a level of selectivity that isn't offered with absorbance or interference, as only the labeled species will be detected. Although this method requires the addition of a fluorescent tag, and poses new challenges in both setup and analysis, the increased capabilities of this system make it ideal for complex mixtures and high affinity interactions.

4.4.2 - Sensitivity, selectivity, and high affinity interactions can be monitored using FDS

Although the FDS is an extremely powerful addition to the Beckman AUCs, likely due to the price and steep learning curve, its adoption has been slow. Therefore, publications illustrating its use are limited, requiring trial and error for determining the optimal setup and conditions with proteins being more challenging than DNA. Although DNA is quite robust and not prone to denaturing or aggregation on its own, proteins can be quite sensitive to both denaturing and aggregation. Most proteins used in our lab, especially histones, require optimal buffer conditions to retain their native state along with minimizing aggregation. At low nM concentrations, proteins, especially when fluorescently labeled, often have the tendency to "stick" to inert surfaces such as the epon centerpiece and quartz/sapphire windows found in AUC cells. Because of this, precautions are needed that otherwise wouldn't be necessary when performing absorbance runs at higher concentrations. Although higher concentrations increase sample consumption, they also often have stabilizing effects on the protein while minimizing loss due to "sticking."

To begin optimizing conditions using fluorescence-detected sedimentation velocity (FDS-SV), we began with yNap1, a protein that has been previously characterized by us using absorbance detected sedimentation velocity (AU-SV) [62]. yNap1 has a sedimentation coefficient

of 4.5 at 0.32 M ionic strength and oligomerizes into higher order species as the ionic strength is decreased (Fig. 4.8) [62]. Alexa 488 was conjugated to a cysteine mutant of yNap1 (cysteine mutant D201C does not appear to impact oligomerization or histone binding) using a maleimide linkage. Alexa 488 was chosen over other labels such as GFP or fluorescein because of its high fluorescence quantum yield, insensitivity to pH, and superior photostability. FDS-SV was performed using either 1nM or 5nM concentrations of 488-yNap1 at 0.32 M ionic strength to determine if the sedimentation coefficient obtained from absorbance optics using uM concentrations could be replicated (Fig. 4.8). Using van Holde-Weischet analysis, we found that 5 nM 488-yNap1 produced a good signal, and near perfect correspondence with the absorbance plot of yNap1. This was not the case when using 1 nM 488-yNap1, as the data was unusable producing negative sedimentation coefficients (Fig. 4.8). This could be caused by the protein either sticking to the glass windows or the epoxy centerpiece. The use of an inert carrier protein such as BSA, lysozyme, or κ-casein has been shown to minimize the effects due to sticking [130].

Our lab has previously characterized the yNap1-histone interactions through fluorescent quenching using similar concentrations of either labeled histones or Nap1. We therefore chose similar buffer conditions containing BSA [1]. Our group along with others have found that high concentrations of BSA contributes to the overall fluorescent signal, therefore, low concentrations were used that had little impact on the overall signal [128]. We found that 1 nM 488-yNap1 at 0.32 M ionic strength, in presence of 0.075 mg/mL of BSA, produced similar van Holde-Weischet plots as 5 nM 488-yNap1 without BSA (FDS) and 7.5 μM yNap1 (Abs) (Fig. 4.8). Since we did not observe an increase in the sedimentation coefficient with the presence of BSA, we also conclude BSA did not interact with yNap1 (Fig. 4.8). Although we found BSA to prevent sticking in our system, it is likely that these additives will need to be optimized individually for each system under investigation.

Zhao et al. found that FDS-SV is capable of detecting picomolar binding affinities using enhanced green fluorescent protein and anti-GFP IgG [128]. We set out to determine whether we
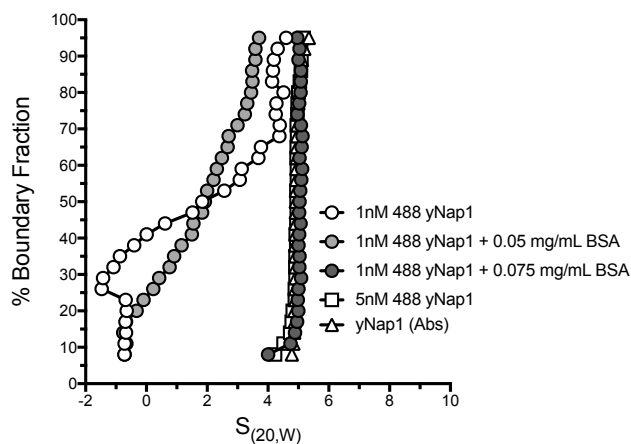
Figure 4.8. Optimization of buffer conditions is required for low nM detection
van Holde-Weischet analysis of different conditions tested to achieve optimal sensitivity when detecting 488 labeled yNap1. As a control, AU-SV was performed using unlabeled yNap1 (Abs).
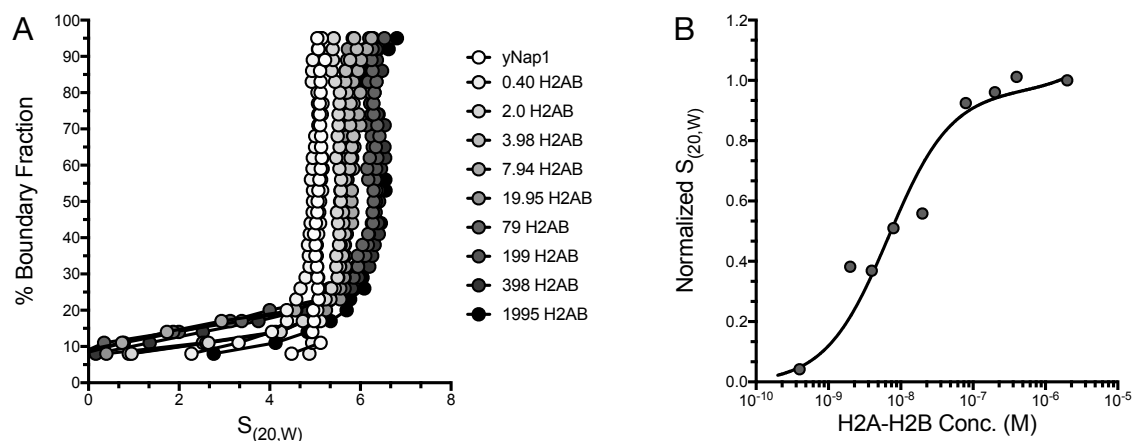
Figure 4.9. The Aviv Fluorescent Detection System (FDS) can be used to obtain low nM binding affinities
A) 1nM 488 yNap1 with increasing molar ratios of unlabeled H2A-H2B was used with FDS-SV and analyzed using the van Holde-Weischet analysis. **B)** Sedimentation data was plotted as a function of yNap1 concentration (nM) and fit using non-linear regression using GraphPad Prism to obtain a K_D of 6.77 ± 2.48 nM which agrees with our previously published data [1].

could detect nanomolar binding affinities using 488-yNap1 and H2A-H2B. Our lab has previously

shown that yNap1 binds H2A-H2B with low nanomolar affinity, using both fluorescence quenching

and Förster resonance energy transfer (FRET) [1, 60]. Using the conditions optimized for 1nM

488-yNap1, and taking advantage of the large number of samples that can be analyzed in a single

FDS-SV experiment, we prepared a series of samples containing 1n M 488-yNap1 with increasing

molar ratios of unlabeled H2A-H2B (Fig. 4.9A). One of the challenges associated with

fluorescence is maintaining a linear relationship between the fluorescence signal and

concentration, which may impact concentration dependent data such as association constants,

or in some cases, dissociation constants. Although it has been shown that the Aviv FDS maintains

a linear relationship up to 500 nM [137], we avoided this issue by keeping fluorescently labeled

yNap1 well below the K_D of yNap1:H2A-H2B.. Keeping the labeled probe well below the K_D and

then titrating H2A-H2B to concentrations well above the K_D, we can make the assumption that

yNap1$_{bound}$ is equal to yNap1$_{total}$, eliminating the need to know the exact concentration (eqn. 14).

The K_D can then be determined by monitoring the change in sedimentation, as it is proportional

to the fraction bound (*Fb*). Plotting the sedimentation coefficient as a function of H2A-H2B

concentration, the binding affinity was then determined with equation 14 using nonlinear

regression through GraphPad Prism (Fig. 4.9B).

$$yNap1 + (H2A - H2B) \leftrightharpoons yNap1 \cdot (H2A - H2B)$$
$$Fb = \frac{[H2A - H2B]}{([H2A - H2B] + K_D)} \tag{14}$$

Using this method, we determined yNap1 bound H2A-H2B with a K_D of 6.77 $\pm$ 2.48 nM, which is

in agreement with previous published quenching results of 7.8 nM [1, 60].

One of the major advantages to the fluorescent detection system compared to using either

absorbance or interference is the ability to monitor specific species that are tagged with a 488

fluorophore. This is especially useful when trying to monitor the interaction between very large

species and very small species as the overall change in sedimentation may be too small to
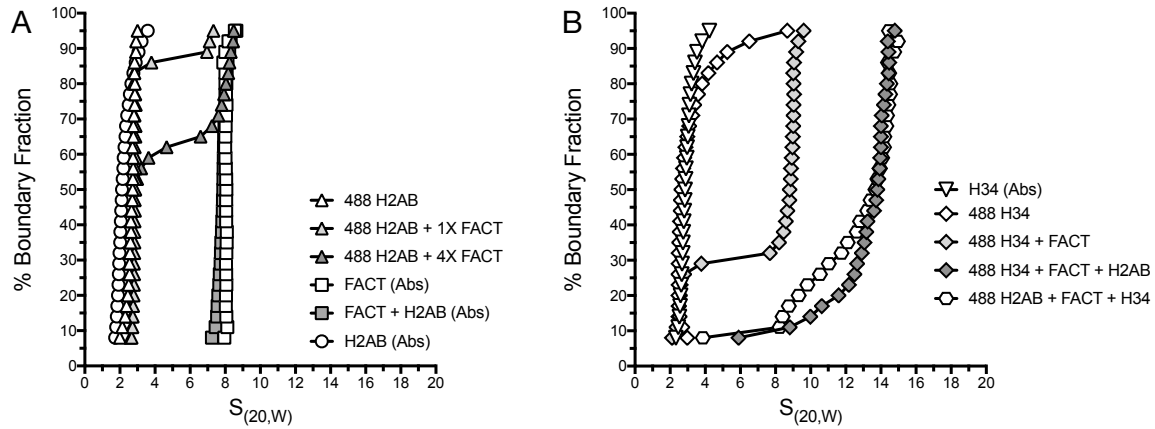
Figure 4.10. Aviv Fluorescent Detection System allows for both specificity and selectivity with excellent sensitivity

A) van Holde-Weischet analysis for FDS-SV that was performed monitoring the change in sedimentation of 488-(H2A-H2B) with increasing molar ratios of FACT. Data collected using absorbance optics shows minimal change between FACT and FACT+H2A-H2B whereas by following labeled H2A-H2B a significant change is observed using FDS-SV. **B)** FDS-SV confirmed that FACT can bind H2A-H2B and H3-H4 simultaneously.

observe. This was the case when H2A-H2B was added to the histone chaperone FACT[3] (facilitates chromatin transcription). Using SV-AUC, addition of H2A-H2B to FACT resulted in negligible changes in sedimentation, making it difficult to determine if complex formation has occurred (Fig. 4.10A). Using FDS-SV, FACT was added to 488-(H2A-H2B) at 1:1 or 1:4 molar ratios of 488-(H2A-H2B):FACT. With H2A-H2B being the only protein visible to the FDS, we could clearly observe that the addition of FACT caused a shift in sedimentation of labeled H2A-H2B that would otherwise have been indistinguishable using the absorbance optics (Fig. 4.10A).

The ability to specifically track individual species using FDS-SV has proven to be extremely valuable. FDS-SV allowed us to confirm biding that was otherwise not detectable using absorbance optics. This technique also allows us to validate binding interactions by separately labeling each of the binding partners. This was accomplished using FACT and core histones H2A-H2B and H3-H4. By monitoring 488-(H3-H4), we confirmed that H3-H4 and FACT interact (Fig. 4.10B). H2A-H2B was then added to determine whether both core histone complexes could simultaneously bind FACT (Fig. 4.11B). An increase in sedimentation when H2A-H2B was added indicates H2A-H2B bound the 488-(H3-H4)-FACT complex (Fig. 4.10B). Switching the label from H3-H4 to H2A-H2B validated that both core histones did in fact bind FACT (Fig. 4.10B). The sensitivity and selectivity of FDS-SV allows us to obtain pM to nM binding constants along with characterizing complex mixtures, which would not be possible using traditional detectors equipped on the current Beckman Coulter analytical ultracentrifuges.

4.5 - Conclusions

Analytical ultracentrifugation has been and will continue to be a powerful method to characterize macromolecules in solution. In particular, molecular mass, shape, and biological interactions can be characterized with greater accuracy than other techniques that require

---

[3] Tao Wang provided reagents along with experimental design for all experiments using FACT. Daniel Krzizike performed and analyzed all AUC experiments regarding FACT.

standards. Until recently, sedimentation equilibrium was the primary method of molecular mass determination, whereas sedimentation velocity was used to obtain hydrodynamic information. With advances in both computing and analysis software, sedimentation velocity can now be used in place of sedimentation equilibrium for many applications, with the advantage of providing more information in less time. By fitting both diffusion and sedimentation transport processes, accurate molecular mass determination is now possible using sedimentation velocity.

Accurate molecular mass determination from sedimentation velocity data is only possible by fitting both sedimentation and diffusion. This is quite complex and requires the use of two-dimensional spectral analysis coupled with a genetic algorithm and Monte Carlo analysis, all of which is available through the UltraScan software [71, 72, 78, 134]. Using this method, our lab has gone from primarily using AUC to determine homogeneity/heterogeneity with van Holde-Weischet analysis to accurately determining molecular masses and stoichiometry of DNA, proteins, protein-protein interactions, and protein-DNA interactions.

Limiting factors to SV-AUC are sensitivity and selectivity of the absorbance optics. The absorbance optics monitor anything in the cell that absorbs light at a selected wavelength, with a detection limit of ~0.1 – 1 OD. Therefore, the AUC can only detect low μM amounts of most proteins, eliminating the possibility of detecting nM binding affinities. With the lack of being able to detect specific solutes within a cell, the absorbance optics are incapable of distinguishing between absorbing species. This really becomes an issue when species sediment at similar rates or when monitoring interactions between a very large species and a very small species where the change in sedimentation is minimal. These limitations can be resolved with the optional Aviv fluorescence detection system that is commercially available for the XL series analytical ultracentrifuges. The FDS provides much greater sensitivity than the standard optics for the XL series as it can detect labeled molecules in the high pM to low nM range. This allows for detection of binding affinities in the pM to nM range that would otherwise not be possible with the absorbance optics as we have shown with yNap1 and histones H2A-H2B. The FDS is also highly

selective, as it will only detect solutes labeled with a fluorophore excitable at 488 nm. This makes it possible to follow specific solutes, resolving any issues that arise when two species sediment at similar rates, or when binding cannot be detected due to the overall change in sedimentation being minimal. This was shown with the histone chaperone FACT and core histones H2A-H2B and H3-H4.

We have shown that the current XL series AUC can be a very powerful instrument for characterizing macromolecules. Accurate molecular masses are highly dependent on the solutes partial specific volume and buffer density. As we have shown, for homogenous species we were able to achieve accurate molecular masses, but as the mixture became more heterogeneous the accuracy decreased, specifically, because it is not possible to assign partial specific volumes to each of the species present. With the new developments of multi-wavelength detection this might become a possibility in the future. This would allow for the detection of multiple wavelengths in a single run, which is not possible with the current XL series optics. This would allow greater selectivity, as solutes can be detected based on unique absorbance spectra. Likewise, a solute's absorbance spectrum may change based on interactions which could be used as another level of detection.

From the beginning, analytical ultracentrifugation has seen its highs and lows, with the highs being the development of new hardware and software and the lows being the field becoming stagnant due to the lack of hardware/software evolution. With the soon to be released Beckman Coulter Optima AUC, and the CFA by Spin Analytical, exciting advancements are coming to the field of AUC.

4.6 – Materials and Methods

4.6.1 - Reagents

Saccharomyces cerevisiae Nap1 was expressed and purified as previously described [59], with the exception they were from the pHAT4 plasmid and contained mutations D201C, C200,

249, 272, 414A to facilitate labeling. *Xenopus laevis* H2A-H2B-T112C, *Xenopus laevis* H2A-H2B, *Xenopus laevis* H3-H4-E63C were expressed and purified as described previously [66, 67]. All DNA sequences used are based off the "601" nucleosome positioning sequence [68]. 601-207 was prepared as previously described [4, 69]. FACT complex was purified as previously described by Tao Wang [138].

4.6.2 - Sedimentation velocity analytical ultracentrifugation

Sedimentation velocity analytical ultracentrifugation (SV-AUC) experiments were performed using a Beckman Coulter Optima XL-I or XL-A analytical ultracentrifuge equipped with an optional Aviv fluorescence detection system (FDS) using either an An50Ti or An60Ti rotor (Beckman Coulter) with standard epon two-channel centerpiece cells. Samples were diluted to desired concentrations ranging from ~0.2 – ~0.8 OD (absorbance) or Alexa 488 labeled samples were set to nM concentrations (fluorescence). Sedimentation was then monitored using either the absorbance optics (intensity mode at 260 or 280nm) or fluorescence optics (emission 488, excitation >505) at 20°C using speeds ranging from 20,000 RPM to 45,000 RPM depending on the sample and rotors used. Before performing fluorescent runs with FDS the focal height was adjusted based on each sample.

Analysis was performed using UltraScan 3 software [78]. Partial specific volumes of sample were determined based on sequence using UltraScan 3. Time invariant and radial invariant noise was subtracted from the sedimentation velocity data by two-dimensional-spectrum analysis (2DSA) followed by genetic algorithm refinement and Monte Carlo analysis [71-73]. Sedimentation coefficient distributions G(s) were obtained with enhanced van Holde-Weischet analysis [74]. Calculations were performed on the UltraScan LIMS cluster at the Bioinformatics Core Facility at the University of Texas Health Science Center at San Antonio and the Lonestar cluster at the Texas Advanced Computing Center supported by NSF Teragrid Grant #MCB070038.

Chapter 5 – Summary and future directions

Histone chaperones have been implicated in almost every aspect of chromatin regulation, with the mechanism being largely unknown. Specifically, nucleosome assembly proteins have been characterized as multifunctional chaperones that are capable of binding both core histones and linker histones. We focused our research on characterizing Nap family members using various biochemical techniques, to gain mechanistic insight into how these chaperones mediate chromatin regulation.

Nap family members share a conserved core region that is flanked by disordered N- and C-terminal tails varying in both length and charge. Suspecting that the charge of the tails may be linked to chromatin regulation through processes like post-translational modifications, we began by performing thermodynamic assays between yeast Nap1 and core histones H2A-H2B and H3-H4. We found that the tails of yNap1 have a profound effect on histone binding. By calculating the change in free energy, we found that H2A-H2B is the preferred binding partner of yNap1. The change in energy was reduced with removal of the tails indicating the highly charged tails modulate histone selectivity. With charge impacting selectivity, it is entirely feasible for the cell to regulate Nap through tail modifications such as polyglutamylation [43].

We then set out to determine the conservation of Nap family members Vps75, Nap2, and SET in regards to self-association, histone binding, and histone removal from DNA. Although these chaperones have similar structures, they vary in many aspects. For example, at low ionic strength we have shown that SET does not self-associate into higher order complexes, whereas we observed higher order complexes with Nap1, Nap2, and Vps75. We also observed asymmetric binding in regards to histones. At low ionic strength, addition of sub-saturating amounts of histones to Vps75 caused higher order complexes consistent with Vps75 remaining in a tetrameric form, whereas WT Nap1 splits into a dimeric structure. Removal of the N- and C-terminal tails

impacted histone splitting of Nap1, as we observed binding similar to that of Vps75, further indicating the tails are involved in regulation.

Characterization of yNap1, Nap2, human Nap1, and SET in regards to histone removal indicated this function is not conserved. We found that each of the Nap family members bind H2A-H2B with nM affinities, but only yNap1 and its human counterpart could efficiently remove H2A-H2B from DNA. Lastly, we confirmed previously published results showing H3-H4 does not productively bind DNA when added at low ionic strength [7]. By comparing H3-H4 assembly onto DNA by systematically lowering the ionic strength with Nap1-mediated H3-H4 assembly, we concluded the mechanism behind Nap1-mediated H3-H4 assembly is much like salt reconstitution in that it eliminates unfavorable ionic interactions.

With a substantial amount of this work being performed with analytical ultracentrifugation, we found we could improve our existing capabilities by employing new detection methods and software analysis. Two primary methods exist with AUC, sedimentation velocity and sedimentation equilibrium, with sedimentation equilibrium being the preferred method for molecular mass determination. With advancements in software analysis, we were able to accurately assign the stoichiometry and molecular mass of Nap family members at different ionic strengths in the presence and absence of core histones using sedimentation velocity. By monitoring the OD, we were also able to quantify H3-H4-induced DNA aggregation along with the efficiency of Nap to prevent/restore this aggregation. Sedimentation velocity experiments are ideal as they can be done in a much shorter time period along with gaining hydrodynamic information about size and shape that otherwise isn't available when performing sedimentation equilibrium. With the added fluorescence detection system, we were also able to gain a level of sensitivity and selectivity that isn't possible with the traditional absorbance optics.

With the increased selectivity of the fluorescence detection system, there are still questions remaining that I feel could be answered using this technique. We observed increased sedimentation coefficients when Nap was added to arrays containing excess H3-H4. We were

103

unable to definitively define whether the increase was due to formation of a ternary complex or Nap-aided H3-H4 assembly onto the array. By individually labeling either Nap or H3-H4, we can answer this question as we would be able to specifically observe sedimentation of the labeled species.

Further investigation into the tails of Nap family members could support our theory about the tails being critical for regulation. As we have found the tails of yNap1 function in histone selectivity and are critical for preventing non-nucleosomal interactions, creating tail truncations of other Nap family members along with modifying the tails altering the overall charge would give mechanistic insight as to whether ionic interactions contribute to specificity and ultimately contribute to chromatin regulation and dynamics.

References

1.   Andrews, A.J., et al., *A thermodynamic model for Nap1-histone interactions.* J Biol Chem, 2008. **283**(47): p. 32412-8.

2.   G., R., *Introduction to Analytical Ultracentrifugation.* 1993: Beckman Instruments, Inc. .

3.   Hansen, J.C., *Conformational dynamics of the chromatin fiber in solution: Determinants, Mechanisms, and Functions.* Annu Rev Biophys Biomol Struct, 2002. **31**: p. 361-92.

4.   Dyer, P.N., et al., *Reconstitution of nucleosome core particles from recombinant histones and DNA.* Methods Enzymol, 2004. **375**: p. 23-44.

5.   Luger, K., et al., *Crystal structure of the nucleosome core particle at 2.8 Å resolution.* Nature, 1997. **389**: p. 251-259.

6.   White, C.L., R.K. Suto, and K. Luger, *Structure of the yeast nucleosome core particle reveals fundamental changes in internucleosome interactions.* Embo J, 2001. **20**(18): p. 5207-18.

7.   Wilhelm, F.X., et al., *Reconstitution of chromatin: assembly of the nucleosome.* Nucleic Acids Res, 1978. **5**(2): p. 505-21.

8.   Laskey, R.A., et al., *Nucleosomes are assembled by an acidic protein which binds histones and transfers them to DNA.* Nature, 1978. **275**(5679): p. 416-20.

9.   Hewish, D.R. and L.A. Burgoyne, *Chromatin sub-structure. The digestion of chromatin DNA at regularly spaced sites by a nuclear deoxyribonuclease.* Biochem Biophys Res Commun, 1973. **52**(2): p. 504-10.

10.   Luger, K. and T.J. Richmond, *The histone tails of the nucleosome.* Curr Opin Genet Dev, 1998. **8**(2): p. 140-146.

11.   Baxevanis, A.D., et al., *A variety of DNA-binding and multimeric proteins contain the histone fold motif.* Nucleic Acids Res, 1995. **23**(14): p. 2685-91.

12.   Olins, D.E. and A.L. Olins, *Chromatin history: our view from the bridge.* Nat Rev Mol Cell Biol, 2003. **4**(10): p. 809-14.

13.   Allen, M.J., et al., *Atomic force microscope measurements of nucleosome cores assembled along defined DNA sequences.* Biochemistry, 1993. **32**(33): p. 8390-6.

14.   Dehghani, H., G. Dellaire, and D.P. Bazett-Jones, *Organization of chromatin in the interphase mammalian cell.* Micron, 2005. **36**(2): p. 95-108.

15.   Finch, J.T. and A. Klug, *Solenoidal model for superstructure in chromatin.* Proc. Natl. Acad. Sci. U. S. A., 1976. **73**: p. 1897-1901.

16.   Schalch, T., et al., *X-ray structure of a tetranucleosome and its implications for the chromatin fibre.* Nature, 2005. **436**(7047): p. 138-41.

17.   Song, F., et al., *Cryo-EM study of the chromatin fiber reveals a double helix twisted by tetranucleosomal units.* Science, 2014. **344**(6182): p. 376-80.

18.   Tremethick, D.J., *Higher-order structures of chromatin: the elusive 30 nm fiber.* Cell, 2007. **128**(4): p. 651-4.

19.   Grigoryev, S.A. and C.L. Woodcock, *Chromatin organization - the 30 nm fiber.* Exp Cell Res, 2012. **318**(12): p. 1448-55.

20.   Maeshima, K., S. Hihara, and M. Eltsov, *Chromatin structure: does the 30-nm fibre exist in vivo?* Curr Opin Cell Biol, 2010. **22**(3): p. 291-7.

21.   Maeshima, K., et al., *Nucleosomal arrays self-assemble into supramolecular globular structures lacking 30-nm fibers.* Embo j, 2016. **35**(10): p. 1115-32.

22.   Strahl, B.D. and C.D. Allis, *The language of covalent histone modifications.* Nature, 2000. **403**(6765): p. 41-5.

23.   Bannister, A.J. and T. Kouzarides, *Regulation of chromatin by histone modifications.* Cell Res, 2011. **21**(3): p. 381-95.

24. Kouzarides, T., *Chromatin modifications and their function.* Cell, 2007. **128**(4): p. 693-705.

25. Tropberger, P. and R. Schneider, *Going global: novel histone modifications in the globular domain of H3.* Epigenetics, 2010. **5**(2): p. 112-7.

26. Albig, W. and D. Doenecke, *The human histone gene cluster at the D6S105 locus.* Hum Genet, 1997. **101**(3): p. 284-94.

27. Li, A., et al., *Phosphorylation of histone H2A.X by DNA-dependent protein kinase is not affected by core histone acetylation, but it alters nucleosome stability and histone H1 binding.* J Biol Chem, 2010. **285**(23): p. 17778-88.

28. Suto, R.K., et al., *Crystal structure of a nucleosome core particle containing the variant histone H2A.Z.* Nat Struct Biol, 2000. **7**(12): p. 1121-1124.

29. Thakar, A., et al., *H2A.Z and H3.3 histone variants affect nucleosome structure: biochemical and biophysical studies.* Biochemistry, 2009. **48**(46): p. 10852-7.

30. Sevilla, A. and O. Binda, *Post-translational modifications of the histone variant H2AZ.* Stem Cell Res, 2014. **12**(1): p. 289-95.

31. Hondele, M. and A.G. Ladurner, *The chaperone-histone partnership: for the greater good of histone traffic and chromatin plasticity.* Curr Opin Struct Biol, 2011. **21**(6): p. 698-708.

32. Philpott, A., T. Krude, and R.A. Laskey, *Nuclear chaperones.* Semin Cell Dev Biol, 2000. **11**(1): p. 7-14.

33. Ransom, M., B.K. Dennehey, and J.K. Tyler, *Chaperoning histones during DNA replication and repair.* Cell, 2010. **140**(2): p. 183-95.

34. De Koning, L., et al., *Histone chaperones: an escort network regulating histone traffic.* Nat Struct Mol Biol, 2007. **14**(11): p. 997-1007.

35. Eitoku, M., et al., *Histone chaperones: 30 years from isolation to elucidation of the mechanisms of nucleosome assembly and disassembly.* Cell Mol Life Sci, 2008. **65**: p. 414-44.

36. Park, Y.J., et al., *Nucleosome assembly protein 1 exchanges histone H2A-H2B dimers and assists nucleosome sliding.* J Biol Chem, 2005. **280**(3): p. 1817-25.

37. Park, Y.J. and K. Luger, *Histone chaperones in nucleosome eviction and histone exchange.* Curr Opin Struct Biol, 2008. **18**: p. 282-9.

38. Park, Y.J. and K. Luger, *Structure and function of nucleosome assembly proteins.* Biochem Cell Biol, 2006. **84**(4): p. 549-58.

39. Eissenberg, J.C., and Elgin, Sarah CR, *Heterochromatin and Euchromatin.* eLS. John Wiley & Sons Ltd, Chichester, 2014.

40. Ohtomo, H., et al., *C-terminal acidic domain of histone chaperone human NAP1 is an efficient binding assistant for histone H2A-H2B, but not H3-H4.* Genes Cells, 2016. **21**(3): p. 252-63.

41. Marciano, G. and D.T. Huang, *Structure of the human histone chaperone FACT Spt16 N-terminal domain.* Acta Crystallogr F Struct Biol Commun, 2016. **72**(Pt 2): p. 121-8.

42. Dennehey, B.K., et al., *The C terminus of the histone chaperone Asf1 cross-links to histone H3 in yeast and promotes interaction with histones H3 and H4.* Mol Cell Biol, 2013. **33**(3): p. 605-21.

43. Regnard, C., et al., *Polyglutamylation of nucleosome assembly proteins.* J Biol Chem, 2000. **275**(21): p. 15969-76.

44. Onikubo, T., et al., *Developmentally Regulated Post-translational Modification of Nucleoplasmin Controls Histone Sequestration and Deposition.* Cell Rep, 2015.

45. Hammond, C.M., et al., *The histone chaperone Vps75 forms multiple oligomeric assemblies capable of mediating exchange between histone H3-H4 tetramers and Asf1-H3-H4 complexes.* Nucleic Acids Res, 2016. **44**(13): p. 6157-72.

46.   Bowman, A., et al., *The histone chaperones Vps75 and Nap1 form ring-like, tetrameric structures in solution.* Nucleic Acids Res, 2014. **42**(9): p. 6038-51.

47.   Ishimi, Y., et al., *A protein which facilitates assembly of nucleosome-like structures in vitro in mammalian cells.* J Biochem, 1983. **94**(3): p. 735-44.

48.   Park, Y.J. and K. Luger, *The structure of nucleosome assembly protein 1.* Proc Natl Acad Sci U S A, 2006. **103**(5): p. 1248-53.

49.   Miyaji-Yamaguchi, M., et al., *Involvement of nucleocytoplasmic shuttling of yeast Nap1 in mitotic progression.* Mol Cell Biol, 2003. **23**(18): p. 6672-84.

50.   Mosammaparast, N., et al., *Nuclear import of histone H2A and H2B is mediated by a network of karyopherins.* J Cell Biol, 2001. **153**(2): p. 251-62.

51.   Mosammaparast, N., C.S. Ewart, and L.F. Pemberton, *A role for nucleosome assembly protein 1 in the nuclear transport of histones H2A and H2B.* Embo J, 2002. **21**(23): p. 6527-38.

52.   Park, Y.J., S.J. McBryant, and K. Luger, *A beta-hairpin comprising the nuclear localization sequence sustains the self-associated states of Nucleosome Assembly Protein 1.* JMB, 2008. **375**: p. 1076-85.

53.   Okuwaki, M., K. Kato, and K. Nagata, *Functional characterization of human nucleosome assembly protein 1-like proteins as histone chaperones.* Genes Cells, 2010. **15**(1): p. 13-27.

54.   D'Arcy, S., et al., *Chaperone Nap1 Shields Histone Surfaces Used in a Nucleosome and Can Put H2A-H2B in an Unconventional Tetrameric Form.* Mol Cell, 2013. **51**(5): p. 662-77.

55.   Luebben, W.R., N. Sharma, and J.K. Nyborg, *Nucleosome eviction and activated transcription require p300 acetylation of histone H3 lysine 14.* Proc Natl Acad Sci U S A, 2010. **107**(45): p. 19254-9.

56.   Chen, X., et al., *Histone Chaperone Nap1 Is a Major Regulator of Histone H2A-H2B Dynamics at the Inducible GAL Locus.* Mol Cell Biol, 2016. **36**(8): p. 1287-96.

57.   Aguilar-Gurrieri, C., et al., *Structural evidence for Nap1-dependent H2A-H2B deposition and nucleosome assembly.* EMBO J, 2016. **35**(13): p. 1465-82.

58.   Newman, E.R., et al., *Large multimeric assemblies of nucleosome assembly protein and histones revealed by small-angle X-ray scattering and electron microscopy.* J Biol Chem, 2012. **287**(32): p. 26657-65.

59.   McBryant, S.J., et al., *Preferential binding of the histone (H3-H4)2 tetramer by NAP1 is mediated by the amino-terminal histone tails.* J Biol Chem, 2003. **278**(45): p. 44574-83.

60.   Andrews, A.J., et al., *The Histone Chaperone Nap1 Promotes Nucleosome Assembly by Eliminating Nonnucleosomal Histone DNA Interactions.* Mol Cell, 2010. **37**(6): p. 834-842.

61.   Mosammaparast, N., B.C. Del Rosario, and L.F. Pemberton, *Modulation of histone deposition by the karyopherin kap114.* Mol Cell Biol, 2005. **25**(5): p. 1764-78.

62.   McBryant, S.J. and O.B. Peersen, *Self-Association of the Yeast Nucleosome Assembly Protein 1.* Biochemistry, 2004. **43**(32): p. 10592-10599.

63.   Vlijm, R., et al., *NAP1-assisted nucleosome assembly on DNA measured in real time by single-molecule magnetic tweezers.* PLoS One, 2012. **7**(9): p. e46306.

64.   Tachiwana, H., et al., *Nap1 regulates proper CENP-B binding to nucleosomes.* Nucleic Acids Res, 2013. **41**(5): p. 2869-80.

65.   Mao, Z., et al., *Anp32e, a higher eukaryotic histone chaperone directs preferential recognition for H2A.Z.* Cell Res, 2014. **24**(4): p. 389-99.

66.   Park, Y.J., et al., *Histone chaperone specificity in Rtt109 activation.* Nature structural & molecular biology, 2008. **15**(9): p. 957-64.

67. Luger, K., T.J. Rechsteiner, and T.J. Richmond, *Expression and purification of recombinant histones and nucleosome reconstitution.* Methods in molecular biology, 1999. **119**: p. 1-16.

68. Lowary, P.T. and J. Widom, *New DNA sequence rules for high affinity binding to histone octamer and sequence-directed nucleosome positioning.* J Mol Biol, 1998. **276**(1): p. 19-42.

69. Carruthers, L.M., et al., *Assembly of defined nucleosomal and chromatin arrays from pure components.* Methods Enzymol, 1999. **304**: p. 19-35.

70. Hieb, A.R., et al., *Fluorescence strategies for high-throughput quantification of protein interactions.* Nucleic Acids Res, 2012. **40**(5): p. e33.

71. Brookes, E., W. Cao, and B. Demeler, *A two-dimensional spectrum analysis for sedimentation velocity experiments of mixtures with heterogeneity in molecular weight and shape.* Eur Biophys J, 2010. **39**(3): p. 405-14.

72. Demeler, B. and E. Brookes, *Monte Carlo analysis of sedimentation experiments.* Colloid and Polymer Science, 2008. **286**(2): p. 129-137.

73. Brookes, E.H. and B. Demeler, *Parsimonious Regularization using Genetic Algorithms Applied to the Analysis of Analytical Ultracentrifugation Experiments.* Gecco 2007: Genetic and Evolutionary Computation Conference, Vol 1 and 2, 2007: p. 361-368.

74. Demeler, B. and K.E. van Holde, *Sedimentation velocity analysis of highly heterogeneous systems.* Anal Biochem, 2004. **335**(2): p. 279-88.

75. Gorbet, G., et al., *A parametrically constrained optimization method for fitting sedimentation velocity experiments.* Biophys J, 2014. **106**(8): p. 1741-50.

76. Toth, K.F., J. Mazurkiewicz, and K. Rippe, *Association states of nucleosome assembly protein 1 and its complexes with histones.* J Biol Chem, 2005. **280**(16): p. 15690-9.

77. Demeler, B., et al., *Characterization of reversible associations by sedimentation velocity with UltraScan.* Macromol Biosci, 2010. **10**(7): p. 775-82.

78. Demeler, B. *UltraScan (current version), A comprehensive software package for the analysis of sedimentation experiments. Dept. of Biochemistry, The University of Texas Health Science Center*. Available from: http://www.ultrascan.uthscsa.edu.

79. Hanna Rose, W. and U. Hansen, *Active repression mechanisms of eukaryotic transcription repressors.* Trends Genet, 1996. **12**(6): p. 229-34.

80. Ellison, M.J. and D.E. Pulleyblank, *The assembly of an H2A2,H2B2,H3,H4 hexamer onto DNA under conditions of physiological ionic strength.* J Biol Chem, 1983. **258**(21): p. 13307-13.

81. Akey, C.W. and K. Luger, *Histone chaperones and nucleosome assembly.* Curr Opin Struct Biol, 2003. **13**(1): p. 6-14.

82. Burgess, R.J. and Z. Zhang, *Histone chaperones in nucleosome assembly and human disease.* Nat Struct Mol Biol, 2013. **20**(1): p. 14-22.

83. Gurard-Levin, Z.A., J.P. Quivy, and G. Almouzni, *Histone chaperones: assisting histone traffic and nucleosome dynamics.* Annu Rev Biochem, 2014. **83**: p. 487-517.

84. Zlatanova, J., C. Seebart, and M. Tomschik, *Nap1: taking a closer look at a juggler protein of extraordinary skills.* FASEB J, 2007. **21**(7): p. 1294-310.

85. Su, D., et al., *Structure and histone binding properties of the Vps75-Rtt109 chaperone-lysine acetyltransferase complex.* J Biol Chem, 2011. **286**(18): p. 15625-9.

86. Bonangelino, C.J., E.M. Chavez, and J.S. Bonifacino, *Genomic screen for vacuolar protein sorting genes in Saccharomyces cerevisiae.* Mol Biol Cell, 2002. **13**(7): p. 2486-501.

87. Selth, L. and J.Q. Svejstrup, *Vps75, a new yeast member of the NAP histone chaperone family.* J Biol Chem, 2007. **282**(17): p. 12358-62.

88. Park, Y.J., et al., *Histone chaperone specificity in Rtt109 activation.* Nat Struct Mol Biol, 2008.

89.   Tsubota, T., et al., *Histone H3-K56 acetylation is catalyzed by histone chaperone-dependent complexes.* Mol Cell, 2007. **25**(5): p. 703-12.

90.   Han, J., et al., *The Rtt109-Vps75 histone acetyltransferase complex acetylates non-nucleosomal histone H3.* J Biol Chem, 2007. **282**(19): p. 14158-64.

91.   Kuo, Y.M., et al., *Utilizing targeted mass spectrometry to demonstrate Asf1-dependent increases in residue specificity for Rtt109-Vps75 mediated histone acetylation.* PLoS One, 2015. **10**(3): p. e0118516.

92.   Recht, J., et al., *Histone chaperone Asf1 is required for histone H3 lysine 56 acetylation, a modification associated with S phase in mitosis and meiosis.* Proc Natl Acad Sci U S A, 2006. **103**(18): p. 6988-93.

93.   Driscoll, R., A. Hudson, and S.P. Jackson, *Yeast Rtt109 promotes genome stability by acetylating histone H3 on lysine 56.* Science, 2007. **315**(5812): p. 649-52.

94.   Fillingham, J., et al., *Chaperone Control of the Activity and Specificity of the Histone H3 Acetyltransferase Rtt109.* Mol Cell Biol, 2008.

95.   Berndsen, C.E., et al., *Molecular functions of the histone acetyltransferase chaperone complex Rtt109-Vps75.* Nat Struct Mol Biol, 2008.

96.   English, C.M., et al., *Structural basis for the histone chaperone activity of Asf1.* Cell, 2006. **127**(3): p. 495-508.

97.   Bowman, A., et al., *The histone chaperones Nap1 and Vps75 bind histones H3 and H4 in a tetrameric conformation.* Mol Cell, 2011. **41**(4): p. 398-408.

98.   Tang, Y., et al., *Structure of the Rtt109-AcCoA/Vps75 complex and implications for chaperone-mediated histone acetylation.* Structure, 2011. **19**(2): p. 221-31.

99.   McBryant, S.J., et al., *Preferential binding of the histone (H3-H4)2 tetramer by NAP1 is mediated by the amino-terminal histone tails.* The Journal of biological chemistry, 2003. **278**(45): p. 44574-83.

100.   Brookes, E., W. Cao, and B. Demeler, *A two-dimensional spectrum analysis for sedimentation velocity experiments of mixtures with heterogeneity in molecular weight and shape.* European biophysics journal : EBJ, 2010. **39**(3): p. 405-14.

101.   Demeler, B. and K.E. van Holde, *Sedimentation velocity analysis of highly heterogeneous systems.* Analytical biochemistry, 2004. **335**(2): p. 279-88.

102.   Gorbet, G., et al., *A parametrically constrained optimization method for fitting sedimentation velocity experiments.* Biophysical journal, 2014. **106**(8): p. 1741-50.

103.   Tang, Y., et al., *Structure of Vps75 and implications for histone chaperone function.* Proceedings of the National Academy of Sciences of the United States of America, 2008. **105**(34): p. 12206-11.

104.   Bowman, A., et al., *The histone chaperones Vps75 and Nap1 form ring-like, tetrameric structures in solution.* Nucleic acids research, 2014. **42**(9): p. 6038-51.

105.   Eickbush, T.H. and E.N. Moudrianakis, *The histone core complex: an octamer assembled by two sets of protein-protein interactions.* Biochemistry, 1978. **17**(23): p. 4955-64.

106.   D'Arcy, S., et al., *Chaperone Nap1 shields histone surfaces used in a nucleosome and can put H2A-H2B in an unconventional tetrameric form.* Molecular cell, 2013. **51**(5): p. 662-77.

107.   Mattiroli, F., et al., *DNA-mediated association of two histone-bound CAF-1 complexes drives tetrasome assembly in the wake of DNA replication.* Elife, 2017. **6**.

108.   Andrews, A.J., et al., *A thermodynamic model for Nap1-histone interactions.* The Journal of biological chemistry, 2008. **283**(47): p. 32412-8.

109.   D'Arcy, S. and K. Luger, *Understanding histone acetyltransferase Rtt109 structure and function: how many chaperones does it take?* Curr Opin Struct Biol, 2011. **21**(6): p. 728-34.

110.   Rinde., T.S.a.H., *The Ultra-Centrifuge, a New Instrument for the Determination of Size and Distribution of Particle in Amicroscopic Colloids.* J. Am. Soc., 1924. **46(12)**: p. 2677-2693.

111.   Nichols, T.S.a.J.B., *Determination of Size and Distribution of Size of Particle by Centrifugal Methods.* J. Am. Soc., 1923. **45**(12): p. 2910-2917.

112.   Svedberg, T., Pederson, K.O., *The Ultracentrifuge.* 1940: Oxford, Clarendon Press.

113.   Meselson, M., F.W. Stahl, and J. Vinograd, *Equilibrium Sedimentation of Macromolecules in Density Gradients.* Proc Natl Acad Sci U S A, 1957. **43**(7): p. 581-8.

114.   Vinograd, J., et al., *The twisted circular form of polyoma viral DNA.* Proc Natl Acad Sci U S A, 1965. **53**(5): p. 1104-11.

115.   Laue, T.M. and W.F. Stafford, 3rd, *Modern applications of analytical ultracentrifugation.* Annu Rev Biophys Biomol Struct, 1999. **28**: p. 75-100.

116.   Laue, T.M., *Sedimentation equilibrium as thermodynamic tool.* Methods Enzymol, 1995. **259**: p. 427-52.

117.   Williams, J.W., et al., *The Theory of Sedimentation Analysis.* Chemical Reviews, 1958. **58**(4): p. 715-806.

118.   Fujita, H., *Foundations of ultracentrifugal analysis.* 1975: Wiley; New York.

119.   *Analytical Ultracentrifugation: Techniques and Methods*, ed. S.E.H. David Scott, Arther Rowe. December 16, 2005.

120.   Einstein, A., *Über die von der molekularkinetischen Theorie der Wärme geforderte Bewegung von in ruhenden Flüssigkeiten suspendierten Teilchen.* Annalen der Physik, 1905. **322**(8): p. 549-560.

121.   Lamm, O., *Die Differentialgleichung der Ultrazentrifugierung.* Ark. Mat. Astr. Fys., 1929. **21B:1-4**.

122.   Dam, J., et al., *Sedimentation velocity analysis of heterogeneous protein-protein interactions: Lamm equation modeling and sedimentation coefficient distributions c(s).* Biophys J, 2005. **89**(1): p. 619-34.

123.   Balbo, A., et al., *Studying multiprotein complexes by multisignal sedimentation velocity analytical ultracentrifugation.* Proc Natl Acad Sci U S A, 2005. **102**(1): p. 81-6.

124.   Schuck, P., *Sedimentation analysis of noninteracting and self-associating solutes using numerical solutions to the Lamm equation.* Biophysical Journal, 1998. **75**(3): p. 1503-12.

125.   Cole, J.L., et al., *Analytical ultracentrifugation: Sedimentation velocity and sedimentation equilibrium.* Biophysical Tools for Biologists: Vol 1 in Vitro Techniques, 2008. **84**: p. 143-179.

126.   Demeler, B., *Methods for the design and analysis of sedimentation velocity and sedimentation equilibrium experiments with proteins.* Curr Protoc Protein Sci, 2010. **Chapter 7**: p. Unit 7 13.

127.   MacGregor, I.K., A.L. Anderson, and T.M. Laue, *Fluorescence detection for the XLI analytical ultracentrifuge.* Biophys Chem, 2004. **108**(1-3): p. 165-85.

128.   Zhao, H., M.L. Mayer, and P. Schuck, *Analysis of protein interactions with picomolar binding affinity by fluorescence-detected sedimentation velocity.* Anal Chem, 2014. **86**(6): p. 3181-7.

129.   Kingsbury, J.S. and T.M. Laue, *Fluorescence-detected sedimentation in dilute and highly concentrated solutions.* Methods Enzymol, 2011. **492**: p. 283-304.

130.   Kroe, R.R. and T.M. Laue, *NUTS and BOLTS: Applications of fluorescence-detected sedimentation.* Analytical Biochemistry, 2009. **390**(1): p. 1-13.

131.   Brown, P.H. and P. Schuck, *Macromolecular size-and-shape distributions by sedimentation velocity analytical ultracentrifugation.* Biophys J, 2006. **90**(12): p. 4651-61.

132.   Schuck, P., *Size-distribution analysis of macromolecules by sedimentation velocity ultracentrifugation and lamm equation modeling.* Biophys J, 2000. **78**(3): p. 1606-19.

133. van Holde, K.E. and W.O. Weischet, *Boundary analysis of sedimentation-velocity experiments with mondisperse and paucidisperse solutes.* Biopolymers, 1978. **17**: p. 1387-1403.

134. Brookes, E. and B. Demeler, *Genetic algorithm optimization for obtaining accurate molecular weight distributions from sedimentation velocity experiments.* Analytical Ultracentrifugation VIII, 2006. **131**: p. 33-40.

135. Cao, W. and B. Demeler, *Modeling analytical ultracentrifugation experiments with an adaptive space-time finite element solution for multicomponent reacting systems.* Biophys J, 2008. **95**(1): p. 54-65.

136. Brown, P.H., et al., *Density contrast sedimentation velocity for the determination of protein partial-specific volumes.* PLoS One, 2011. **6**(10): p. e26221.

137. Lyons, D.F., et al., *Are fluorescence-detected sedimentation velocity data reliable?* Anal Biochem, 2013. **437**(2): p. 133-7.

138. Winkler, D.D., et al., *Histone chaperone FACT coordinates nucleosome interaction through multiple synergistic binding events.* J Biol Chem, 2011. **286**(48): p. 41883-92.

139. Muto, S., et al., *Relationship between the structure of SET/TAF-Ibeta/INHAT and its histone chaperone activity.* Proc Natl Acad Sci U S A, 2007. **104**(11): p. 4285-90.

140. Kawase, H., et al., *NAP-I is a functional homologue of TAF-I that is required for replication and transcription of the adenovirus genome in a chromatin-like structure.* Genes Cells, 1996. **1**(12): p. 1045-56.

141. Okuwaki, M., et al., *Assembly and disassembly of nucleosome core particles containing histone variants by human nucleosome assembly protein I.* Mol Cell Biol, 2005. **25**(23): p. 10639-51.

142. Hieb, A.R., Arcy, S. D., Kramer, M. A, White, A. E., and Luger, K., *Fluorescence strategies for high-throughput quantification of protein interactions.* Nucleic Acids Res, 2011.

143. Dechassa, M.L., et al., *Structure and Scm3-mediated assembly of budding yeast centromeric nucleosomes.* Nat Commun, 2011. **2**: p. 313.

Appendix 1

Functional comparison between Nap family members

A1.1 - Introduction

Nap is conserved among all eukaryotes from yeast to humans. In higher eukaryotes, there are several homologues of Nap, including SET and Nap1-like proteins such as Nap1L4 (also known as Nap2). These Nap family members share a similar core region but differ in their N- and C-terminal tails, with respect to their length, charge, or both [53]. Structurally, each Nap subunit contains a long dimerization helix forming a homodimer [48]. Dimeric Nap1 contains a negatively charged surface on the 'underside' of the α-β domain that is responsible for histone binding [54]. Although the core domain is conserved among Nap family members, there are differences such as the β-hairpin found in yNap1 but not in the structurally similar histone chaperone SET [48, 139]. The β-hairpin in yNap1 contains a nuclear localization sequence allowing Nap1 to shuttle histones from the cytoplasm to the nucleus [49, 51, 52, 61]. At low ionic strength, the β-hairpin has also been shown to mediate yNap1 oligomerization [52].

Nap1 like proteins have been found to associate with histone variants H2A.X, H2A.Z, and macro H2A1.2 in cell extracts along with being involved in processes such as histone disassembly [53]. Specifically, SET has been shown to act as a substitute for yNap1 in chromatin assembly and disassembly in vitro [38, 140, 141]. Nap2 has been shown to mediate nucleosome assembly through H2A-H2B interactions along with nucleosome disassembly through H2ABbd-H2B eviction, indicating that Nap2 may also be specific to histone variants [53]. With the core region being conserved among Nap family members, functional differences may be due to the variation found in the N- and C-terminal tails. As several groups have shown Nap family members mediate nucleosome assembly by interacting with core histones, we posed the question as to how conserved are Nap family members in relation to function?

A1.2 - Results

A1.2.1 - H2A-H2B binding is not conserved among Nap family members

Using the HIFI (<u>H</u>igh-throughput <u>I</u>nteractions by <u>F</u>luorescent <u>I</u>ntensity) assay developed by our lab we obtained binding affinities for Nap family members mNap2 and SET so we could determine if H2A-H2B binding is a conserved trait among family members [142]. The reactions were performed under the same conditions as for yNap1 (Chapter 2). These conditions included labeling H2A-H2B with a donor fluorophore and kept at a constant concentration while yNap1, labeled with an acceptor fluorophore, was titrated while monitoring the FRET signal. The apparent K_D was then determined using GraphPad Prism (Fig. A1.1A). We found that both mNap2 and SET bound H2A-H2B with low nanomolar affinity, although not as tightly as yNap1 (mNap2 was ~ 2 fold weaker and SET was ~3.5 fold weaker) (Table A1.1).

We next looked at histone selectivity between dimers containing H2A-H2B and H2A variants H2A.X-H2B and H2A.Z-H2B. We previously found that yNap1 binds both variants with low nanomolar affinity, so we used these binding affinities to determine chaperone selectivity by calculating the difference in free energy ($\Delta\Delta G^o$) between the different variants. Similar to yNap1, both Nap2 and SET preferentially bind H2A-H2B over H2A variants, with H2A.Z binding being preferred over H2A.X (Fig. A1.2A-B). We also looked at selectivity between yNap1 and Nap2 or SET by calculating the difference in free energy ($\Delta\Delta G^o$). We found H2A-H2B and H2A variants H2A.X and H2A.Z preferentially bind yNap1 over both Nap2 and SET (Fig. A1.2C-D).

A1.2.2 - hNap1 and Nap2 oligomerize at lower ionic strength, but SET does not

yNap1 and Vps75, both members of the Nap family, have been shown to self-associate at low ionic strength ((Chapter 2, and [62]). We therefore wanted to determine if this was a feature that was conserved among all Nap family members, using sedimentation velocity analytical ultracentrifugation (SV-AUC). Consistent with the sedimentation coefficient of dimeric yNap1

(~4.5S), we observed human Nap1 (hNap1), Nap2, and SET all have sedimentation coefficients between 4-5S at 300 mM NaCl (Fig. A1.3A-C (white diamonds)). Lowering the ionic strength to 150 mM NaCl caused an increase in sedimentation for hNap1 and Nap2, whereas SET remained unchanged (Fig. A1.3A-C (white circles)).

Recent literature suggests that Nap family members may bind histones at low ionic strength and form higher order complexes [45, 57]. In Chapter 3, we show this to be true when histones were added to Vps75 or Nap1 at sub-saturating concentrations. Saturating concentrations of histones splits the Vps75 or Nap1 tetramer into two homodimers that bind core histones with a 2:2 stoichiometry. Using SV-AUC we found that in the presence of H2A-H2B, SET forms complexes that are consistent with a tetrameric species, likely a SET homodimer bound to two H2A-H2B heterodimers, as we did not observe self-association at low ionic strength (Fig A1.3C & D). A shift in sedimentation was not observed when H2A-H2B was added to Nap2, suggesting that the higher order complex formed at low ionic strength could be blocking the binding of H2A-H2B. Alternatively, the Nap2 oligomer is split by the presence of H2A-H2B and adopts a higher order conformation similar to that without histones (Fig. A1.3D).

A1.2.3 - Not all Nap family members mediate disruption of non-nucleosomal histone DNA interactions

Nucleosome formation is a sequential process beginning with H3-H4 binding DNA followed by H2A-H2B deposition. This process can be blocked if H2A-H2B first binds, creating non-nucleosomal H2A-H2B:DNA interactions. It has been previously reported that yNap1 prevents these non-nucleosomal interactions and Nap1-like proteins are known to be involved in histone disassembly [60]. We therefore wanted to determine if this function was conserved among other Nap family members. Employing the same methodology used in Chapter 2 with yNap1 using SV-AUC, H2A-H2B or H2A variants H2A.X and H2A.Z were incubated with 207x3 DNA. Either hNap1, Nap2, or SET was then added and the change in sedimentation monitored using SV-AUC

(Fig A1.4A-D). Using yNap1 as a control, we first looked at whether yNap1 could remove H2A variants in the same manner as canonical H2A-H2B. Consistent with binding affinities, we found that yNap1 could effectively remove both H2A.X-H2B and H2A.Z-H2B from 207x3 DNA with no apparent differences from canonical H2A-H2B (Fig. A1.4A). We then looked at the human counterpart of yNap1, hNap1. Similar to yNap1, hNap1 removed H2A-H2B and both H2A variants from 207x3 DNA with the same molar ratios to yNap1 (Fig. A1.4B). We next tested Nap2, a member of the Nap family that is ubiquitously expressed and thought to mediate nucleosome assembly through H2A-H2B interactions, and found it lacked removal activity for H2A-H2B and H2A variants H2A.X and H2A.Z (Fig. A1.4C). Lastly, we looked at SET, as we observed it bound H2A-H2B with low nanomolar affinity (Table A1.1). We found minimal removal activity for SET, although it did produce sedimentation curves that were more vertical/homogenous than in the absence of SET (Fig. A1.4D). This could indicate SET can bind H2A-H2B and variants, but lacks the ability to remove/outcompete the DNA for the histones (Fig. A1.4D).

A1.2.4 - Nucleosomal array "cleanup" is not a conserved activity for all Nap family members

Histones are produced in the cytoplasm and transported to the nucleus. If not properly chaperoned, these histones may bind free DNA through non-nucleosomal interactions, or the linker region between assembled nucleosomes which might inhibit linker histone binding [56]. Using nucleosomal arrays, we decided to look at how the addition of either H2A-H2B or H3-H4 impacts sedimentation using SV-AUC, and how this might be relieved by histone chaperones. We first looked at just 601-207x12 DNA, as that is the DNA used for assembling the arrays. Consistent with 207x3 DNA, we found that neither Nap2 nor SET removed H2A-H2B from the DNA, but did produce homogenous curves indicating they may bind the histones, but lack the ability to outcompete DNA (Fig. 5A). We then looked at how the presence of nucleosomes would impact these results, as histones may not bind the linker region with the same affinity as free DNA. Using

SV-AUC, we found that neither Nap2 nor SET could efficiently remove H2A-H2B from the linker region of nucleosomal arrays (Fig. A1.5B).

Lastly, we looked at how these chaperones functioned in the presence of H3-H4 instead of H2A-H2B. Using the same methodology as for H2A-H2B, H3-H4 was added to preassembled 207x12mer nucleosomal arrays followed by the addition of yNap1, Nap2, or SET. Similar to free DNA (Chapter 2 Fig. 2.10), we found H3-H4 bound poorly to the nucleosomal arrays when added at low ionic strength, as we saw minimal shifts in sedimentation (Fig. A1.6A). Addition of yNap1, Nap2, or SET caused a shift in sedimentation, indicating the species became larger (Fig. A1.6B). Initially, we assumed this was due to the chaperone binding, forming a ternary complex, but further analysis revealed that this may not be the case. An advantage of SV-AUC over other methods, such as gel electrophoresis, is the ability to observe all species present using first principles. Besides monitoring the species based on size and shape, we can also monitor the change in absorbance, which is directly proportional to concentration. By plotting the concentration as a function of sedimentation, we found that the addition of H3-H4 to nucleosomal arrays decreased the absorbance. Generally speaking, a decrease in absorbance indicates aggregation, meaning that the addition of H3-H4 to the nucleosomal array caused the array to aggregate and fall out of solution, leading to loss in absorbance (Fig. A1.6C & E). This aggregation was reversed in the presence of histone chaperones. yNap1 has the biggest impact followed by Nap2 and SET (Fig. A1.6D & F). One could speculate that this is simply due to the absorbance contribution of the histone chaperones. Therefore, we monitored the absorbance at both 260 nm (primarily observe DNA) and 280 nm (primarily observe protein) (Fig. A1.6D & F). With the absorbance at 280 nm we can see the presence of histone chaperones at ~5S and then the histones in the nucleosomal array that start at ~35S (Fig. A1.6F). At 260, the presence of histone chaperones is minimal indicating that we are primarily focused on the DNA sedimenting at ~35-40S. Together, this data allows us to conclude that yNap1 has the greatest impact on removing array aggregation caused by excess H3-H4, with Nap2 and SET displaying similar (but lower) activity (Fig. A1.6E).

A1.3 - Discussion

In this work we looked at of the propensity of various Nap family members to self-associate at low ionic strength, bind histones, and remove/assemble, using FRET and sedimentation velocity analytical ultracentrifugation. We found that Nap family members are conserved in their ability to bind H2A-H2B and H2A histone variants H2A.X and H2A.Z, as each preferred canonical H2A-H2B (Fig. A1.1). Although many features of yNap1 are conserved among family members, ionic dependent self-association was not, as we did not observe self-association with SET. SET has been shown to act as a replacement for yNap1, with SET being structurally similar [139, 140]. With Nap1 likely existing as a tetrameric species and SET as a dimeric species at biological ionic strength, these results indicate these two chaperones are mechanistically different when binding histones [46, 62].

When we looked at other Nap family members, self-association was observed with Nap2 and human Nap1, indicating it is not just limited to yNap1. Shifts in the sedimentation coefficients with the addition of histones H2A-H2B to yNap1 and SET at low ionic strength indicated binding were not impacted by self-association (Fig. A1.3D). A shift in sedimentation was not observed for Nap2; this could be due to minimal binding between Nap2 and H2A-H2B, or that H2A-H2B split the tetrameric Nap2 complex toformed a similar Nap2:H2A-H2B tetrameric complex (Fig. A1.3D). Since the van Holde-Weischet plots of Nap2 and Nap2 with H2A-H2B almost exactly superimpose, several extra copies of H2A-H2B would need to bind Nap2 to make up similar molecular mass, along with forming a structure that is similar in shape. Since we, along with others, have shown that Nap2 binds H2A-H2B (Fig. A1.1, Table A1.1), it is therefore more likely that the higher order complex formed at low ionic strength blocks H2A-H2B from binding.

yNap1 has been found to have many functions such as histone removal, histone assembly, and histone storage, making it an all-purpose histone chaperone. We therefore wanted to determine if any of these functions were conserved among Nap family members. We specifically looked at histone removal as it has been shown that Nap functions in histone

disassembly [53, 60]. We found that this function was conserved in human Nap1, for both canonical H2A-H2B and H2A variants (Fig. A1.4A-D, Fig. A1.5A-B). This was not the case for Nap2 and SET, as both had minimal removal activity indicating that histone removal/nucleosome disassembly might not be their primary function within the cell (Fig. A1.4A-D, Fig. A1.5A-B).

We then looked at how these chaperones functioned with H3-H4 by adding it to nucleosomal arrays. As with free DNA, we found that H3-H4 caused aggregation when added to the arrays at low ionic strength (Chapter 2 Fig 2.10, Fig A1.6A, C, & E). Addition of yNap1, Nap2, and SET caused increased sedimentation coefficients leading us to conclude that they may be binding the complex (Fig. A1.6B). Further investigation revealed that instead of binding, they may be aiding in H3-H4 assembly on the nucleosomal array (Fig. A1.6D & F). With sedimentation velocity analytical ultracentrifugation, the absorbance of the solution is monitored as it sediments. This allows us to record the initial DNA or array absorbance and then compare it to the absorbance in the presence of excess histones. We found that the addition of H3-H4 to the nucleosomal array caused a significant decrease in absorbance indicating aggregation that was reversed in the presence of histone chaperones (Fig. A1.6). One could speculate that the increase in absorbance is due to the presence of histone chaperones, as absorbance optics monitor the overall absorbance of the sample as a whole. By monitoring both 260 nm and 280 nm, we were able to dismiss the idea that just the presence of the histone chaperones caused the increase in absorbance. If this were the case, we would have seen only an increase in absorbance at 280 nm, as that primarily monitors the protein in the sample. With the observed increase of absorbance at 260 nm, we can conclude the histone chaperones are reducing aggregation caused by H3-H4.

Together this data suggests that although Nap family members have a conserved core region, the function of Nap family members is not conserved [38, 48]. Each of the Nap family members contain N- and C-terminal tails that vary in length and charge. As we have shown with yNap1, altering length and charge of the tails will impact histone binding (Chapter 2). Likewise,

118

self-association of histone chaperones also impacts the stoichiometry of histone binding. Therefore, regulation of histone chaperones may be linked to the oligomeric state, along with the N- and C-terminal tails.
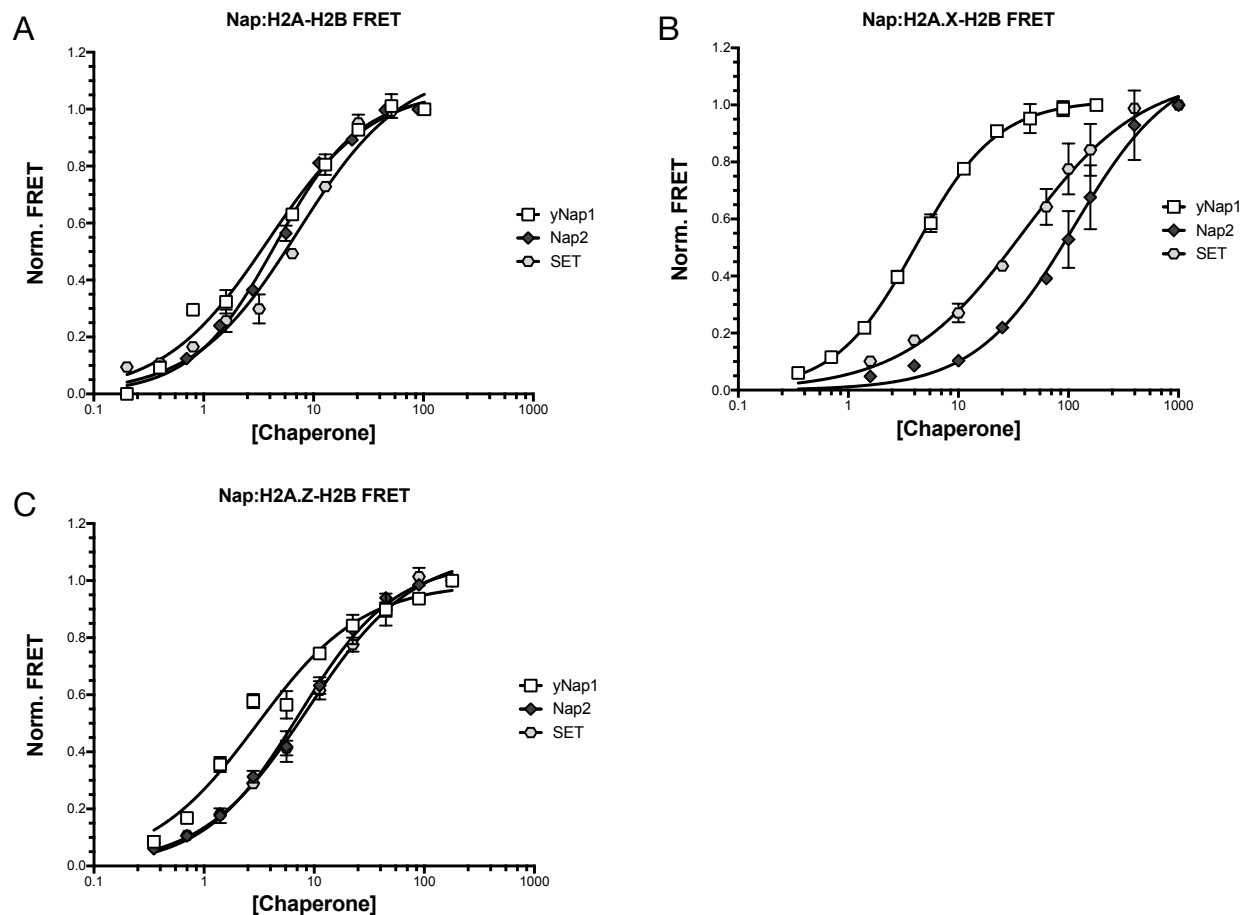
Figure A1.1. H2A-H2B binding is not conserved among Nap family members. Normalized fluorescence as a function of yNap1 WT (squares), Nap2 (diamonds), or SET (hexagon) binding histones **(A)** H2A-H2B, **(B)** H2A.X-H2B, or **(C)** H2A.Z-H2B at 0.32M ionic strength. Apparent dissociation constants were determined through GraphPad Prism and listed in Table A1. yNap1 binding data was taken from chapter 2. Error bars stem from two replicates.

TABLE A1.1. Values of the observed disassociation constants calculated for Nap family members binding to H2A-H2B, H2A.X-H2B, and H2A.Z-H2B at 0.32M ionic strength. Error stems from 2 replicates. *yNap1-H2A-H2B binding affinity was taken from chapter 2-Table 2.1

Nap	-H2AB K_D (M)	-H2A.X-H2B K_D (M)	-H2A.Z-H2B K_D (M)
yNap1	$2.01 \pm 0.94 \times 10^{-9}$*	$5.98 \pm 2.62 \times 10^{-9}$	$4.04 \pm 1.15 \times 10^{-9}$
mNap2	$4.88 \pm 0.35 \times 10^{-9}$	$124.10 \pm 9.62 \times 10^{-9}$	$8.09 \pm 0.10 \times 10^{-9}$
SET	$7.13 \pm 1.74 \times 10^{-9}$	$37.80 \pm 4.82 \times 10^{-9}$	$12.73 \pm 4.38 \times 10^{-9}$
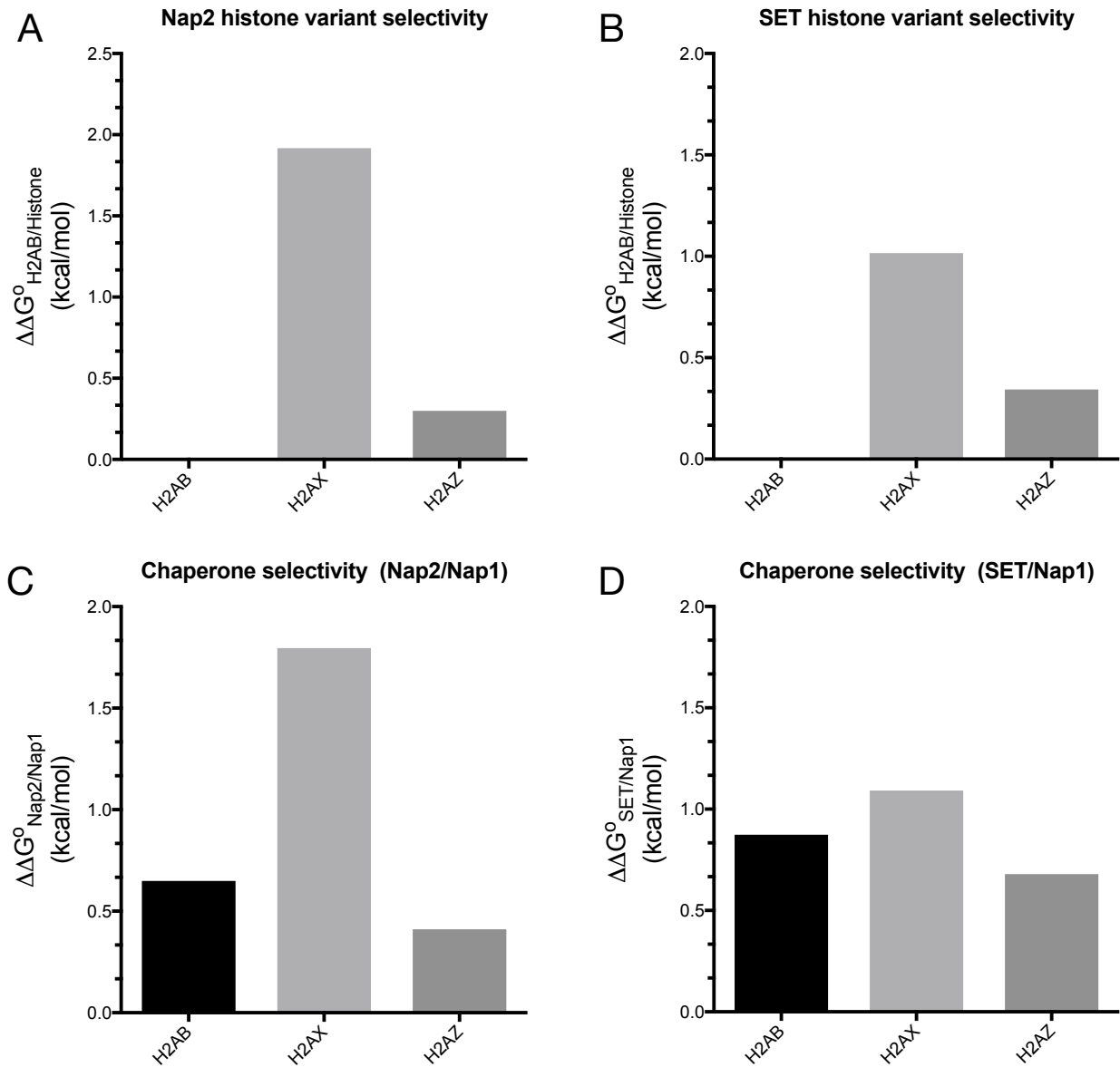
Figure A1.2. Change in free energy indicates Nap family members prefer H2A-H2B over H2A variants.
Histone selectivity was calculated by determining the change in free energy between H2A-H2B and H2A variants binding Nap1 family members. **A & B)** Change in free energy indicates that both Nap2 and SET have preferential binding for H2A-H2B followed by H2A variant H2A.Z-H2B. **C & D)** Change in free energy indicates that yNap1 is the preferential binding partner for H2A-H2B and H2A variants.
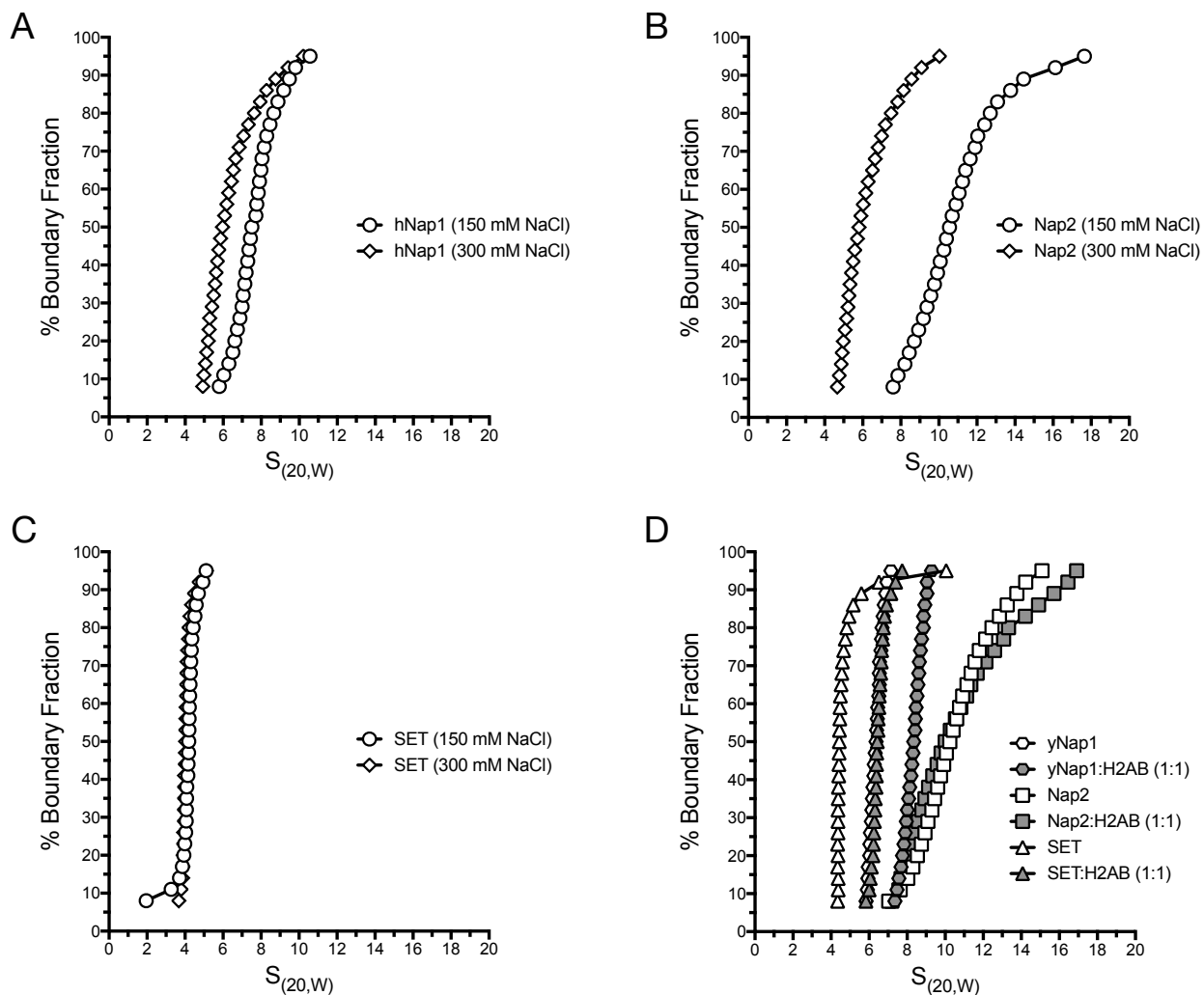
Figure A1.3. Ionic strength-dependent oligomerization of Nap family members
Sedimentation velocity was performed to determine if Nap family members displayed salt-dependent behavior **A & B)** At 150mM NaCl (circles)we observe Nap family members hNap1 and mNap2 self-associate into higher order species when compared to 300 mM NaCl (diamonds) **C)** SET remains in the same state at both 150 mM NaCl (circles) and 300mM NaCl (diamonds). **D)** Sedimentation velocity was used to determine H2A-H2B binding to Nap family members yNap1 (hexagon), Nap2 (squares), and SET (triangles). H2A-H2B was added to Nap family members at a 1:1 ratio at 200 mM NaCl. Chaperones alone are shown in open white symbols and dark grey symbols represent the addition of H2A-H2B.
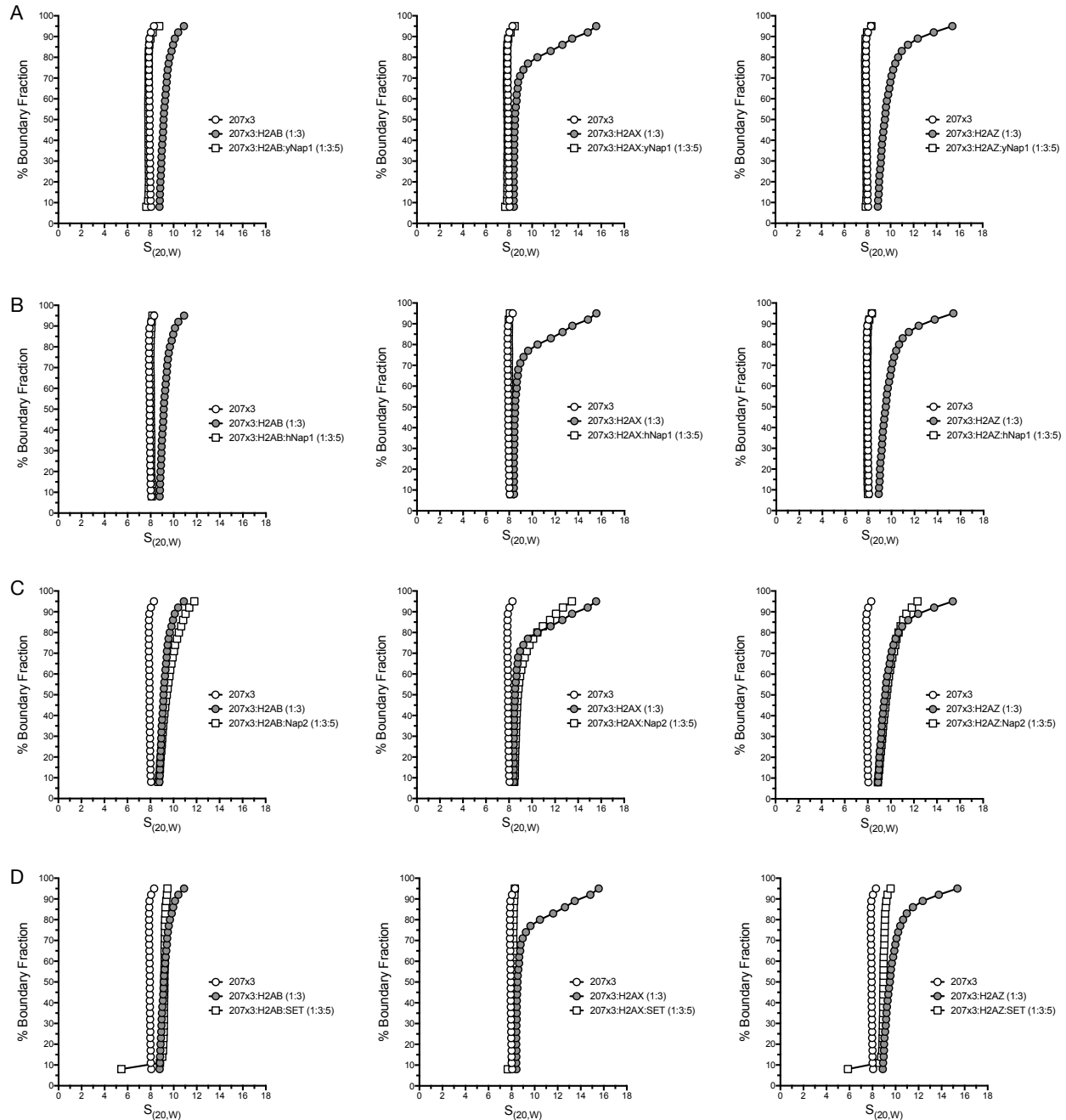
Figure A1.4. Prevention of non-nucleosomal H2A-H2B interactions is not conserved among Nap family members. Sedimentation velocity was performed to monitor the interaction of Nap family members in the presence of 207x3 DNA with 3-fold molar excess of histones H2A-H2B (Left), H2A.X-H2B (Middle), or H2A.Z-H2B (Right). 5-fold molar excess of either **A)** yNap1, **B)** hNap1, **C)** Nap2, or **D)** SET was then added and the change in sedimentation monitored.
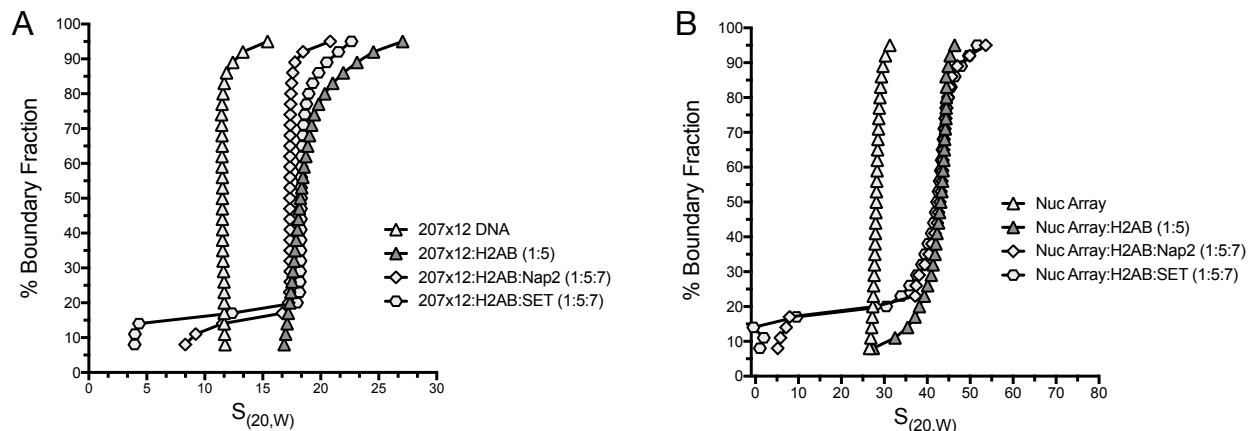
Figure A1.5. Removal of nonspecifically bound H2A-H2B from 207x12 DNA or 207x12 nucleosomal arrays is not conserved among Nap family members. A) SV was performed to monitor the impact of Nap2 (diamonds) or SET (hexagon) with 207x12 DNA + 5-fold molar excess H2A-H2B. **B)** SV was performed to monitor the impact of Nap2 (diamonds) or SET (hexagon) in the presence of nucleosomal arrays containing 5-fold molar excess H2A-H2B to determine whether removal of nonspecifically bound H2A-H2B removal is conserved among Nap family members. Need a conclusion statement: Unlike Nap1, Nap2 and SET could not remove H2A-H2B from 207-12 DNA or arrays.
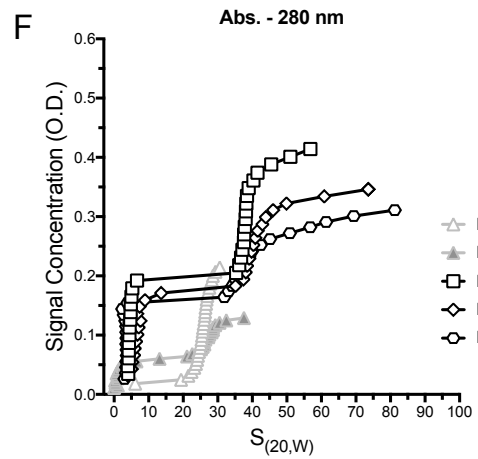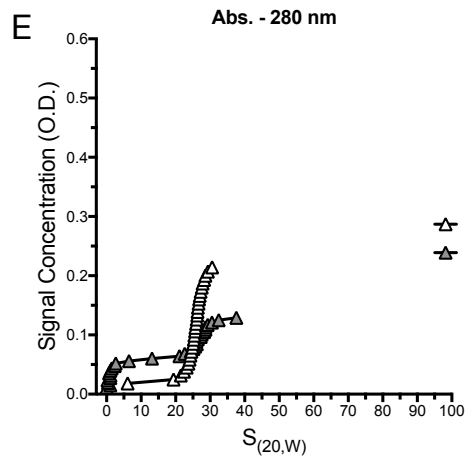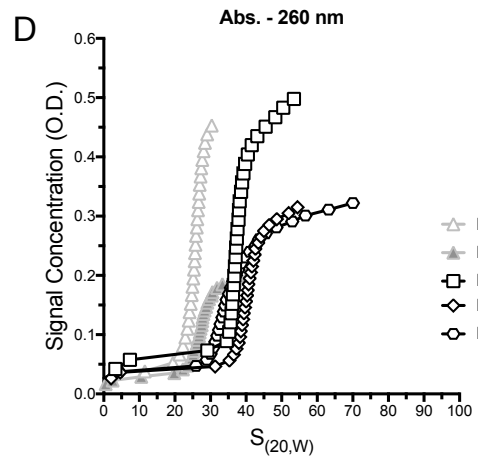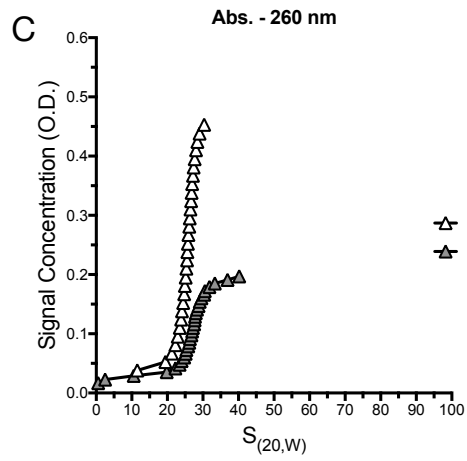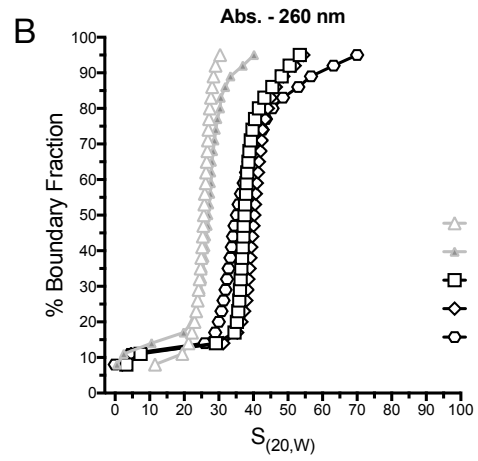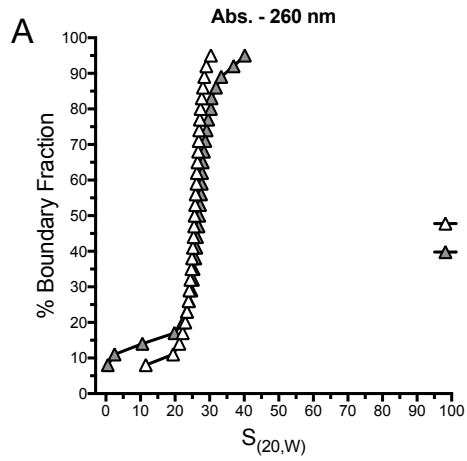
Figure A1.6. Functional comparison of H3-H4 removal between Nap family members in using sedimentation velocity. A) The addition of 2-fold molar excess H3-H4 to nucleosomal arrays caused minimal changes in sedimentation **B)** Addition of 5-fold molar excess Nap family members yNap1 (squares), Nap2 (diamonds), or SET (hexagon) to the H3-H4 saturated array resulted in an increased S value. **C)** Using data from (A), the signal concentration was plotted as a function of sedimentation instead of %Boundary fraction. This revealed that the addition of H3-H4 causes a reduction in absorbance. **D)** Data from (B) with signal concentration plotted as a function of sedimentation reveals the addition of histone chaperones restores absorbance values. **E)** Monitoring the absorbance at 280 nm allows us to track protein instead of DNA. Addition of H3-H4 to the array causes a significant tail representing unbound H3-H4. **F)** Monitoring the absorbance at 280 nm reveals that the addition of Nap family members to the array causes significant tailing of the sedimentation profile indicating the presence of histone chaperones not bound to the array. The increase in absorbance at both 260 and 280 nm indicates the chaperones are not contributing to the overall increase in absorbance.

Appendix 2

H2A-H2B binds nonspecifically to DNA

Introduction:

Using MNase digestion assays we investigated the impact of excess H2A-H2B on free DNA and in the presence of nucleosomes. We found free DNA was digested rapidly by MNase whereas in the presence of H2A-H2B, the DNA was digested less rapidly (Fig. A2.1)[4]. The lack of any distinct bands representing a defined protection region indicated H2A-H2B bound the DNA nonspecifically. We also looked at how H2A-H2B impacted digestion of mononucleosomes and trinucleosomes (Fig. A2.1). Addition of excess H2A-H2B to both mononucleosomes and trinucleosomes increased resistance to MNase digestion (Fig. A2.2). Using trinucleosomes, we observed rapid digestion in the linker region between the nucleosomes when H2A-H2B was not present (Fig. A2.2). Using excess H2A-H2B, we observed clearly defined bands representing trinucleosomes, dinucleosomes, and mononucleosomes suggesting H2A-H2B bound the linker region providing protection from MNase digestion.

Materials and Methods:

Micrococcal nuclease (MNase) digestion assays were performed using previously established protocols with canonical mononucleosomes and trinucleosomes [38, 48]. Mono and trinucleosomes were reconstituted using the dilution technique with purified *Xenopus laevis* octamer on 601-207bp DNA (or 601-621bp DNA for trinucleosomes) [143]. ~5 µg (0.17µM) of nucleosomes or DNA were used for each Micrococcal Nuclease digestion (MNase). MNase was performed with and without samples containing *Xenopus laevis* H2A/H2B. 3-fold molar excess H2A/H2B was added for a final concentration of 0.51 µM and allowed to incubate for 5 minutes

---

[4] Figures were taken from published paper Chen, X., et al. (2016) give proper reference number.

before the digestion occurred. MNase was added to each reaction and digestion occurred at room temperature for the indicated times. The reactions were then quenched by adding EDTA for a final concentration of 12.5 mM. The DNA was isolated from the histones by adding SDS and proteinase K for final concentrations of 0.5% and 0.2 mg/mL and incubated at 50^0 C for 30 minutes. Phenol-chloroform extraction was performed followed by ethanol precipitation. The samples were separated on a 6% native gel and stained with SYBR Gold.

Publication:

This was a collaboration project resulting in authorship in the following paper:

Chen, X., et al. (2016). "Histone Chaperone Nap1 Is a Major Regulator of Histone H2A-H2B Dynamics at the Inducible GAL Locus." Mol Cell Biol **36**(8): 1287-1296.
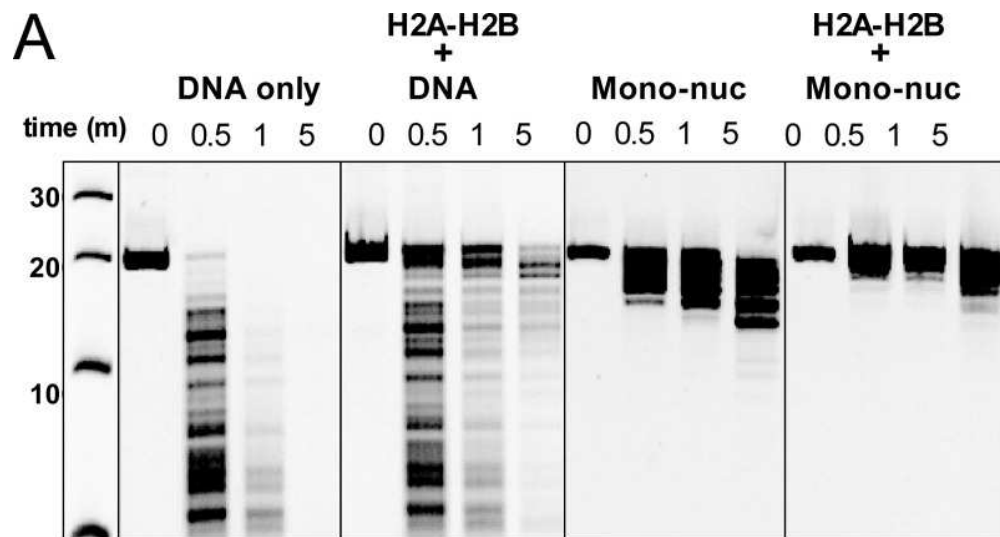
Figure A2.1. H2A-H2B accumulation protects DNA from MNase digestion. (A) *In vitro* analysis of chromatin with and without excess H2A-H2B. Shown are data from PAGE analysis of MNase digestion of naked DNA alone, DNA with H2A-H2B, mononucleosomes (Mono-nuc), and mononucleosomes with H2A-H2B, assessed on a 207-bp DNA fragment.
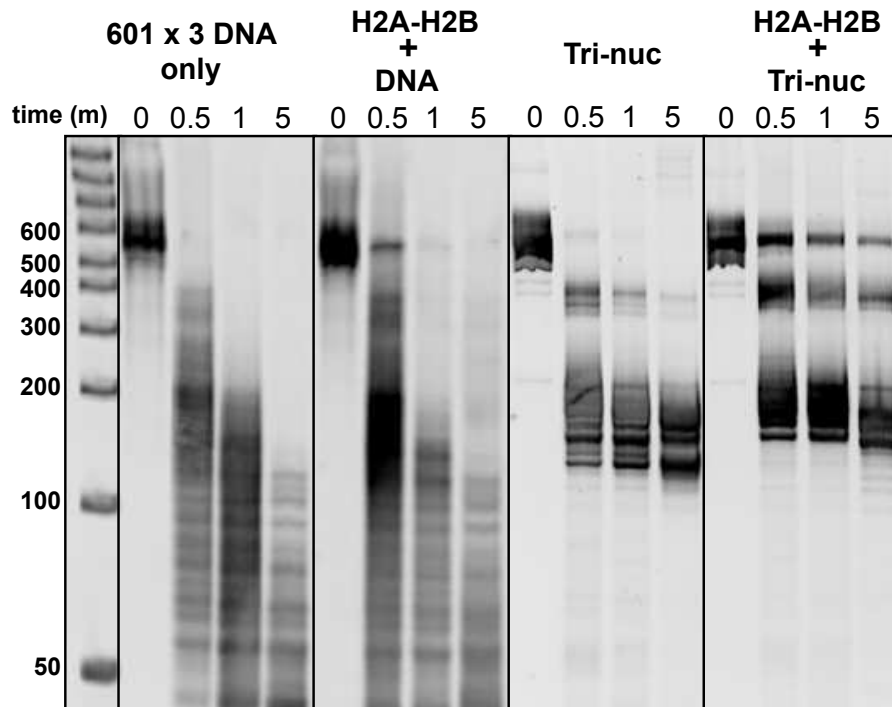
Figure A2.2. H2A-H2B accumulation protects DNA from MNase digestion. Analyses of MNase digestion of A) a 621 bp 601 (601 x 3) DNA fragment capable of forming tri-nucleosomes, composed of three consecutive 207 bp Widom 601 nucleosome positioning sequences with linker DNA MNase digestion of naked DNA alone (first panel), DNA with H2A-H2B (second panel), chromatin (third panel), and chromatin with excess H2A-H2B (fourth panel).

Supplementary Figures for Chapter 3
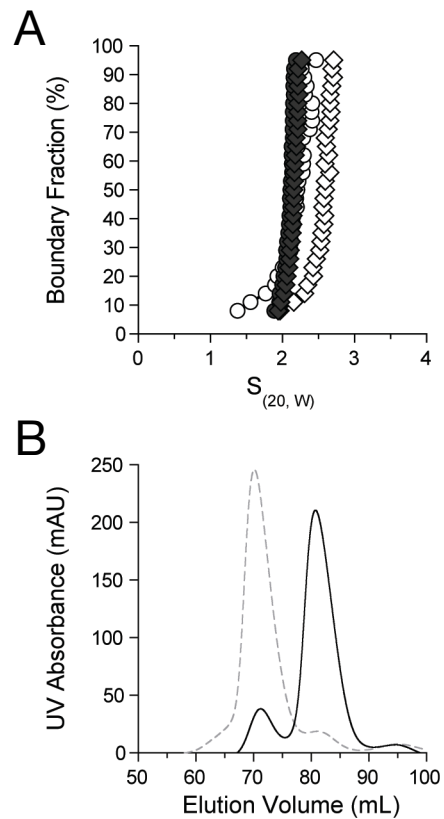
Figure S3.1. Comparison of H3-H4 and TM-H3-H4
(A) Sedimentation velocity of H3-H4 (white) or TM-H3-H4 (black) at 150 mM (circles) or 300 mM (diamonds) NaCl. **(B)** SEC of H3-H4 (dashed trace) or TM-H3-H4 (solid trace) at 2 M NaCl.
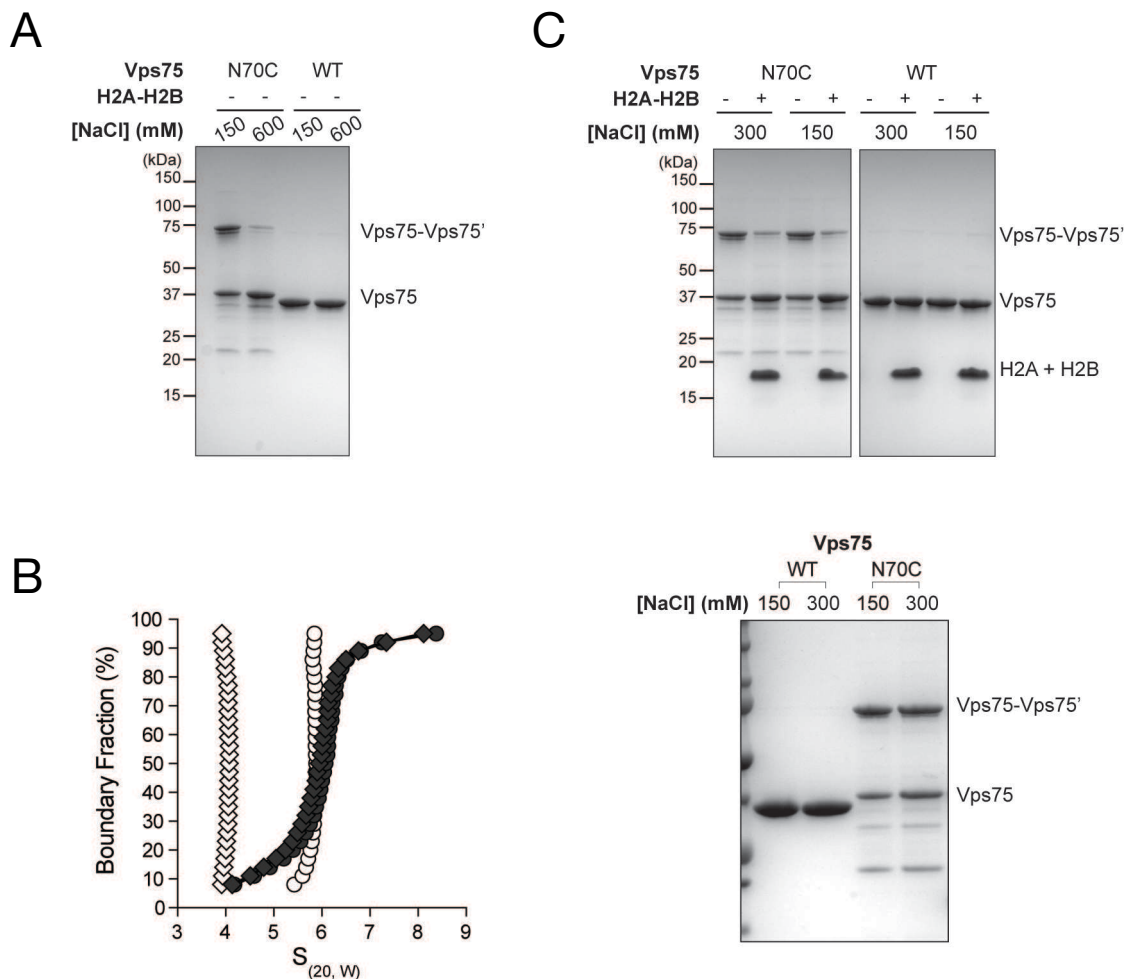
Figure S3.2. The Vps75 tetramer splits into two histone-bound Vps75 dimers
(A) Vps75-N70C and wild type Vps75 were incubated without reducing agent. Samples were resolved by SDS-PAGE without reducing agent and visualized with Coomassie Blue. Vps75- N70C disulphide bond formation depends on ionic strength, while wild type Vps75 does not form disulphide bonds. **(B)** Sedimentation velocity of disulphide-bonded Vps75-N70C at 150 mM (black circles) or 300 mM (black diamonds) NaCl. For reference, plots are also shown for wild type Vps75 at 150 mM (white circles) or 300 mM (white diamonds) NaCl. (C) Vps75- N70C and wild type Vps75 were incubated with an equimolar amount of H2A-H2B without reducing agent. Samples were analyzed as in A. H2A-H2B inhibits disulphide bond formation of Vps75-N70C.
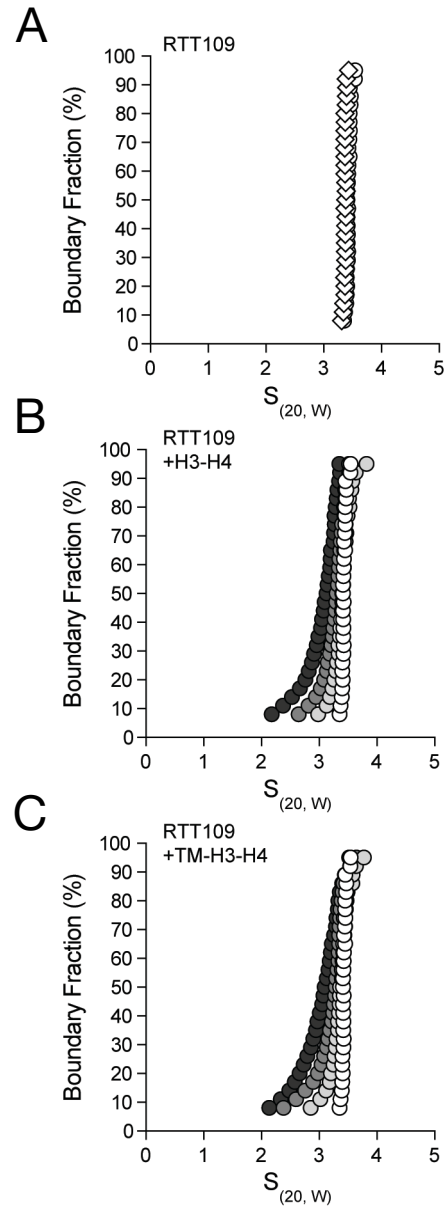
Figure S3.3. RTT109 does not stably interact with H3-H4 or TM-H3-H4
Sedimentation velocity of RTT109 alone (A) or with 0 to 2 molar equivalents of (B) H3-H4 or (C) TM-H3-H4. Experiments were done at 150 mM (circles) or 300 mM (diamonds) NaCl. RTT109 alone is shown in white, while RTT109 with 0.5, 1 or 2 molar equivalents of histones is shown in light grey, dark grey or black respectively.

Supplementary Table 1 - Molecular weights and frictional ratios obtained from SV-AUC

A

Measured MWs of Vps75 at 150 mM and 300 mM NaCl (Fig. 3.1A)

[NaCl] (mM)	Measured MW (Da) [95% CI]	f/f_o [95% CI]	Theoretical MW (Da) Measured MW/Theoretical MW
150	132190 [125500 – 138880]	1.6 [1.6 – 1.7]	131114 (Tetramer) [1.01]
300	66636 [66332 – 66940]	1.6 [1.5 – 1.6]	65557 (Dimer) [1.02]

B

Abundance (%) and Measured MWs (Da) [95% CI] of Vps75•H2A-H2B Complexes at 300 mM NaCl (Fig. 3.2A)

Molar equivalents of H2A-H2B

Vps75:H2A-H2B	Theoretical MW (Da)	0.5	1	2	f/f_o
0:1	27706	n.d.	10% 27090 [24806 – 29375]	22% 25333 [23442 – 27225]	1.2 – 1.4
2:1	93263	85% 87387 [79731 – 95044]	89% 93901 [89155 – 98646]		1.6 – 1.7
2:2	120969	n.d.	n.d.	78% 108120 [102830 – 113410]	

C

Abundance (%) and Measured MWs (Da) [95% CI] of Vps75•H2A-H2B Complexes at 150 mM NaCl (Fig. 3.2C)

Molar equivalents of H2A-H2B

Vps75:H2A-H2B	Theoretical MW (Da)	0.5	1	2	3	f/f_o
0:1	27706	n.d.	n.d.	15% 20638 [17620 – 23657]	28% 20980 [19205 – 22755]	1.2 – 1.3
2:1	93263	n.d.	n.d.	n.d.	n.d.	
2:2	120969	n.d.	56% 112150 [100820 – 123470]	71% 117100 [109870 – 124340]	70% 117190 [111110 – 123270]	1.4
4:1	158820	n.d.	41% 173160 [157430 – 188880]	14% 168290 [155810 – 180770]	n.d.	1.5 – 1.6
4:2	186526	92% 184590 [181440 – 187730]	n.d.	n.d.	n.d.	1.4 – 2.1

D

	Measured MWs of Vps75 with an equimolar amount of TM-H3-H4 at 150 mM and 300 mM NaCl (Fig. 3.2E)		
[NaCl] (mM)	Measured MW (Da) [95% CI]	f/f_o [95% CI]	Theoretical MW (Da) Measured MW/Theoretical MW
150	118990 [114810 – 123170]	1.5 [1.5 – 1.6]	118979 (2:2) [1.00]
300	105520 [104490 – 106550]	1.4 [1.4 – 1.4]	92268 (2:1) [1.14]

E

	Measured MWs of Nap1 with an equimolar amount of H2A-H2B at 150 mM and 300 mM NaCl (Fig. 3.3A & C)		
[NaCl] (mM)	Measured MW (Da) [95% CI]	f/f_o [95% CI]	Theoretical MW (Da) Measured MW/Theoretical MW
150	162020 [145400 – 178630]	1.7 [1.6 – 1.7]	151103 (2:2) [1.07]
300	154330 [146980 – 161680]	1.7 [1.7 – 1.7]	151103 (2:2) [1.02]

F

Abundance (%) and Measured MWs (Da) [95% CI] of Vps75•Rtt109 Complexes at 150 mM NaCl

Vps75:Rtt109	Theoretical MW (Da)	Molar equivalents of Rtt109 0.5	1	f/f_o
0:1	49045	n.d.	n.d.	
2:1	115681	95.73 108440 [103970-112900]	49% 117110 [104270-129960]	1.31– 1.36
2:2	165805	n.d.	41% 158340 [143170-173520]	1.43

G

Abundance (%) and Measured MWs (Da) [95% CI] of Vps75•Rtt109 Complexes at 300 mM NaCl

Vps75:Rtt109	Theoretical MW (Da)	Molar equivalents of Rtt109 0.5	1	f/f_o
0:1	49045	10% 54514 [50620-58407]	20% 40296 [36710-43882]	1.21-1.36
2:1	115681	75% 120110 [114450-125770]	63% 122880 [116740-129010]	1.44– 1.49
2:2	165805	n.d.	n.d.	

TABLE S1. (A-G) SV was performed to determine molecular mass (Da) and gross shape (f/f_o) using two-dimensional spectrum analysis.